



Kíssila Botelho Goliath

**Flexural Behavior of I-Section Textile
Reinforced Concrete Beams**

Tese de Doutorado

Thesis presented to the Programa de Pós
Graduação em Engenharia Civil of PUC-Rio in
partial fulfillment of the requirements for the
degree of Doutor em Engenharia Civil

Advisor: Prof. Daniel Carlos Taissum Cardoso
Co-supervisor: Prof. Flávio de Andrade Silva

Rio de Janeiro
April 2022



Kíssila Botelho Goliath

**Flexural Behavior of I-Section Textile
Reinforced Concrete Beams**

Tese de Doutorado

Tese apresentada como requisito parcial para obtenção do grau de Doutor pelo Programa de Pós Graduação em Engenharia Civil of PUC-Rio. Aprovada pela Comissão Examinadora abaixo.

Prof. Daniel Carlos Taissum Cardoso

Advisor

Civil and Environmental Eng. Dept. – PUC-Rio

Prof. Flávio de Andrade Silva

Co-supervisor

Civil and Environmental Eng. Dept. – PUC-Rio

Prof. Luiz Fernando Martha

Civil and Environmental Eng. Dept. – PUC-Rio

Prof. José Roberto Moraes D’Almeida

Chemical and Materials Eng. Dept. – PUC-Rio

Prof. Claudia Maria de Oliveira Campos

Federal Fluminense University

Prof. Julio Jeronimo Holtz Silva Filho

Federal University of Rio de Janeiro

Rio de Janeiro, April 8th, 2022

All rights reserved.

Kíssila Botelho Golith

Graduated in Civil Engineering at Universidade Estadual do Norte Fluminense Darcy Ribeiro in 2015 and obtained her M.Sc. Degree in Civil Engineering from the Universidade Estadual do Norte Fluminense Darcy Ribeiro in 2017. The area of interest encompasses reinforced concrete, cement-based composites, and experimental research.

Bibliographic data

Golith, Kíssila Botelho

Flexural behavior of i-section textile reinforced concrete beams / Kíssila Botelho Golith ; advisor: Daniel Carlos Taissum Cardoso ; co-advisor: Flávio de Andrade Silva. – 2022.

165 f. : il. color. ; 30 cm

Tese (doutorado)–Pontifícia Universidade Católica do Rio de Janeiro, Departamento de Engenharia Civil e Ambiental, 2022.

Inclui bibliografia

1. Engenharia Civil e Ambiental - Teses. 2. Concreto Têxtil. 3. Tecido de carbono. 4. Impregnações minerais. 5. Coating polimérico. 6. Temperatura. I. Cardoso, Daniel Carlos Taissum. II. Silva, Flávio de Andrade. III. Pontifícia Universidade Católica do Rio de Janeiro. Departamento de Engenharia Civil e Ambiental. IV. Título.

CDD: 624

Acknowledgments

To Prof. Daniel Cardoso, my advisor, for all the knowledge transmitted. Thank you for believing in me, for the encouragement, patience and dedication, doing everything possible for the development of this research. To Prof. Flavio Silva, my co-supervisor, my special thanks for agreeing to guide me alongside Prof. Daniel. Thanks for supporting and guiding me within the lab and for all the contributions.

To the technical staff of LEM-DEC, Euclides, José Nilson, Marques, Jhansen, Rogério and Bruno, for all the technical and emotional support provided to me during my time at the laboratory. In general, I would like to thank all the professors, technical staff and employees of PUC-Rio.

To my mother, Wilma, without her I never thinking about pos graduate and I would not have gotten this far. She always knew how to understand my absences, my afflictions, my fears and share my little achievements. I am proud to say that I admire her, I follow her examples and that thanks to her I am completing another stage of my life. For all her efforts in making my dreams come true and her love.

To the Zacarias family, especially Igor, Jorge and Cláudia. This journey would not have been possible without your care and unconditional support along this path. I have no words to say how grateful I am to have you by my side. Thanks for everything!

To my soul sister and college friend, Juliana Trindade, who is always by my side even with miles away, sharing with me all the joys and concerns throughout the doctoral period. You were fundamental in every way!

To my longtime friend, coach and best teacher ever, Andrey Escala. Your friendship made a great contribution and was of great value. I will not be forgotten.

During these five years I had the opportunity to make friends for life and I could not fail to thank the Fernanda Salgado, Tathiana Caram, Priscila Vieira, Felipe Pinheiro, Victor Nogueira, Thiago Carnavale and Thomas Lima. Thank you for

sharing ideas, knowledge, victories, difficulties, beers and so many moments together.

This study was financed in part by the Coordenação de Aperfeiçoamento de Pessoal de Nível Superior – Brasil (CAPES) – Finance Code 001.

Abstract

Botelho Goliath, Kíssila; Carlos Taissum Cardoso, Daniel (Advisor); de Andrade Silva, Flávio (Co-supervisor). **Flexural Behavior of I-Section Textile Reinforced Concrete Beams**. Rio de Janeiro, 2022. 165 p. Tese de Doutorado – Departamento de Engenharia Civil e Ambiental, Pontifícia Universidade Católica do Rio de Janeiro.

The present research aims to perform an experimental investigation on the short and long-term flexural behavior of I-section textile reinforced concrete (TRC) beams. Four types of carbon fabric were used, differentiated by the mesh dimensions and yarn cross-section, as well as by the fabric coating. The samples were identified according to the name of the coating, being styrene butadiene rubber (SBR) and SBR impregnated with sand (SND), acrylate (ACR) and epoxy (EPX) resin. Initially, four-point bending tests were performed in I-beams, considering SBR fabric and the following conditions: (a) plain cementitious matrix; (b) plain matrix and sand-coated textile; and (c) strain hardening cement-based composite (SHCC) matrix. The main goal was to correlate the improvements on interface and matrix properties with the crack pattern, failure mode and ductility. A theoretical method was used to evaluate the flexural behavior of the beams and good agreement was achieved with the experimental results. In the next step, the mechanical properties of different types of carbon-TRC and their interface were studied through direct tensile, pullout and compression tests. The influence of different test configurations and the effectiveness of the parameters obtained in these tests were verified for the performance prediction of TRC beams tested in bending in a monotonic way. The study was able to indicate the most suitable characterization methods to derive mechanical properties to be used in analytical methods, as well as to show the influence of different testing parameters on the load capacity of the composite. Finally, the long-term behavior of I-section beams reinforced with carbon fabric under sustained loading of 4 kN was investigated. An analytical model was used to analyze the results in terms of effective textile moduli, concrete tensile strength and the nominal bond stress. The model showed that SBR textile is strongly affected by

sustained load. SND, ACR and EPX beams formed new cracks during creep and the reduction in effective modulus observed was not accompanied by increase in crack width. It was confirmed the great influence of adhesion between fabric and matrix on the load capacity of the composite, the decrease in matrix strength due to fabric incorporation, as well as the divergence of the conditions of composite characterization tests.

Keywords

Textile reinforced concrete; Carbon fabric; Beam Long-term behavior; structural design

Resumo

Botelho Goliath, Kíssila; Carlos Taissum Cardoso, Daniel (Advisor); de Andrade Silva, Flávio (Co-supervisor). **Comportamento à Flexão de Vigas de Seção-I de Concreto Reforçado com Tecido**. Rio de Janeiro, 2022. 165 p. Tese de Doutorado – Departamento de Engenharia Civil e Ambiental, Pontifícia Universidade Católica do Rio de Janeiro.

Esta pesquisa tem por objetivo a análise experimental do comportamento à flexão, a curto e longo prazo, de vigas de seção I de concreto reforçado com tecido de carbono (*Textile Reinforced Concrete* - TRC). Foram utilizados quatro tipos de tecido de carbono, sendo eles diferenciados pelas dimensões da malha e seção transversal dos cordões, assim como pelo revestimento do tecido. As amostras foram identificadas de acordo com o nome do revestimento, sendo eles de estireno butadieno (SBR) e SBR com impregnação de areia (SND), acrilato (ACR) e epóxi (EPX). Inicialmente, foram realizados ensaios de flexão em quatro pontos nas vigas, considerando o tecido SBR e as seguintes condições: (a) matriz cimentícia simples; (b) matriz simples e têxtil revestido de areia; e (c) matriz *strain hardening cement-based composite* (SHCC). O principal objetivo foi correlacionar as melhorias nas propriedades da interface e da matriz com o padrão de fissuração, modo de falha e ductilidade. Foi utilizado um método teórico para avaliação do comportamento à flexão das vigas, que obteve boa concordância com os resultados experimentais. Na etapa seguinte, as propriedades mecânicas de diferentes tipos de TRC e sua interface foram estudadas através de ensaios de tração direta, arrancamento e compressão. A influência de diferentes configurações de ensaio e a eficácia dos parâmetros obtidos nestes ensaios foram verificados para a previsão do desempenho de vigas de TRC ensaiadas em flexão de forma monotônica. O estudo foi capaz de indicar os métodos de caracterização mais adequados para derivar propriedades mecânicas a serem utilizadas em métodos analíticos, assim como a influência dos diferentes parâmetros de ensaio na capacidade de carga do compósito. Finalmente, foi investigado o comportamento de longo duração das vigas de seção sob carregamento permanente de 4 kN. Um modelo analítico foi

usado para analisar os resultados em termos de módulo efetivo do tecido, resistência à tração do concreto e tensão nominal de aderência. O modelo mostrou que o tecido SBR é fortemente afetado pela carga permanente. As vigas SND, ACR e EPX formaram novas fissuras durante os ensaios de fluência e a redução do módulo efetivo observada não foi acompanhada pelo aumento da abertura da fissura. Confirmou-se a grande influência da adesão entre tecido e matriz na capacidade de carga do compósito, a diminuição da resistência da matriz devido à incorporação do tecido, bem como a divergência das condições dos ensaios de caracterização do compósito.

Palavras – chave

Concreto reforçado com tecido; Tecido de carbono; Comportamento à longo prazo de vigas; Projeto estrutural

Table of contents

Acknowledgments	4
Abstract	6
Resumo	8
Table of contents	10
List of figures	13
List of tables	17
List of Equations	18
1 Introduction	19
1.1. Motivation	19
1.2. Objectives	20
1.3. Thesis organization	21
2 Literature review	22
2.1. Overview	22
2.2. Concrete Matrix	23
2.2.1. Fiber reinforced concrete	25
2.3. Fabric Reinforcement	28
2.3.1. Carbon Textiles	30
2.4. Textile Reinforced Concrete	30
2.5. Hybrid Fiber Reinforced Composites	31
2.6. Composite characterization	33
2.6.1. Fabric-Matrix Interface	33
2.6.2. Tensile Test	36

2.6.3. Compression Test	40
2.7. TRC Beams	41
2.8. Design Models	45
2.9. Flexural creep behavior of TRC	46
2.10. References	48
3 Flexural behavior of carbon-TRC I-section beams	63
3.1. Introduction	63
3.2. Experimental Program	66
3.2.1. Materials and Mechanical Characterization	66
3.3. Results and Discussions	72
3.4. Conclusions	84
3.5. References	85
4 Material characterization of carbon-TRC composites	98
4.1. Introduction	98
4.2. Experimental program	100
4.2.1. Materials	100
4.2.2. Composite characterization	101
4.3. Results and Discussions	107
4.3.1. Pullout Test	107
4.3.2. Compression Test	109
4.3.3. Tensile Test	112
4.4. Influence of Material Parameters on Beam Response	118
4.5. Conclusions	122
4.6. References	123
5 Flexural creep of carbon-TRC beams	128
5.1. Introduction	128
5.2. Experimental program	131
5.2.1. Materials	131
5.2.2. I-section beams production	132
5.2.3. Overview of Experimental Program	133
5.3. Results and discussion	138

5.3.1. Short-term Monotonic Tests	138
5.3.2. Long-term Tests	142
5.4. Conclusions	151
5.5. References	152
6 General Conclusions	161
6.1. Suggestions for Future Works	163
7 APPENDIX A	164

List of figures

Figure 2.1 - TRC application examples (a) TRC barrel vault shells as roof elements [47]; (b) Pedestrian bridge Albstadt-Ebingen (solidiam GmbH) [48]; (c) Roof structure of TRC shells at RWTH Aachen [49]; (d) TRC pedestrian bridge [50].	23
Figure 2.2 - The CUBE – Henn Architecture [52].	23
Figure 2.3 – Behavior of plain concrete and FRC in compression (adopted by [65]).	26
Figure 2.4 – Tensile behavior of FRC [65].	27
Figure 2.5 – Tensile behavior of FRC [65].	28
Figure 2.6 - Different fabric structure: (a) weft insertion knit fabric, (b) short weft knit fabric, and (c) woven fabric (plain weave) [69].	29
Figure 2.7 - Textile made of (a) carbon [70], (b) AR-glass[72], (c) basalt [90], (d) PBO [77] and (e) sisal fiber [80].	30
Figure 2.8 - Stress-profile for different impregnations of textiles a) uncoated, b)SBR-coated fabric, c) fabric with sand-epoxy impregnation and d) fully impregnated fabric (adapted from [6]).	34
Figure 2.9 - Pullout test setup - (a) single yarn [96] e (b) yarn from textile [23].	35
Figure 2.10 - Pullout-slip response and shear strength diagram [21].	36
Figure 2.11 - Clevis grip method with (a) screws[113] and (b) with glued metal tabs [72]; and (c) clamp grip method [113].	38
Figure 2.12 - Typical stress versus strain curve of direct tensile test for TRC and bare fabric.	39
Figure 2.13 – TRC in compression [33].	41
Figure 2.14 - CLC test setup [32].	41
Figure 2.15 – Sectional geometry tested by [124].	42
Figure 2.16 – Sectional geometry and test set-up analyzed by [33].	43
Figure 2.17 – Cross-sections and reinforcement layout of beams tested by [119].	44
Figure 2.18 – Dimensions of the T-beams tested by [93].	45

Figure 3.1 – (a) Compression test set up and (b) Mechanical response of the concrete matrices in compression test.	68
Figure 3.2 - Pullout test: (a) Set up scheme; (b) overview of test setup; (c) average bond stress versus average slip.	69
Figure 3.3 - (a) Positioning of the reinforcement in the form and (b) concrete being cast in the form.	71
Figure 3.4 - Four-point Bending Test: (a) overview of test setup; (b) scheme of test and cross-section (dimensions in mm).	72
Figure 3.5 - Failure mode of beams: (a) RT-M1; (b) ST-M1; (c) RT-M2 beams.	74
Figure 3.6 - Load-deflection curves: (a) for full test; (b) detail for low deflections.	75
Figure 3.7 - Tensile stress trajectory.	75
Figure 3.8 - Moment-curvature relations (a) and initial moment stages in detail (b).	76
Figure 3.9 -DIC analysis of the (a) RT-M1, (b) ST-M1 and (c) RT-M2 beams; (d) Moment vs average crack opening; (e) mean crack spacing vs curvature. ...	78
Figure 3.10 - Tension stiffening model adopted for TRC with fiber reinforced concrete.....	79
Figure 3.11– Constitutive relationships assumed in the model.	80
Figure 3.12 – Comparison between moment-curvature relations obtained theoretically and experimentally.	81
Figure 3.13– Comparison between moment vs crack opening relations obtained theoretically and experimentally.	83
Figure 3.14 - Figure 3.14 – Comparison with experimental moment vs average curvature relations available in literature: a) Valeri et al. [33]; b) Preinstorfer et al. [8].	84
Figure 4.1 -Carbon fabrics with different coating conditions: a) SBR, b) SND, c) ACR and d) EPX.	101
Figure 4.2 - Pullout test: (a) Set up scheme and dimensions (in mm) and (b) overview of test setup.	102
Figure 4.3 - Overview of test setup of (a) compression test and specimen dimensions (in mm) and (b) CLC test and specimen dimensions (in mm).	104
Figure 4.4 - Tensile Test: (a) dimensions (in mm), (b) DIC scheme and (c) clevis grip detail.	106

Figure 4.5 - Tensile test with steel tabs glued with different gauge lengths.	107
Figure 4.6 - Representative bond stress versus slip curves.	108
Figure 4.7 - Results of compression tests for (a) different carbon textiles and (b) SBR samples under different testing conditions.....	110
Figure 4.8 - Failure mode of CLC specimens: (a) M-C-30 (b) SBR-C-30-L and (c) SBR-C-40-L.....	110
Figure 4.9 - Representative curve for tensile test.	113
Figure 4.10 - Tensile stress vs strain curve for (a) SBR-S-1-450, SND-S-1-450, ACR-S-1-450 and (d) EPX-S-1-450.....	114
Figure 4.11 - Representative tensile stress vs strain curve for SBR specimens: (a) effect of cross section, (b) effect of testing setup and (c) effect of gauge length.	117
Figure 4.12 - Idealized constitutive laws.....	119
Figure 4.13 - Influence of different parameters on the flexural response of TRC beams.....	121
Figure 4.14 - Influence of different tensile test on flexural response of SBR-carbon TRC.	121
Figure 5.1 - Carbon fabrics with different coating conditions: a) SBR, b) SND, c) ACR and d) EPX.	131
Figure 5.2– (a) Reinforcement assemble cage detail and (b) concrete casting process.	133
Figure 5.3– Flowchart representation of experimental program process.	134
Figure 5.4– Overview of the (a) scheme of test and (b) four-point bending setup and cross-section beam.....	135
Figure 5.5 - (a) Scheme of flexural creep test and (b) details of the instrumentation and load application; (c) flexural creep test setup.	137
Figure 5.6– Failure mode of beams in monotonic test: a) SBR; b) SND; ACR and EPX.....	138
Figure 5.7– Load-deflection curves from monotonic test for beams with different textile reinforcements and reinforcing ratios.....	140
Figure 5.8– Cracking pattern of beams not in scale, only for crack pattern observation purposes): a) SBR; b) SND; c) ACR; d) EPX.	141
Figure 5.9– Moment vs average crack opening.....	142

Figure 5.10– Flexural creep test graphical representation of the (a) process and (b) creep parameters over time.....	143
Figure 5.11– Load-deflection curves comparing the monotonic test with the creep process for a) SBR, b) SND, c) ACR and d) EPX.....	145
Figure 5.12– Long-term deflections: a) deflection-time curves and b) evolution of creep deflection coefficients.....	146
Figure 5.13– Cracking pattern of beams obtained using DIC: a) SBR; b) SND; c) ACR; d) EPX.....	149
Figure 5.14– Moment vs maximum crack opening for: a) SBR; b) SND; c) ACR and d) EPX beams.	150
Figure 5.15– Failure mode of beams after residual bending tests: a) SBR; b) SND; ACR and EPX.....	151
Figure 7.1– Models adopted for theoretical analysis: a) moment vs curvature; b) moment vs crack opening.....	164

List of tables

Table 3.1 - Composition for cementitious matrices per m ³ and main compressive properties.	67
Table 3.2 - Summary of experimental results.....	73
Table 3.3– Properties adopted in theoretical model.	82
Table 5.1– Carbon fabric properties reported by manufacturers.....	132
Table 5.2– Summary of short-term monotonic tests results.....	139
Table 5.3– Summary of long-term tests results.....	143
Table 5.4– Long-term evolution of parameters related to overall beam performance.	145
Table 5.5– Long-term evolution of parameters associated to cracking.....	149

List of Equations

Eq. 3.1.....	78
Eq. 3.2.....	81
Eq. 3.3.....	81
Eq. 5.1.....	147
Eq. 5.2.....	148
Eq. 7.1.....	165
Eq. 7.2.....	165
Eq. 7.3.....	165

1 Introduction

1.1. Motivation

The construction industry is increasingly seeking materials with high strength and good durability, among which composites arise as an attractive candidate. Composite materials are obtained through the macroscopic combination of two or more chemically distinct constituent materials – matrix and reinforcement – to obtain a new material with particular properties. In a typical composite, the matrix binds the reinforcement together and provides protection to the reinforcement, while the reinforcement is responsible for the composite's strength and stiffness

Textile reinforced concrete (TRC) is a cementitious composite material characterized by a matrix of fine aggregate concrete (mortar) and an open mesh fabric reinforcement. The combination of these materials results in a product with high mechanical strength and good durability that can be used to produce new thin-walled structural elements or to strengthen existing structures.

The use of carbon fiber fabrics as reinforcement of TRC has been investigated by many authors and it has been shown that excellent mechanical performance can be achieved in tension [1–9] and bending [10–15]. However, the behavior of these structures depends on the properties of the matrix and fiber used, as well as on the interface between these two materials. Adhesion between matrix and fiber is the bond component of the interface and has been the subject of many studies [16,17,26,27,18–25]. Although the presence of the fabric within matrix may affect composite's compressive strength negatively, few works have addressed this topic [28–33].

For successful application of TRC as a structural material, validated design methods based on appropriate values of mechanical and bond properties determined through experimental tests are required. Nevertheless, there is still a gap in the knowledge regarding this correlation between characterization techniques and structural design approaches. Since there is no specific standard or code for the mechanical characterization or design of TRC composites, different material

characterization methods, specimens' geometries and procedures to measure the deformation and crack pattern have been used for different research groups, with variations in results. Currently, a new report is being prepared by the Technical Committee 292-MCC: Mechanical Characterization and Structural design of Textile Reinforced Concrete.

Although there are many publications in the literature about carbon TRC, there is still no sufficient data regarding the behavior of this material in a structural level, both for short and long-term loading conditions. The creep behavior of TRC remains a gap in the knowledge, while appropriate comprehension of the phenomenon is relevant for the design of structural members. So far, there is no sufficient experimental data available [34–38] on the overall behavior of TRC members to allow studying the complex interaction between phases of the composite and developing methodologies for a long-term prediction of the behavior. Highlighting, no research on creep in TRC structural members was found to date. Thus, this research aims to evaluate the performance of I-section TRC beams made with various carbon fabrics and to develop analytical models to correlate the mechanical properties with the structural behavior.

1.2. Objectives

The main goal of this research is to investigate the flexural performance of TRC I-beams made with different carbon fabric conditions and propose analytical models incorporating the influence of material and interface properties. The specific objectives include:

- to evaluate sand-coated and uncoated SBR-laminate carbon-TRC beams comprised of either a high strength matrix and a SHCC matrix to investigate the influence of materials on the interface properties, crack pattern, failure mode and ductility;
- to compare the constitutive laws obtained through different techniques and for various carbon-TRC materials on the theoretical flexural response of carbon-TRC beams, comparing the predictions against experimental results;
- to investigate experimentally the long-term behavior of carbon-TRC I-section structural beams under sustained load and the influence of different coating conditions (SBR, ACR, EPX and SND).

1.3. Thesis organization

This thesis consists of this Introduction, a Literature Review, followed by three chapters structured as individual full papers and Conclusions. Chapter 2 presents a literature review on the topics covered by the thesis, identifying the gaps in the knowledge. Chapter 3 presents an investigation into improved SBR-carbon fabric performance and proposes an analytical model to validate the experimental results. In Chapter 4, different constitutive laws for the TRC are obtained through various characterization methods and their influence on the structural performance prediction is evaluated. Chapter 5 presents the study about long-term behavior of TRC beams. Chapter 6 presents the conclusions and suggestions for future investigations.

2 Literature review

2.1. Overview

Different reinforcement techniques have been developed and studied to replace the conventional steel reinforcement in concrete structures. An example is the ferrocement, which can be considered a precursor of the cement-based composite reinforced with textile. It was used firstly by Frenchman Joseph Louis Lambot in France, in 1855, who constructed a ferrocement boat [39]. However, in the 1960s, this technology started being used in the construction industry to build slender shell structures such as roofs and water tanks. Ferrocement is a composite construction material consisting of single or multiple layers of steel mesh [40]. According to the report of the Committee 549 of the American Concrete Institute (ACI) [41], *“Ferrocement is a type of thin wall reinforced concrete commonly constructed of hydraulic cement mortar reinforced with closely spaced layers of continuous and relatively small size wire mesh. The mesh may be made of metallic or other suitable materials”*. Meshes fabricated using high-performance carbon, glass, or aramid fibers were more recently adopted as a reinforcement strategy, resulting in the so-called textile reinforced concrete (TRC) [39].

Research works on TRC have been extensively carried out in the past decades and the material’s application in load-bearing members is already a reality [42–46]. The TRC can be applied to the exterior and interior of buildings, roofing products, flooring, water and sewage pipes, molded forms, rebar-free applications and various renovation projects. Figure 2.1 presents some examples of its application.



(a)



(b)



Figure 2.1 - TRC application examples (a) TRC barrel vault shells as roof elements [47]; (b) Pedestrian bridge Albstadt-Ebingen (solidiam GmbH) [48]; (c) Roof structure of TRC shells at RWTH Aachen [49]; (d) TRC pedestrian bridge [50].

Many universities have developed initiatives and prototypes to show the material's potential. For example, the world's first building made of carbon concrete – the so-called CUBE (Figure 2.2) – is currently under construction at TU Dresden campus, in Germany. The building is a showcase project of the research project on innovative building materials "C³ - Carbon Concrete Composite", funded by the German Federal Ministry of Education and Research [51].



Figure 2.2 - The CUBE – Henn Architecture [52].

2.2. Concrete Matrix

The composite matrix has the main functions of binding the fibers, providing protection and transferring to them the external forces. In a TRC, the matrix is usually a mortar with a maximum aggregate size of up to 2 mm. However, due to its high mechanical performance, it is considered a fine-grained concrete [53,54].

Concrete with fine aggregate has low stiffness and high strain at break when compared to conventional concrete [53]. The high strength of the matrix is obtained through the use of pozzolanic additions, such as silica fume and fly ash. The use of these materials is beneficial since the pozzolanic reactions densify the matrix and

reduce the available calcium hydroxide in the interface transition zone, improving the adhesion bond between matrix and fiber [55]. It is noteworthy that, by replacing part of the cement with pozzolanic additions, energy consumption and CO₂ emission from conventional cement production are reduced [4]. In addition, it is possible to use a cement with a low clinker content once the fabric does not require passivation by the concrete, further reducing CO₂ emissions.

Partial replacement of cement with fly ash makes cement-based products more economical and the particle morphology improves the rheology of the fresh mix [46]. In general, it has been found that the use of fly ash leads to better workability and offers adequate mechanical properties [1].

Mobasher et al. [46] studied the incorporation of different levels of fly ash in a cement matrix reinforced with glass fabric. The workability of the mixture was improved with the addition, which was attributed to the fineness of the pozzolanic material. All samples tested under direct tensile showed higher strength than the control. However, an optimal content to be incorporated was found to be about 60% in volume. Through Scanning Electron Microscopy (SEM), it was shown that the fly ash fills the capillary voids and the transition zone in the vicinity of the spacing between the uncoated rovings. This explains the greater adhesion with increasing fly ash content.

Silica fume is a pozzolanic material with high reactivity, very small particle size, high surface area and high percentage of amorphous silica. Silica reacts with hydrated calcium hydroxide and contributes to increased adhesion of the matrix-fiber interface [56]. Previous studies [19,57] reported an improvement in the adhesion between the carbon fiber and the matrix with the addition of silica fume and a low water/binder ratio.

With the incorporation of silica fume in the fine-grained concrete, an improvement in density occurs. This is due to the densification of the matrix around the fiber, which has a positive effect on the bond strength [46]. Despite this, the amount of silica used in the mixture must be limited to 10% of the total mass content of the binder, as it is not possible to obtain a fluid consistency for higher contents, affecting its workability [58].

Brittle failure is another characteristic of the cement matrix. The reinforcement with fibers enhances the behavior in this aspect, increasing its tensile strength,

tenacity, ductility and energy absorption capacity, as well as allowing the control of cracking of the material [59–61]. This subject will be discussed further on.

2.2.1. Fiber reinforced concrete

Fiber-reinforced concrete (FRC) is defined by the report of the ACI Committee 116 as a concrete containing dispersed randomly oriented fibers [62]. According to Bentur and Mindess [59], the oldest written record of the use of fibers as reinforcement in brittle matrices forming cement-based composites dates from 4000 B.C., by the Egyptian civilization.

Traditionally, the most common way to reinforce plain concrete is through continuous steel bars. Cement-based matrices are known for their low tensile strength and low ability to deform under tensile stresses [2]. Therefore, the steel bars are positioned in order to withstand the tensile forces to which the structural members are subjected. Short fibers can be also adopted randomly dispersed in the matrix, but this strategy is not as effective in transferring tensile forces. On the other hand, short fibers have a greater potential in terms of cracking control due to their homogeneous distribution inside matrix [59]. According to Bentur and Mindess [59], the use of short fibers is not a substitute for conventional reinforcement. In fact, each type of reinforcement plays a distinct role in the mechanical behavior of the material. The randomly distributed fibers in the cement matrix work as a ‘bridge’ for the transmission of tensile forces between the crack edges. Thus, it can help controlling the crack formation and in the improvement of its distribution along a structural member. In this way, the fibers are used not to improve the strength of the concrete, but to improve the behavior of the concrete once the matrix was cracked. The use of short fibers, therefore, prevents the total loss of load capacity [59,63] and provides ductility and toughness to the material.

The incorporation of fibers in concrete can be adopted for several purposes, such as the improvement of impact performance, fatigue properties and abrasion resistance, reduction in the shear reinforcement rate, in addition to cracking control and improvement of ductility already mentioned [2]. However, despite the numerous advantages, the use of fibers leads to a loss of workability, since a high demand for water is required [54].

The compressive strength and the modulus of elasticity in concrete for the same volume of fibers will vary according to the type of fibers used [64]. However, it is worth mentioning that the post-peak behavior can be significantly affected, showing a softer descending branch as a consequence of the fibers ability to tie the matrix together and to control transverse expansion. Therefore, a more expressive residual strength after rupture can be seen, improving its toughness (Figure 2.3) [65].

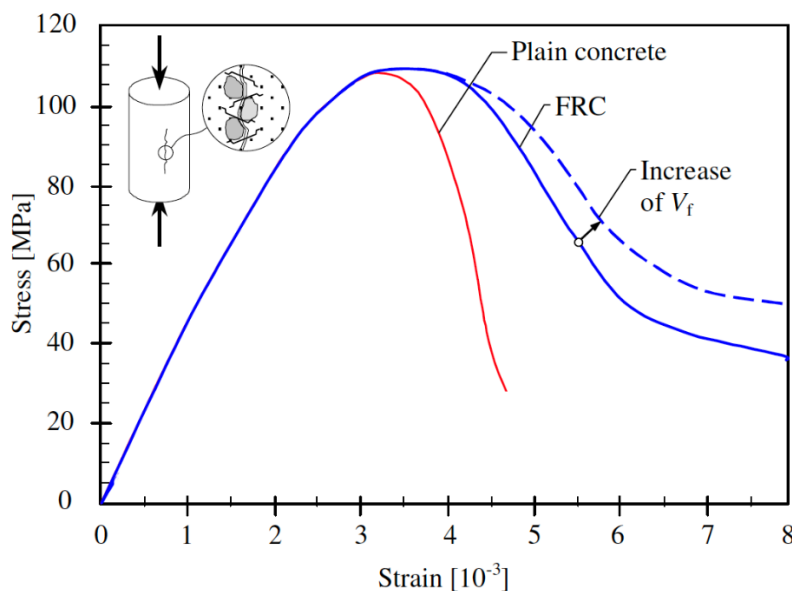


Figure 2.3 – Behavior of plain concrete and FRC in compression (adopted by [65]).

Currently, there are several types of short fibers available for use in cementitious matrices, such as glass, steel, carbon, poly-vinyl alcohol (PVA), polypropylene (PP) and natural fibers. Choosing the type of short fiber will vary according to their physical/chemical properties, material, or their mechanical properties [2].

The tensile behavior of FRC can be classified as strain softening or strain hardening, which will depend on the post-cracking strength behavior, as shown in Figure 2.4 [59]. Regarding the strain-softening behavior, a stress decay after initial cracking occurs with increasing strains and a single localized crack is formed. On the other hand, the strain-hardening behavior is characterized by a post-cracking increasing resistance, with the formation of several cracks before reaching the stress peak. The volumetric fraction of fibers will determine the transition between the two types of behavior for a given type of fiber and mixture [59,65].

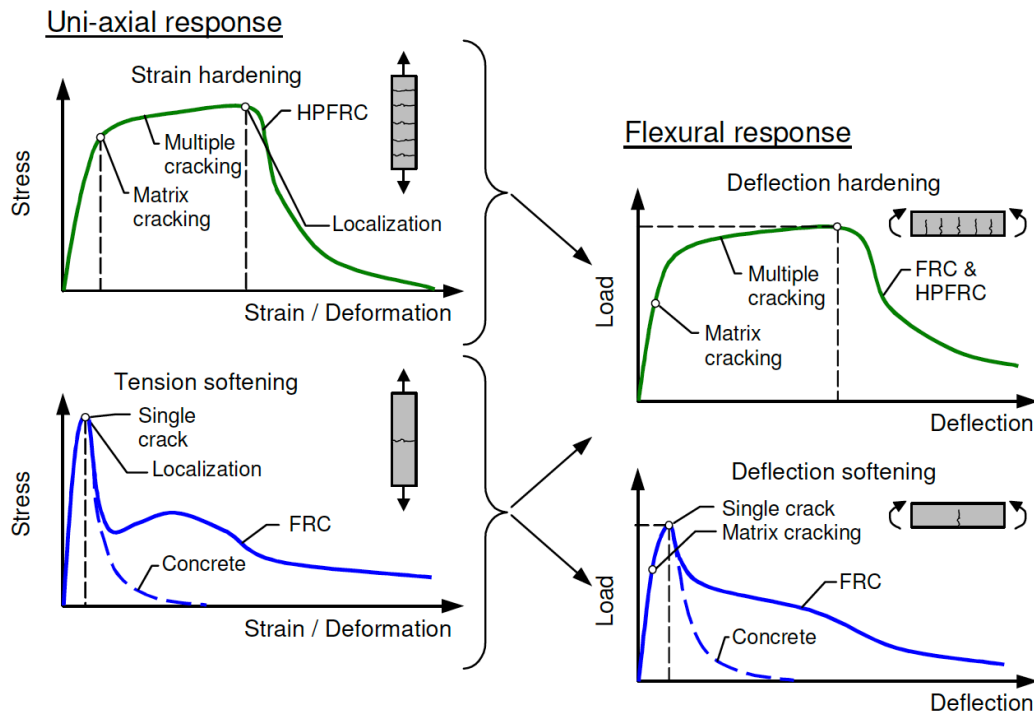


Figure 2.5 – Tensile behavior of FRC [65].

2.3. Fabric Reinforcement

Textiles are fibers in a form multifilament yarns structured as a bi- or three-dimensional open mesh [53]. The 3D is capable of withstanding forces in its main plane as well as in the direction perpendicular to it, whereas 2D or planar structures can support loads only acting on their plane [54]. They can offer excellent corrosion resistance and are lightweight materials, with high tensile strength and high potential to be used as reinforcement in cement-based matrices. In order to increase the efficiency of the composites, the warp yarns must be oriented parallel to the direction of main tensile stresses of the component. The transverse yarns are sometimes described as “non-structural” [68], although these are also responsive in the case of stresses not orthogonal to loading.

Fabrics can be differentiated according to the manufacturing process, mesh dimensions, cross-section shape and dimensions, type of coating and/or fiber material. It can be also classified according to the way longitudinal and transverse strands are connected, e.g. woven, knitted, braided or nonwoven [53,69] (Figure 2.6).

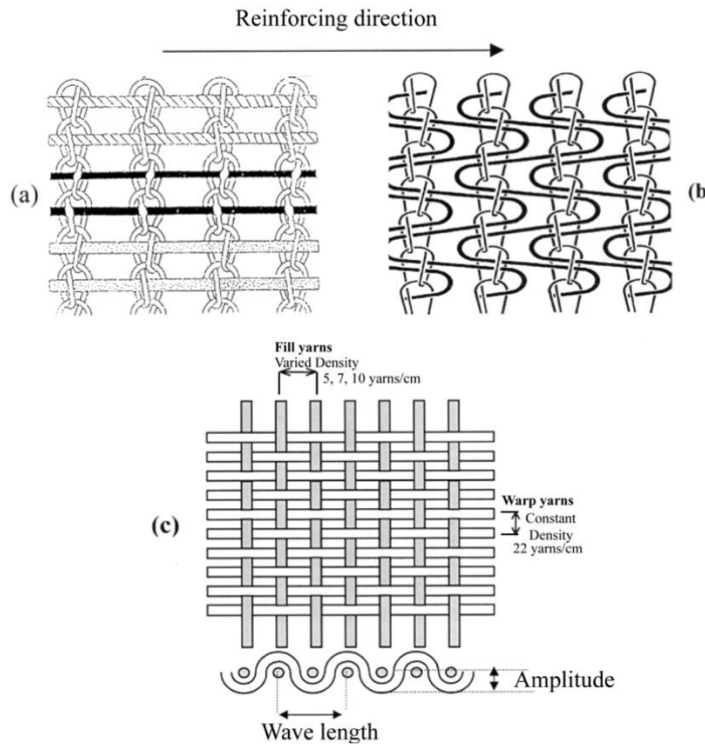
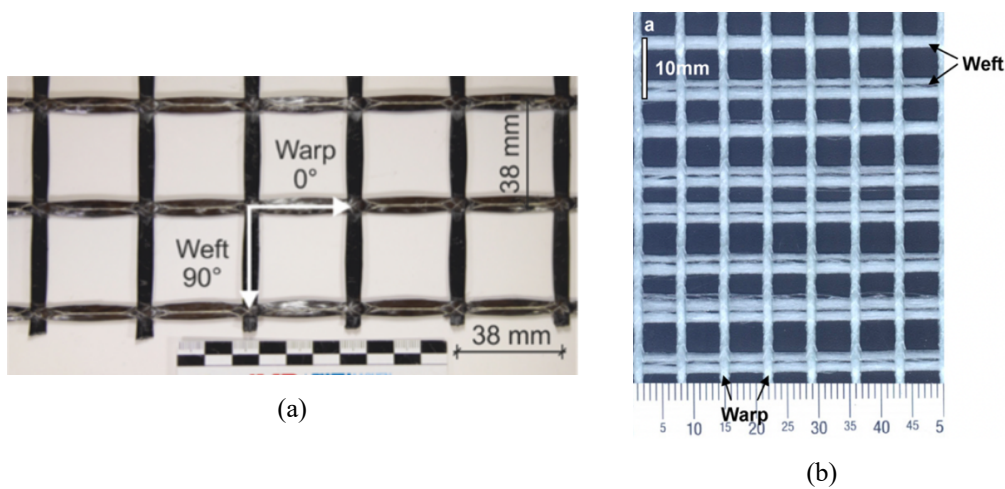


Figure 2.6 - Different fabric structure: (a) weft insertion knit fabric, (b) short weft knit fabric, and (c) woven fabric (plain weave) [69].

In general, textiles are composed by fibers such as carbon [14,26,70], alkali-resistant glass [71,72], basalt [73,74], PBO [75–77] and natural [13,78–80] (Figure 2.7). In order to keep the dry fibers together, to protect them, and to improve bond and better activation of internal filaments, textiles can be impregnated with a polymer matrix, e.g., styrene-butadiene rubber (SBR) [81–83], epoxy (EPX) [84–86] or acrylate (ACR) [87–89]. These polymeric impregnations yields different fabric flexibility and bond between matrix and textile.



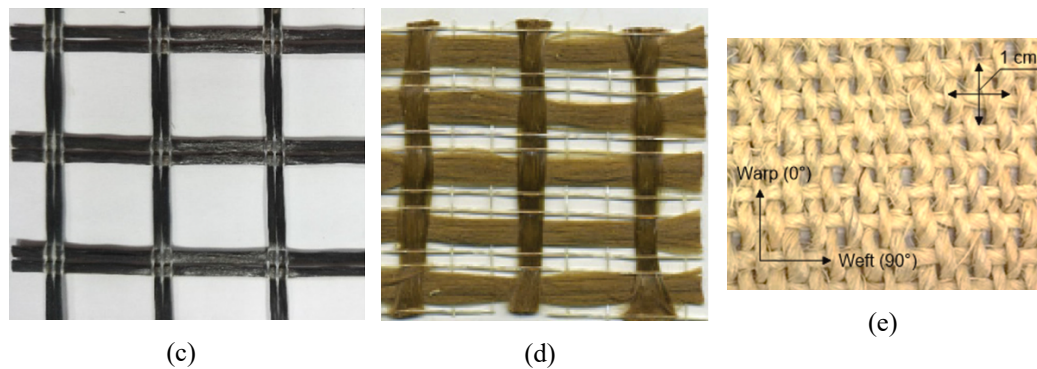


Figure 2.7 - Textile made of (a) carbon [70], (b) AR-glass[72], (c) basalt [90], (d) PBO [77] and (e) sisal fiber [80].

2.3.1. Carbon Textiles

Carbon fibers are known for their high tensile strength and Young's modulus, superior durability and its effectiveness as reinforcement in cement-based matrix compared to others fibers used in TRC [91]. The modulus of elasticity and the tensile strength of carbon fiber mainly depend on its manufacturing process, which are based on the different raw materials used, i.e. polyacrylonitrile (PAN) or petroleum and pitch [59].

The carbon fibers are found in the form of tows, composed of several filaments with a diameter between 7-15 μm [56,92]. They are inert to most chemicals and are therefore suitable for use in an alkaline environment such as concrete. In addition to the aforementioned properties, carbon fibers exhibit negligible creep behavior, low density, low heat expansion and high resistance against acid, alkaline and organic solvents [53].

Despite the advantages presented by the carbon fiber, this uncoated fiber has low adhesion to the cementitious matrix and currently has a high cost when compared to conventional reinforcing steel or to glass fibers. However, carbon offers more cost-effectiveness compared to other fibers and its importance as a reinforcement in concrete is increasing [59].

2.4. Textile Reinforced Concrete

As previously mentioned, the most traditional way of reinforcing concrete (RC) elements is through steel bars. Despite conferring numerous positive properties to concrete, such as strength and stiffness, RC has a low strength-to-weight ratio. In

addition, it is important to highlight the need for an adequate concrete cover to protect the reinforcement against corrosion.

Cement matrix composites with textiles are presented as an alternative to overcome the deficiencies presented by reinforced concrete. Recent studies have directed the use of textile concrete to produce thin, lightweight and modular structures, as aforementioned showed (Figure 2.1) [42,93].

Among the main advantages found in TRC, its high tensile strength and pseudo ductile behavior characterized by large deformations and the formation of multiple cracks before failure can be highlighted [15]. With their excellent mechanical properties, TRC has a wide field of applications both for the construction of new structures and for the repairing and strengthening of existing structures. One of the main advantages of using TRC over RC elements is its corrosion resistance, which eliminates the need for large concrete covers, allowing to fabricate thin-walled slender concrete members [42,53,54].

Since there is no specific standard or code for the mechanical characterization or design of TRC composites, different material characterization methods, specimens' geometries, and procedures to measure the deformation and crack pattern are used for different research groups. Thus, variations in results have been found in the literature [2,7,9,94].

TRC presents a complex behavior and the design of structural members depends on a full characterization of the constituents, as well as of the interaction between them. The fabric and the matrix are usually characterized through simple uniaxial tensile and compressive, respectively, while the composite performance is evaluated through pullout and tensile tests. Although the influence of the fabric within matrix on compressive strength should be considered in the design, only few authors [29–33,95] have investigated this topic.

2.5. Hybrid Fiber Reinforced Composites

Many authors [60,64,89,96–101] have observed that the use of short fibers dispersed in the TRC matrix allows to control the width of the crack, providing a network of fine cracks. Hybrid fiber reinforced composites consisting of strain-hardening based-cement composite (SHCC) matrices and continuous textile reinforcement should yield a better crack control and damage tolerance, showing a

more pronounced multiple cracking behavior. In addition, the use of the SHCC matrices leads to high inelastic deformations with a consequent pseudo-ductile behavior along with higher energy dissipation capacity [100–102].

Hinzem and Brameshuber [64] investigated the improvement in first crack forces and the development of a more ductile behavior in fine-grained concretes reinforced with alkali resistant glass fiber fabric through the incorporation of short fibers of glass, aramid, carbon and PVA in the matrix. Two mixtures were used, one as a reference and the other with an increase in the content of cement and silica fume for the incorporation of fibers. An increase in the first crack load was observed with the addition of all types of fiber in the matrix. The post-cracking behavior of the material depends on the short fibers that are activated after the first crack. By increasing first crack load, the fibers must be able to absorb the increase in energy released in the crack, without an unstable decrease in the load in the tensile test. With a good bond between matrix and fiber, in addition to a more uniform load transfer to the textile, the combination between textile and short fibers may lead to a stiffer behavior in the cracking phase.

In the research carried out by Silva and Silva [96], rectangular section TRC beams were tested without and with the addition of short steel fibers and compared to RC beams without and with short steel fibers. According to Silva [15], the main difference between textile concrete and reinforced concrete beams is the ductility. Reinforcing steel exhibits a yield plateau and can provide a more ductile behavior to the structural member; unlikely, carbon fabric has a brittle behavior. However, it has been proven that the addition of short steel fibers can contribute to mitigate this negative aspect of carbon fabric, providing a more ductile behavior to the beams.

In the work carried out by Barhum and Mechtcherine [97], the interaction between short fibers and continuous fibers in cementitious matrix composites was evaluated through bilateral pullout tests. It was observed that the addition of short fibers led to a considerably higher final pullout force, indicating a better bond between the strand and the matrix. In addition to obtaining greater pullout forces, the displacements measured when reaching the final force decreased slightly. This behavior arises as consequence of the confinement provided by the short fibers.

2.6. Composite characterization

2.6.1. Fabric-Matrix Interface

The load bearing behavior of a TRC, as well as of any composite material, is not achieved only by the properties of its constituent materials; the adhesion between reinforcement and matrix plays an important role [103]. In TRC materials, the bond behavior between the fabric and the matrix is one of the main factors affecting the overall behavior of the structure [54,63], such as its strength, crack pattern, ductility and toughness. In general, a stronger bond between materials leads to fracture of the composite, providing a material with high strength, but with low ductility or relatively brittle behavior. On the other hand, weak bonds can cause fiber pullout with lower final strengths [9,104].

Studies show that the geometry of the fabric (woven, knitted, braided or nonwoven, for example) has a great influence on the bond behavior of the composite, as well as the type of fabric and mesh dimensions [18,68,105].

The interaction nature of the cement matrix and the fabric, and individual roving is complex and different from other materials. This is due to the non-homogeneous activation of filaments and the impregnation conditions [6]. According to previous studies [6,106], the distribution of stresses in a yarn with a given cross-section is influenced by the degree of impregnation and the cross-section shape.

The yarns of fabrics are made up of several filaments, and it is necessary to distinguish between two groups of filaments within a roving. For uncoated fabrics, the outer filaments are in direct contact with the matrix and have better bond than the inner filaments, which are only activated indirectly through friction; this delayed activation effect is called 'shear lag' [98]. In addition, this uncoated fabric presents a non-uniform stress profile [6], as shown in Figure 2.8a.

For the coated fabrics, the coating is in contact with the cement matrix and is responsible to transfer the stresses to the fibers. The stress profile is strongly influenced by the coating material, as well as by the fraction of the area impregnated, as shown in Figure 2.8b-d.

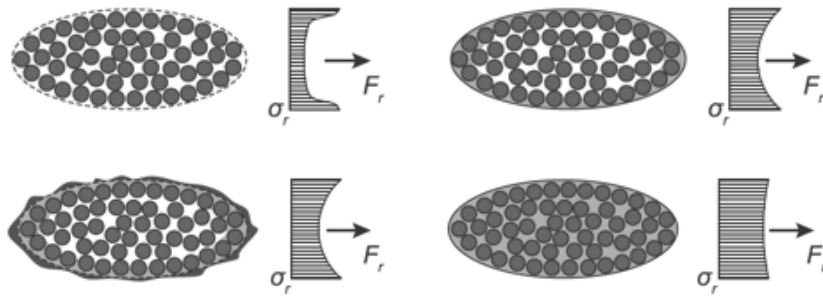
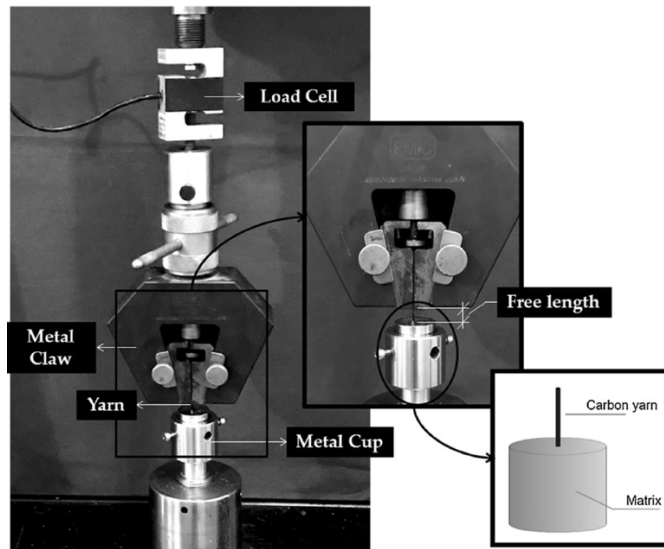


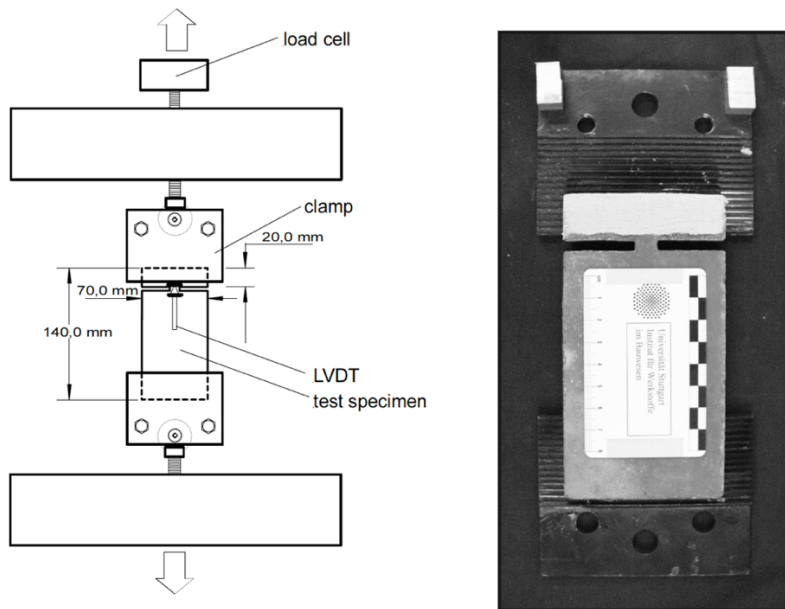
Figure 2.8 - Stress-profile for different impregnations of textiles a) uncoated, b) SBR-coated fabric, c) fabric with sand-epoxy impregnation and d) fully impregnated fabric (adapted from [6]).

Styrene butadiene rubber (SBR) impregnation results in a flexible textile with ease of transportation and handling. However, the use of this polymer leads to poorer activation of inner filaments and bond to the concrete matrix, resulting in a composite with lower stiffness and characterized by wide largely spaced cracks [107]. In contrast to SBR, epoxy resin (EPX) coating results in a rigid textile with good chemical affinity with the cementitious matrices [96]. The acrylic based polymer (ACR) impregnation is stiffer than SBR and yields moderate adherence to the surrounding cementitious matrix [89]; ACR-fabric reinforced TRCs exhibit multiple fine cracking pattern, higher tensile strength and higher energy absorption compared to those reinforced with SBR-fabric [88]. One alternative to improve the bond performance of SBR fabrics is to manually impregnate the textile with epoxy resin and sand [1,23,82,96,108].

The most used method to characterize the bond behavior between matrix-fiber is through pullout tests. Several authors performed the test to better understand the interface behavior of fiber-reinforced cementitious matrix composites. Despite this, there is still a lot of divergence in the literature regarding this set up test. The more traditional pullout test between fiber and matrix is performed using a single yarn, as shown in Figure 2.9a [19,96,109]. However, acknowledging that the textile structure may influence the bond behavior, some studies also performed tests with pullout of yarn from textile (Figure 2.9b) [22,23].



(a)



(b)

Figure 2.9 - Pullout test setup - (a) single yarn [96] e (b) yarn from textile [23].

In Figure 2.9b, a bilateral pullout test configuration developed in the work of Krüger [110] is presented. The sample has asymmetrical anchorage lengths, with one side of the sample having an embedded length of 20 mm and the opposite side a length of 120 mm. This test setup proves to be the most suitable for deriving the slip-stress response between the matrix and a fabric, particularly for carbon fiber fabrics [23].

Through fabric pullout tests of fabrics made of different materials and with various geometries, it has been concluded that the bond behavior is highly

dependent on the fabric type, matrix mix and fabrication method. In addition, the elastic modulus of the fabric yarn can also contribute to the pullout behavior [21].

Figure 2.10 shows a typical pullout response obtained by yarn pulling from a cement matrix. In the load *versus* slip curve, three stages can be distinguished. Stage I corresponds to a linear response, where the yarn is chemically and perfectly bonded to the matrix. In Stage II the response becomes nonlinear on the ascending branch due to initiation of debonding. As debonding progresses along the embedded length, the stiffness of the load-slip curve decreases until the maximum load is reached; at this point, the yarn is completely debonded. Finally, in Stage III the yarn slides out dynamically [21]. In addition, it is possible to see in Figure 2.10 that the nominal bond stress – pullout force divided by yarn nominal embedded surface area – can be correlated to the slip in the linear range through a pullout stiffness parameter κ .

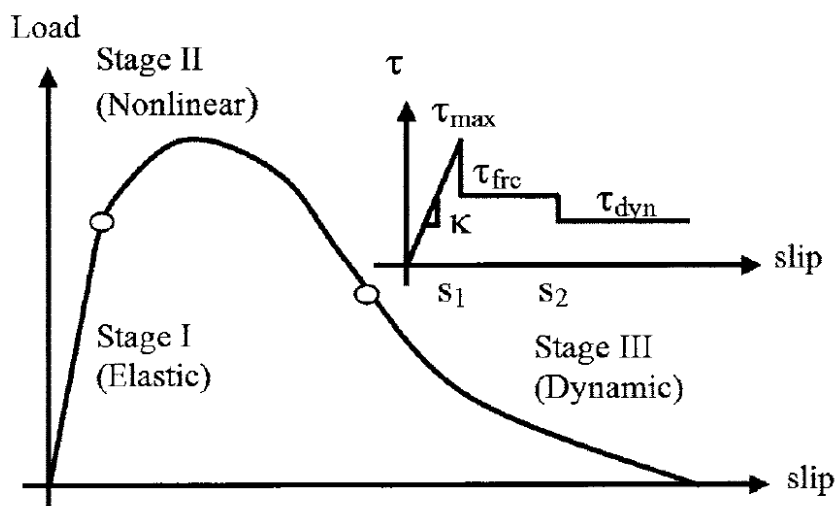


Figure 2.10 - Pullout-slip response and shear strength diagram [21].

To date, there is no study correlating the bond response from pullout test to the performance of structural members. Therefore, more studies are still needed to better understand the best approach for interface characterization.

2.6.2. Tensile Test

There are several factors that influence the tensile performance of the TRC such as the load application strategy, specimen geometry, fabrication procedure and strain measurement technique [2,8,72,94,98,111]. Relevant parameters for the

design of the TRC structures can be obtained from this test such as the composite strength and strain at rupture, the effective modulus and cracking properties (e.g., first crack stress, crack width and spacing with loading).

In general, tensile tests are performed on prismatic samples with clevis (Figures 2.11a and b) or clamp grid method (Figure 2.11c), providing rigid and soft load application, respectively. The clevis grip method – used in this work – is recommended by ACI434.13 [112] and consists in load application through lateral pressure of specimen with screws (Figure 2.11a) or with steel plates glued at the anchorage region (Figure 2.11b). On the other hand, the clamp grip method is characterized by load application through applying a compressive force normal to the plane of the specimen at its ends (Figure 2.11c) [7].

Overall, the tensile behavior is characterized by three stages of response, as seen in Figure 2.12. In Stage I, the matrix is uncracked and is still contributing significantly to resist to the tensile stresses. At this stage it is possible to estimate the tensile modulus of elasticity through an equivalent homogeneous cross section, assuming a perfect bond between the matrix and the textile. The transition between Stages I and II takes place after the appearance of the first crack in the matrix. Thus, in Stage II, the tensile stress exceeds the tensile strength of the concrete and multiple cracks form along the specimen as deformation grows. The length and smoothness of the response will depend on the quality of the bond between the reinforcement and the matrix [53].

After a certain strain, the cracking pattern stabilizes, i.e., no new cracks are formed. In this Stage III, the relation between stress and strain is almost linear, where the cracks formed in the previous stage now begin to open. The slope of the curve is related to the effective modulus of elasticity of the textile, which is related to the bond behavior discussed in Section 2.6.1.

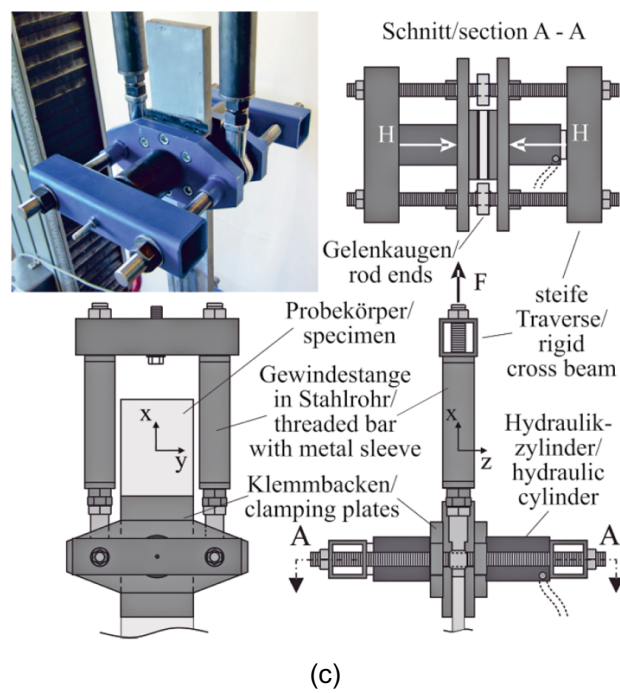
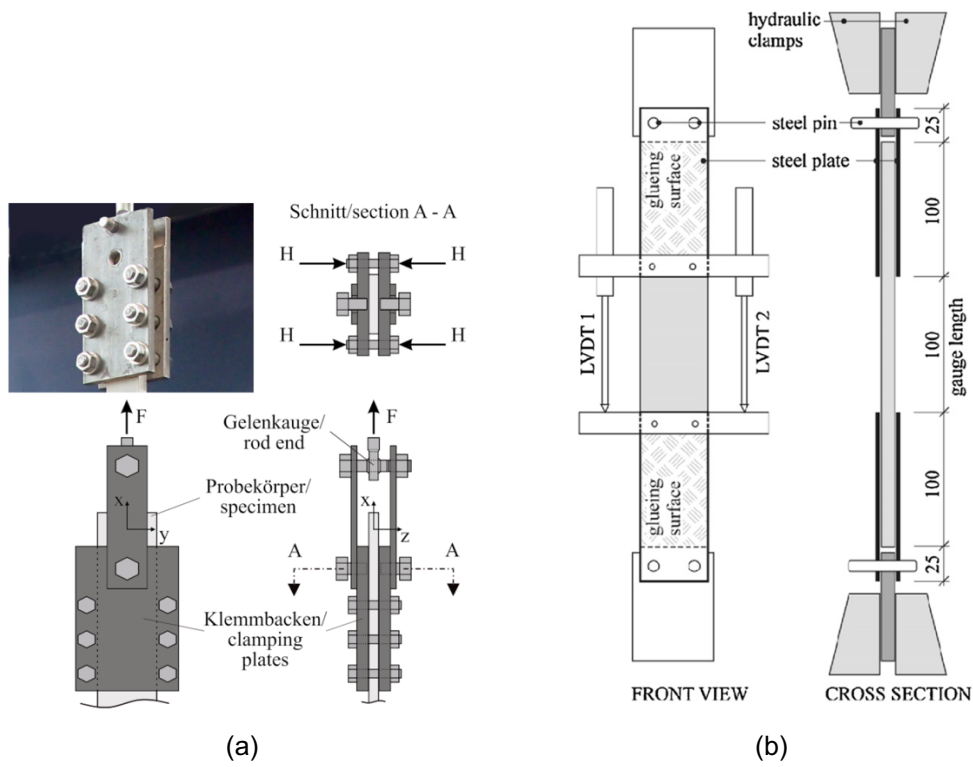


Figure 2.11 - Clevis grip method with (a) screws[113] and (b) with glued metal tabs [72]; and (c) clamp grip method [113].

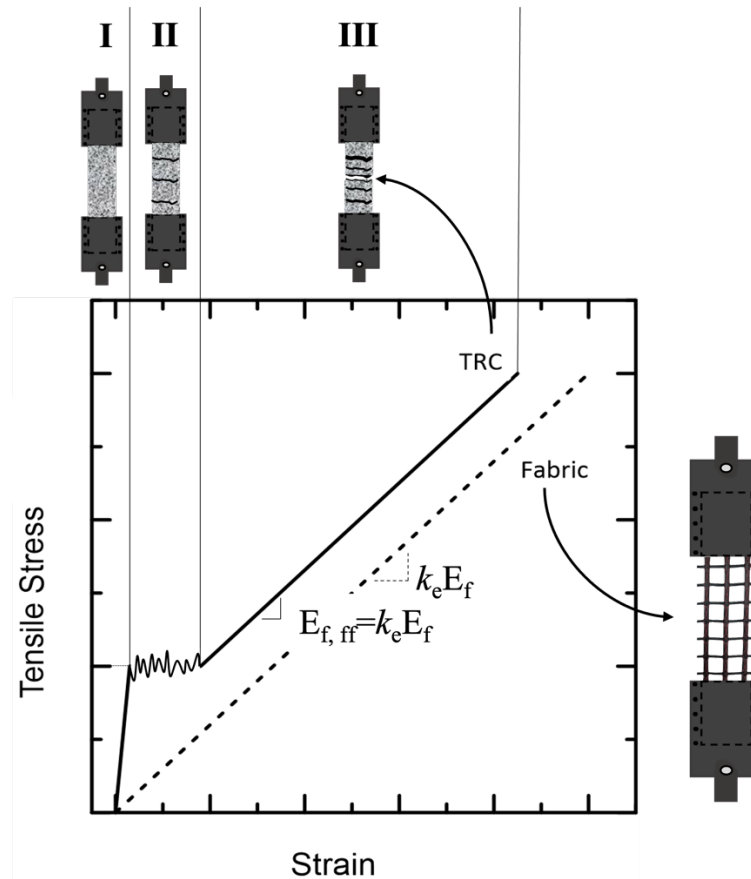


Figure 2.12 - Typical stress versus strain curve of direct tensile test for TRC and bare fabric.

To investigate the pattern of cracks in cementitious matrix composites, the Digital Image Correlation (DIC) technique has been used successfully [2,9,89,98]. According to Tekieli *et al.* [9], DIC is a full-field optical method for measuring the displacement of the surface of an object. The DIC technique consists of high-resolution photographs in a user-defined time interval and Region-of-Interest (ROI) throughout a test. The digital images can be taken for different loading stages, allowing to understand how cracks form and propagate with loading.

In a study carried out by Hegger and Voss [103], where composites reinforced with different types of fabrics were tested under direct tensile, the authors pointed out that the fabric has negligible influence on the stiffness of the uncracked composite, corresponding to Stage I. In other words, the modulus of elasticity of the fabric will only influence the stiffness after the formation of the first crack (Stage II and III), where the higher the modulus of elasticity of the fabric, the greater the stiffness of the cracked composite. Despite having less influence on the stiffness

of the composite, the volumetric fraction of reinforcement used can also influence Stages II and III of the stress-strain curves, as observed in [96].

Another parameter that influences the composite tensile response is the increase in reinforcement volume fraction by adding more layers of reinforcement for a same thickness. Many authors proved the higher tensile strengths of different TRC with the increase of the number of textile layers [3,73,96,114]. In addition, a multiple-cracking pattern with closer and thinner crack was observed [3,115,116]. However, has been also reported in literature a decrease in the effectiveness of the textile reinforcement for increasing reinforcement ratios [115,117].

2.6.3. Compression Test

Regarding the compressive characterization of the textile reinforced concrete, very little information has been reported in the literature [29–33,95]. Bochamann et al. [29] highlighted that the presence of the coated textiles may cause a disruption of the compression field, producing transverse tensile stress. Furthermore, the authors state that the textile forms a plane of weakness in the interface of fabric-matrix, reducing the material capacity against tensile splitting. Valeri et al. [33] performed uniaxial compression test in TRC plates with 60x60x30 mm (length x width x thickness). It was observed a decrease of 35% in the compressive strength when two layers of textile are added and a slight increase in the modulus of elasticity, as showed in Figure 2.13 On the other hand, Hawkins et al. [30] investigated the influence of load application eccentricity in TRC specimen with two layers of textiles with 200x15/30x15/30. The authors reported an improvement in the compressive strength compared to plain concrete, which is attributed to improved compaction of concrete when specimens are produced and to the compliance of the pin supports.

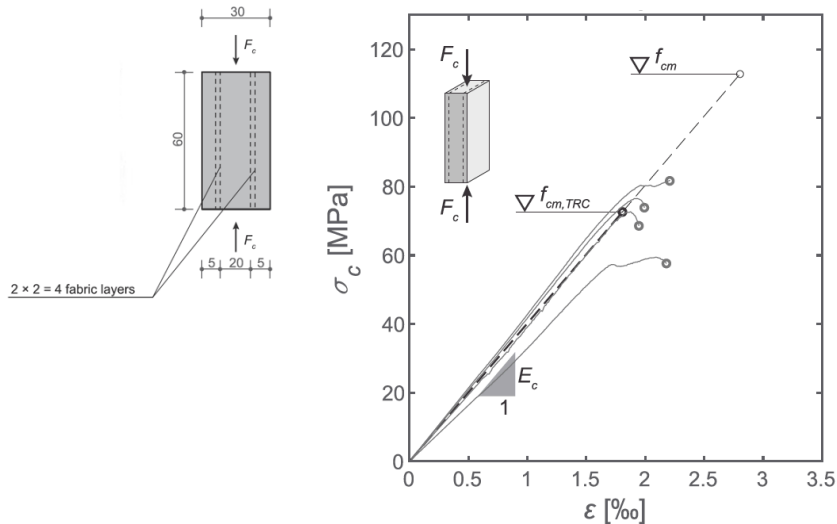


Figure 2.13 – TRC in compression [33].

Santos [31] analyzed the compression behavior of I-section columns and it was proposed the adaptation of a combined loading compression (CLC) test setup (Figure 2.14) used for fiber reinforced polymer materials. TRC specimens with dimensions of 155x15x12 mm with free gauge length of 15 mm were tested and a great improvement in strength was observed when compared to plain matrix tested in cylinder specimens. This difference is likely influenced by the different shapes and scales of specimens.

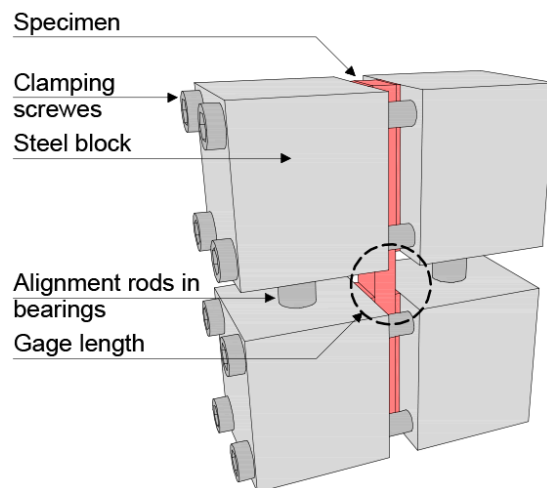


Figure 2.14 - CLC test setup [32].

2.7. TRC Beams

Tests on carbon-TRC I- and T-section beams under bending have already been reported in the literature [33,93,117–124]. The beams vary significantly in length and cross-section type.

Voss and Hegger and Voss [120,122] investigated the parameters that can influence the flexural capacity of I-section TRC beams. According to the authors, the performance was seen to be affected by binding of fabric, reinforcement ratio, fiber orientation and textile impregnation.

Kulas [123] tested I-section beams reinforced with carbon and glass fabric with length of 1000 mm, width of 110 mm and height of 120 mm. To promote beam failure on the side of the measurement field, the shear reinforcement ratio was increased on the side opposite the measurement. Thereby, the author observed beams failure by shear due to insufficient anchorage or delamination of the bottom flange due to insufficient cover at the web-to-flange connection.

Rempel *et al.* [124] investigated I-section beams in four-point bending tests of 1.3 m of length and cross-section dimensions shown in Figure 2.15. The authors used calculation methods of steel-reinforced concrete for calculating the bending moment, i.e., based on simple interaction of the strain distribution. The authors confirm that the method provided a satisfactory prediction for ultimate bending capacity.

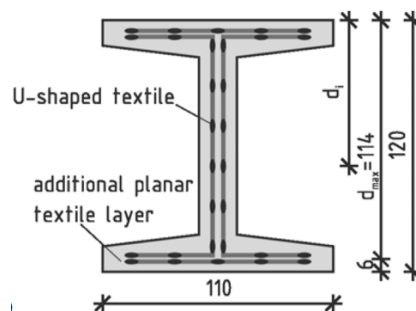


Figure 2.15 – Sectional geometry tested by [124].

Valeri *et al.* [33] investigated two I-shaped beams with a depth of 290 mm and a total length of 2900 mm, without and with concentrated flexural reinforcement made of high-strength stainless steel rebars (Figure 2.16). An enhancement of the bending and deformation capacity was observed and the authors state that adding stainless steel reinforcement is a promising solution to mitigate the deficiencies of TRC. The beams' failure occurred in shear was due to a combined crushing of the web and sliding along delamination cracks by simultaneous crushing of the web and delamination of the flanges. An Elastic-Cracked Stress Fields (ECSF) for beam modeling was proposed by authors. The combination of ECSF with efficiency factors allows suitably estimating the shear response of TRC members.

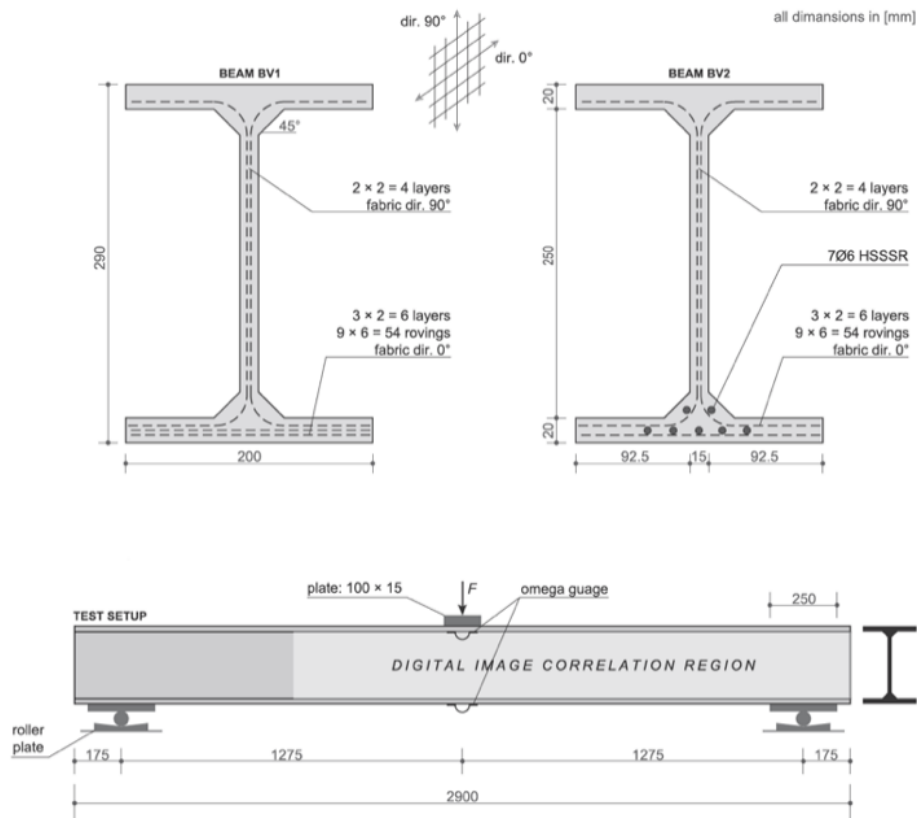


Figure 2.16 – Sectional geometry and test set-up analyzed by [33].

The I-section beams tested in bending by Bielak *et al.* [119] were fabricated using a complex carbon reinforcement layout (Figure 2.17). In tension, carbon-FRP bars were used and epoxy-impregnated biaxial carbon grid was adopted for shear reinforcement. The authors tested different configurations of reinforcement, varying the cross-section and reinforcement layout. The carbon textile as shear reinforcement was efficient for I-beams with large effective depth, providing dense crack pattern and bridging shear cracks efficiently. Geometric and physical nonlinear finite element calculation was used providing accurate results.

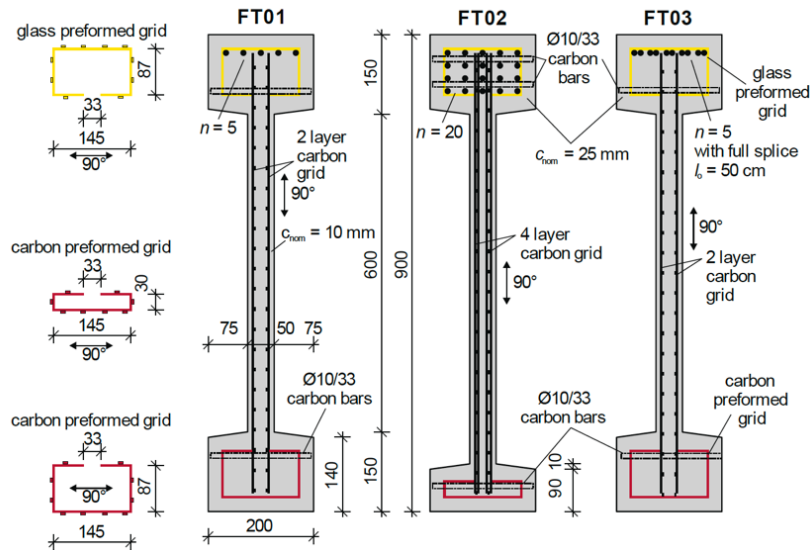


Figure 2.17 – Cross-sections and reinforcement layout of beams tested by [119].

Kromoser *et al.* [93] combined carbon-fiber-reinforced polymers (CFRP) with ultra-high-performance concrete (UHPC) to create very lightweight precast concrete members 6-meter long (Figure 2.18). CFRP rebars were used as bending reinforcement and CFRP textile as shear reinforcement. The authors highlight the need for accurate properties to be provided by the manufacturer, since the structural behavior can be influenced by the CFRP properties (cross section geometry of the roving, the mesh size, the fiber type, the weaving process, the type of impregnation). The authors performed nonlinear finite element analyses to show the potential of the chosen approach due to the close results obtained between the model and the experimental results.

Different reinforcement layout and cross-section dimensions for TRC beams in bending tests were investigated in previous works. Several design models and design strategies were also adopted. However, the influence of constitutive laws obtained for different set-up tests on design methods was not found in literature, as well as the flexural creep behavior of TRC structural elements.

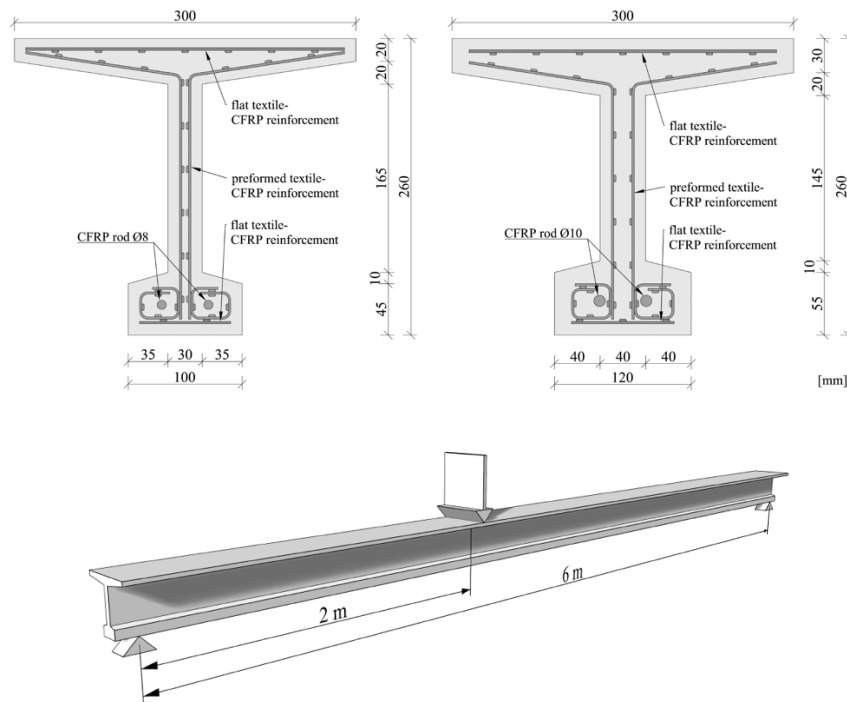


Figure 2.18 – Dimensions of the T-beams tested by [93].

2.8.Design Models

To evaluate the flexural response of TRC beams, the usual cross-sectional analysis adopted for reinforced concrete beams can be used [117,125–127] and moment-curvature relationships can be established. This design approach allows a correlation between material and section properties to other member stiffness and strength. The following hypotheses are considered: i) Bernoulli's principle of plane sections; ii) compatibility of strain between concrete and reinforcement, i.e., perfect bond between constituents; and iii) stresses can be computed from stress-strain curves for each material. The influences of bond performance and shear lag are considered through an correction factors for strength and modulus of elasticity [33].

In taking into account the factors that influence the determination of ultimate tensile force, coefficients k_1 , k_2 and $k_{0,a}$ are adopted. The coefficients k_2 and $k_{0,a}$ consider, respectively, a state of biaxial stress and the slope of the reinforcement in relation to the applied load direction -- both considered equal to 1.0 in the present study. In the case of TRC members subjected to bending, an increase in effectivity has been observed due to curvature of yarns. Thus, when calculating the flexural load capacity, an additional k_{fl} factor is considered [128]. However, these factors do not lead to a clear understanding of the tensile behavior due to the stress

distribution profile in a roving for different coating or impregnation degree (as showed in Figure 2.6). Furthermore, this analysis usually does not consider other effects such as the tension-stiffening effect –the contribution of concrete between cracks –and the effective modulus of elasticity of the composite due to shear lag effect.

In the development of model, the constitutive laws of concrete materials and textile reinforcement should be firstly known, regardless of the cross-section shape. In general, these constitutive laws are experimentally determined in concrete cylinder compression and yarn tensile tests. Thus, diagrams can be converted into idealized models for theoretical prediction. As aforementioned, to take into account the characteristics of TRC it is necessary to consider the effective modulus of elasticity. A major disadvantage of the cross-sectional analysis is that it does not account for the contribution of concrete between cracks and, ultimately, cannot provide information about crack spacing and opening. Although cracking models for TRC have been developed elsewhere [33], to the best of author's knowledge there is presently no cracking model applied to structural members. Such model must be simple and relatively accurate for acceptance among engineers.

2.9. Flexural creep behavior of TRC

TRC has been largely investigated for the past three decades and has been also used for applications in structural load-bearing members under sustained loading. Information on long-term behavior is essential during design stage to ensure appropriate member performance within lifespan.

Non-corrosive reinforcements (e.g. carbon, alkali resistant glass and basalt) increase the durability of structural concrete members [49]. TRC durability was investigated by many authors [10,58,129–132] including the effect of temperature, moisture, alkaline environment and load level on the composite. However, it is of high interest the mechanisms that affect the service life of a structure, i.e. the excessive deflections, crack formation and opening, to provide data about long-term behavior which includes the time-dependent parameters such as creep and fatigue. The fatigue behavior has been analyzed by some authors [84,133,134], but less effort has been devoted to creep so far.

Creep is the main factor to be considered in long-term analyzes and there is insufficient data to provide an adequate framework for long-term assessment of TRC behavior [135]. To describe this phenomenon, it is necessary to understand the sum of the behavior of the cementitious matrix as well as the filaments, the fiber-matrix interface and the filament-filament interface on sustained load [34]. Other aspects that can influence creep resistance such as load level, chemical compositions of the fibers and coatings and environment conditions are important to consider [136]. All factors act combinedly and influence the creep rupture capacity.

The creep behavior results typically on time-dependent curves which can be described as structure deformation under constant load over a certain period. According ACI 440 3R-12 [137], the creep rupture capacity is the stress at which failure occurs during a creep test. Generally, the creep behavior analysis is based on the deflection-time curve and strain-time curves [37]. These curves show three typical stages. The first one is denominated primary creep which corresponds to a decrease in strain rate, attributed to hardening effects. At secondary creep, the strain rate remains constant and eventually reaches a minimum. Finally, the tertiary creep is characterized by an exponential rise in the strain rate until failure; however, this final stage may not occur during testing.

It is possible to estimate the deformation due to creep and concrete cracking at serviceability state through the introduction of a creep coefficient which reduces the Young's modulus of the concrete [49]. As previously described, the analysis of the TRC creep behavior must take into account other properties and there is a lack of information on those mechanisms so far. Tensile creep tests were performed by [34,37,138] on TRC specimens with AR-glass and [136] investigated the creep behavior of the AR-glass filaments on uniaxial tension tests.

Freitag et al. [34] carried out tests in pre-cracked plates on climate chamber at 20°C and relative humidity of 65%. The specimens were manually loaded at load levels between 30 and 80 % of the reference strength (obtained in short-term tests). It was possible to observe a slow strain rate during the primary and secondary strain rise phases. The deformations increased and time-to-failure decreased with increasing load levels.

Uniaxial tension tests were performed by Ortlepp and Jesse [37] at three different load paths. Long-term creep tests were loaded with manual control up to 80% of

reference strength and were conducted for six months. None of the specimens failed at a load level below 60 %. The results clearly show the common three creep stages. They concluded that lifetime decreases under sustained load with an increasing load level. It was also observed that the filament failure and bond failure interact during loading.

In order to develop a mechanical model to predict the long-term behavior of textile reinforced concrete, Seidel et al. [136] performed tensile tests on AR-glass 26-long filaments under constant tensile loads of 80 to 90% of failure load. It was observed a significant increase in elongation on the first day of test, yet it became smaller overtime. It was observed that the initial deformation could be associated with a rearranging of the disordered filaments. This post load application effect increases in relation to the load level and the stretched yarn initial length.

Spelter et al. [138] proposed a testing concept to investigate the long-term durability of the AR-glass TRC under constant load. The tests were conducted at three different temperatures (20, 40 and 60°C) and load levels between 70 and 97%. For the purpose of deriving a time to failure curve and determining a reduction factor for the tensile strength of the carbon textile reinforcement, the testing concept described above [138] was used by [35]. The specimens were exposed to water, temperature and pH solution and pre-cracked up to the final crack pattern. When analyzing the residual capacity, no strength loss was observed for this specimen. An increase of strength was found after more than 5000 h of testing in comparison to the short-term tests. The higher mean ultimate stress was attributed to the alignment of filaments.

It is important to highlight that the results obtained by [34,35,37] cannot be transferred to other material combinations. Further research is needed to be able to quantify the effects of sustained loads in TRC composites with different types of textiles and loading, as well as to understand the performance of structural members.

2.10. References

- [1] Donnini J, Corinaldesi V. Mechanical characterization of different FRCM systems for structural reinforcement. *Constr Build Mater* 2017;145:565–75. <https://doi.org/10.1016/j.conbuildmat.2017.04.051>.

- [2] De Santis S, Hadad HA, De Caso y Basalo F, de Felice G, Nanni A. Acceptance Criteria for Tensile Characterization of Fabric-Reinforced Cementitious Matrix Systems for Concrete and Masonry Repair. *J Compos Constr* 2018;22:04018048. [https://doi.org/10.1061/\(asce\)cc.1943-5614.0000886](https://doi.org/10.1061/(asce)cc.1943-5614.0000886).
- [3] Zhou F, Liu H, Du Y, Liu L, Zhu D, Pan W. Uniaxial tensile behavior of carbon textile reinforced mortar. *Materials (Basel)* 2019;12. <https://doi.org/10.3390/ma12030374>.
- [4] Contamine R, Si Larbi A, Hamelin P. Contribution to direct tensile testing of textile reinforced concrete (TRC) composites. *Mater Sci Eng A* 2011;528:8589–98. <https://doi.org/10.1016/j.msea.2011.08.009>.
- [5] Mesticou Z, Bui L, Junes A, Si Larbi A. Experimental investigation of tensile fatigue behaviour of Textile-Reinforced Concrete (TRC): Effect of fatigue load and strain rate. *Compos Struct* 2017;160:1136–46. <https://doi.org/10.1016/j.compstruct.2016.11.009>.
- [6] Valeri P, Fernández Ruiz M, Muttoni A. Tensile response of textile reinforced concrete. *Constr Build Mater* 2020;258:119517. <https://doi.org/10.1016/j.conbuildmat.2020.119517>.
- [7] Arboleda D, Carozzi FG, Nanni A, Poggi C. Testing Procedures for the Uniaxial Tensile Characterization of Fabric-Reinforced Cementitious Matrix Composites. *J Compos Constr* 2016;20:04015063. [https://doi.org/10.1061/\(asce\)cc.1943-5614.0000626](https://doi.org/10.1061/(asce)cc.1943-5614.0000626).
- [8] Rampini MC, Zani G, Colombo M, di Prisco M. Mechanical behaviour of TRC composites: Experimental and analytical approaches. *Appl Sci* 2019;9. <https://doi.org/10.3390/app9071492>.
- [9] Tekieli M, De Santis S, de Felice G, Kwiecień A, Roscini F. Application of Digital Image Correlation to composite reinforcements testing. *Compos Struct* 2017;160:670–88. <https://doi.org/10.1016/j.compstruct.2016.10.096>.
- [10] Kong K, Mesticou Z, Michel M, Si Larbi A, Junes A. Comparative characterization of the durability behaviour of textile-reinforced concrete (TRC) under tension and bending. *Compos Struct* 2017;179:107–23. <https://doi.org/10.1016/j.compstruct.2017.07.030>.
- [11] D’Ambrisi A, Focacci F. Flexural Strengthening of RC Beams with Cement-Based Composites. *J Compos Constr* 2011;15:707–20.

- [https://doi.org/10.1061/\(asce\)cc.1943-5614.0000218](https://doi.org/10.1061/(asce)cc.1943-5614.0000218).
- [12] Williams Portal N, Nyholm Thrane L, Lundgren K. Flexural behaviour of textile reinforced concrete composites: experimental and numerical evaluation. *Mater Struct Constr* 2017;50:1–14. <https://doi.org/10.1617/s11527-016-0882-9>.
- [13] Teixeira FP, de Andrade Silva F. On the use of natural curauá reinforced cement based composites for structural applications. *Cem Concr Compos* 2020;114. <https://doi.org/10.1016/j.cemconcomp.2020.103775>.
- [14] Halvaei M, Latifi M, Jamshidi M. Study of the microstructure and flexural behavior of cementitious composites reinforced by surface modified carbon textiles. *Constr Build Mater* 2018;158:243–56. <https://doi.org/10.1016/j.conbuildmat.2017.10.044>.
- [15] Silva RM de C. Comportamento mecânico de concretos têxteis reforçados com tecido de carbono : aspectos materiais e estruturais 2018:140.
- [16] Krüger M, Reinhardt H-W, Fichtlscherer M. Bond behaviour of textile reinforcement in reinforced and prestressed concrete. *Otto-Graf-Journal* 2001;12:33–50.
- [17] Banholzer B, Brockmann T, Brameshuber W. Material and bonding characteristics for dimensioning and modelling of textile reinforced concrete (TRC) elements. *Mater Struct Constr* 2006;39:749–63. <https://doi.org/10.1617/s11527-006-9140-x>.
- [18] Peled A, Zaguri E, Marom G. Bonding characteristics of multifilament polymer yarns and cement matrices. *Compos Part A Appl Sci Manuf* 2008;39:930–9. <https://doi.org/10.1016/j.compositesa.2008.03.012>.
- [19] Katz A, Li VC. Bond properties of micro-fibers in cementitious matrix. *Mater Res Soc Symp - Proc* 1995;370:529–37. <https://doi.org/10.1557/proc-370-529>.
- [20] Peled A, Sueki S, Mobasher B. Bonding in fabric-cement systems: Effects of fabrication methods. *Cem Concr Res* 2006;36:1661–71. <https://doi.org/10.1016/j.cemconres.2006.05.009>.
- [21] Sueki S, Soranakom C, Mobasher B, Peled A. Pullout-Slip Response of Fabrics Embedded in a Cement Paste Matrix. *J Mater Civ Eng* 2007;19:718–27. [https://doi.org/10.1061/\(asce\)0899-1561\(2007\)19:9\(718\)](https://doi.org/10.1061/(asce)0899-1561(2007)19:9(718)).
- [22] Williams Portal N, Fernandez Perez I, Nyholm Thrane L, Lundgren K. Pull-

- out of textile reinforcement in concrete. *Constr Build Mater* 2014;71:63–71. <https://doi.org/10.1016/j.conbuildmat.2014.08.014>.
- [23] Xu S, Krüger M, Reinhardt H-W, Ožbolt J. Bond Characteristics of Carbon, Alkali Resistant Glass, and Aramid Textiles in Mortar. *J Mater Civ Eng* 2004;16:356–64. [https://doi.org/10.1061/\(asce\)0899-1561\(2004\)16:4\(356\)](https://doi.org/10.1061/(asce)0899-1561(2004)16:4(356)).
- [24] Li Y, Bielak J, Hegger J, Chudoba R. An incremental inverse analysis procedure for identification of bond-slip laws in composites applied to textile reinforced concrete. *Compos Part B Eng* 2018;137:111–22. <https://doi.org/10.1016/j.compositesb.2017.11.014>.
- [25] Cheng S, Ji J, Meng M. Interfacial response of fibre-to-matrix in textile reinforced concrete between two cracks: Analytical solution. *Compos Struct* 2020;245:112380. <https://doi.org/10.1016/j.compstruct.2020.112380>.
- [26] Dvorkin D, Poursaeed A, Peled A, Weiss WJ. Influence of bundle coating on the tensile behavior, bonding, cracking and fluid transport of fabric cement-based composites. *Cem Concr Compos* 2013;42:9–19. <https://doi.org/10.1016/j.cemconcomp.2013.05.005>.
- [27] Calabrese AS, D’Antino T, Colombi P, Poggi C, Carloni C. Influence of the test set-up on the bond behavior of FRCM composites. *Am Concr Institute, ACI Spec Publ* 2021;SP-345:185–95.
- [28] Bochmann J, Jesse F, Curbach M. Experimental Determination of the Stress-Strain Relation of Fine Grained Concrete Under Compression 2017:11.
- [29] Bochmann J, Curbach M, Jesse F. Influence of artificial discontinuities in concrete under compression load—A literature review. *Struct Concr* 2018;19:559–67. <https://doi.org/10.1002/suco.201700041>.
- [30] Hawkins W, Orr J, Ibell T, Shepherd P. An Analytical Failure Envelope for the Design of Textile Reinforced Concrete Shells. *Structures* 2018;15:56–65. <https://doi.org/10.1016/j.istruc.2018.06.001>.
- [31] Santos FCA dos. Behavior of Textile Reinforced Concrete (TRC) Slender Columns Subject to Compression. Pontificia Universidade Católica do Rio de Janeiro (PUC-Rio), 2018.
- [32] Teixeira, F P. Mechanical Behavior of Natural Fiber Cement Based Composites for Structural Applications, Pontificia Universidade Católica do Rio de Janeiro (PUC-Rio), 2020.
- [33] Valeri P, Ruiz MF, Muttoni A. Modelling of Textile Reinforced Concrete in

- bending and shear with Elastic-Cracked Stress Fields. *Eng Struct* 2020;215:110664. <https://doi.org/10.1016/j.engstruct.2020.110664>.
- [34] Freitag S, Beer M, Jesse F, Weiland S. Experimental investigation and prediction of long-term behavior of textile reinforced concrete for strengthening. In: Hegger J, Brameshuber W, Will N, editors. ICTRC'2006 - 1st Int. RILEM Conf. Text. Reinf. Concr., RILEM Publications SARL; 2006, p. 121–30. <https://doi.org/10.1617/2351580087.012>.
- [35] Spelter A, Bergmann S, Bielak J, Hegger J. Long-term durability of carbon-reinforced concrete: An overview and experimental investigations. *Appl Sci* 2019;9. <https://doi.org/10.3390/app9081651>.
- [36] Bielak J, Spelter A, Will N, Claßen M. Verankerungsverhalten textiler Bewehrungen in dünnen Betonbauteilen. *Beton- Und Stahlbetonbau* 2018;113:515–24. <https://doi.org/10.1002/best.201800013>.
- [37] Ortlepp S, Jesse F. Experimental investigation of static fatigue strength of textile reinforced concrete. ICTRC'2006-1st Int. RILEM Conf. Text. Reinf. Concr., RILEM Publications SARL; 2006, p. 131–40.
- [38] Ali AH, Mohamed HM, Benmokrane B, ElSafty A. Effect of applied sustained load and severe environments on durability performance of carbon-fiber composite cables. *J Compos Mater* 2019;53:677–92. <https://doi.org/10.1177/0021998318789742>.
- [39] Naaman AE. Evolution in Ferrocement and Thin Reinforced Cementitious Composites. *Arab J Sci Eng* 2012;37:421–41. <https://doi.org/10.1007/s13369-012-0187-4>.
- [40] Kaish ABMA, Jamil M, Raman SN, Zain MFM, Nahar L. Ferrocement composites for strengthening of concrete columns: A review. *Constr Build Mater* 2018;160:326–40. <https://doi.org/10.1016/j.conbuildmat.2017.11.054>.
- [41] ACI 549R-97. 549R-2 Aci Committee Report. *ACI Comm Rep* 1997:1–26.
- [42] Rempel S, Kulas C, Will N, Bielak J. Extremely light and slender precast pedestrian-bridge made out of textile-reinforced concrete (TRC). *High Tech Concr. Where Technol. Eng. Meet*, vol. 1, Springer; 2018, p. 2530–7. <https://doi.org/10.1007/978-3-319-59471-2>.
- [43] Scholzen A, Chudoba R, Hegger J. Thin-walled shell structures made of textile-reinforced concrete: Part I: Structural design and construction. *Struct Concr* 2015;16:106–14. <https://doi.org/10.1002/suco.201300071>.

- [44] Scholzen A, Chudoba R, Hegger J. Thin-walled shell structures made of textile-reinforced concrete: Part II: Experimental characterization, ultimate limit state assessment and numerical simulation. *Struct Concr* 2015;16:115–24. <https://doi.org/10.1002/suco.201400046>.
- [45] Schumann A, Michler H, Schladitz F, Curbach M. Parking slabs made of carbon reinforced concrete. *Struct Concr* 2018;19:647–55. <https://doi.org/10.1002/suco.201700147>.
- [46] Hegger J, Kulas C, Schneider HN, Brameshuber W, Hinzen M, Raupach M, et al. TRC Pedestrian Bridge-Design, Load-bearing Behavior and Production Processes of a Slender and Light-weight Construction. *Int RILEM Conf Mater Sci* 2010;I:353–64.
- [47] Sharei E, Scholzen A, Hegger J, Chudoba R. Structural behavior of a lightweight, textile-reinforced concrete barrel vault shell. *Compos Struct* 2017;171:505–14. <https://doi.org/10.1016/j.compstruct.2017.03.069>.
- [48] Helbig T, Unterer K, Kulas C, Rempel S, Hegger J. Fuß- und Radwegbrücke aus Carbonbeton in Albstadt-Ebingen: Die weltweit erste ausschließlich carbonfaserbewehrte Betonbrücke. *Beton- Und Stahlbetonbau* 2016;111:676–85. <https://doi.org/10.1002/best.201600058>.
- [49] Hegger J, Curbach M, Stark A, Wilhelm S, Farwig K. Innovative design concepts: Application of textile reinforced concrete to shell structures. *Struct Concr* 2018;19:637–46. <https://doi.org/10.1002/suco.201700157>.
- [50] Curbach M, Jesse F. Eigenschaften und Anwendung von Textilbeton. *Beton- Und Stahlbetonbau* 2009;104:9–16. <https://doi.org/10.1002/best.200800653>.
- [51] C3project. <http://www.bauen-neu-denken.de>. Accessed February 3 2022. C3 project n.d.
- [52] Henn. No Title 2020. <https://www.henn.com/en/project/c3-cube-tu-dresden>.
- [53] Brameshuber W. Report 36: textile reinforced concrete-state-of-the-art report of RILEM TC 201-TRC. Rilem publications; 2006.
- [54] Papanicolaou CG. *Textile Fibre Composites in Civil Engineering*. 2016.
- [55] Mobasher B, Peled A, Pahilajani J. Pultrusion of fabric reinforced high flyash blended cement composites. *RILEM Tech Meet BEFIB* 2004:1473–82.
- [56] Dvorkin D, Peled A. Effect of reinforcement with carbon fabrics impregnated with nanoparticles on the tensile behavior of cement-based

- composites. *Cem Concr Res* 2016;85:28–38.
<https://doi.org/10.1016/j.cemconres.2016.03.008>.
- [57] Silva FDA, Butler M, Hempel S, Toledo Filho RD, Mechtcherine V. Effects of elevated temperatures on the interface properties of carbon textile-reinforced concrete. *Cem Concr Compos* 2014;48:26–34.
<https://doi.org/10.1016/j.cemconcomp.2014.01.007>.
- [58] Butler M, Mechtcherine V, Hempel S. Experimental investigations on the durability of fibre–matrix interfaces in textile-reinforced concrete. *Cem Concr Compos* 2009;31:221–31.
<https://doi.org/10.1016/j.cemconcomp.2009.02.005>.
- [59] Bentur A, Mindess S. *Fiber Reinforced Cementitious Composites*. CRC Press; 2006.
- [60] Butler M. The Influence of short glass fibres on the working capacity of textile reinforced concrete 2006:45–54.
<https://doi.org/10.1617/2351580087.005>.
- [61] Gong T. On the synergetic action between strain-hardening cement based composites (SHCC) and carbon textile reinforcement under tensile loading 2019. <https://doi.org/10.21012/fc10.235471>.
- [62] ACI Committee 116 "Cement and Concrete Terminology (ACI116-R-00)", "American Concrete Institute, Farmington Hills, Mich., 2000, 73 pp. ACI Comm Rep 2000:73.
- [63] Mobasher B. *Mechanics of fiber and textile reinforced cement composites*. 2011. <https://doi.org/10.1201/b11181>.
- [64] Hinzen M, Brameshuber W. Improvement of Serviceability and Strength of Textile Reinforced Concrete by using Short Fibres. 4th Colloq Text Reinf Struct 2009:261–72.
- [65] Löfgren I. *Fibre-reinforced concrete for industrial construction - A fracture mechanics approach to material testing and structural analysis*. 2005.
- [66] Bayramov F, Taşdemir C, Taşdemir MA. Optimisation of steel fibre reinforced concretes by means of statistical response surface method. *Cem Concr Compos* 2004;26:665–75. [https://doi.org/10.1016/S0958-9465\(03\)00161-6](https://doi.org/10.1016/S0958-9465(03)00161-6).
- [67] Chanvillard G, Banthia N, Aitcin PC. Normalized load-deflection curves for fibre reinforced concrete under flexure. *Cem Concr Compos* 1990;12:41–5.

- [https://doi.org/10.1016/0958-9465\(90\)90034-U](https://doi.org/10.1016/0958-9465(90)90034-U).
- [68] Peled A, Bentur A, Yankelevsky D. Effects of woven fabric geometry on the bonding performance of cementitious composites: mechanical performance. *Adv Cem Based Mater* 1998;7:20–7. [https://doi.org/10.1016/S1065-7355\(97\)00012-6](https://doi.org/10.1016/S1065-7355(97)00012-6).
- [69] Peled A, Bentur A. Fabric structure and its reinforcing efficiency in textile reinforced cement composites. *Compos Part A Appl Sci Manuf* 2003;34:107–18. [https://doi.org/10.1016/S1359-835X\(03\)00003-4](https://doi.org/10.1016/S1359-835X(03)00003-4).
- [70] Bielak J, Adam V, Hegger J, Classen M. Shear capacity of textile-reinforced concrete slabs without shear reinforcement. *Appl Sci* 2019;9. <https://doi.org/10.3390/app9071382>.
- [71] Zhu D, Gencoglu M, Mobasher B. Low velocity flexural impact behavior of AR glass fabric reinforced cement composites. *Cem Concr Compos* 2009;31:379–87. <https://doi.org/10.1016/j.cemconcomp.2009.04.011>.
- [72] Silva F de A, Butler M, Mechtcherine V, Zhu D, Mobasher B. Strain rate effect on the tensile behaviour of textile-reinforced concrete under static and dynamic loading. *Mater Sci Eng A* 2011;528:1727–34. <https://doi.org/10.1016/j.msea.2010.11.014>.
- [73] Du Y, Zhang M, Zhou F, Zhu D. Experimental study on basalt textile reinforced concrete under uniaxial tensile loading. *Constr Build Mater* 2017;138:88–100. <https://doi.org/10.1016/j.conbuildmat.2017.01.083>.
- [74] Du Y, Zhang X, Zhou F, Zhu D, Zhang M, Pan W. Flexural behavior of basalt textile-reinforced concrete. *Constr Build Mater* 2018;183:7–21. <https://doi.org/10.1016/j.conbuildmat.2018.06.165>.
- [75] Focacci F, Antino TD, Carloni C. PBO-FRCM COMPOSITES 2019:15–9.
- [76] Sneed LH, D’Antino T, Carloni C. Investigation of bond behavior of polyparaphenylene benzobisoxazole fiber-reinforced cementitious matrix composite-concrete interface. *ACI Mater J* 2014;111:569–80. <https://doi.org/10.14359/51686604>.
- [77] Ombres L. Analysis of the bond between Fabric Reinforced Cementitious Mortar (FRCM) strengthening systems and concrete. *Compos Part B Eng* 2015;69:418–26. <https://doi.org/10.1016/j.compositesb.2014.10.027>.
- [78] Pereira MV, Fujiyama R, Darwish F, Alves GT. On the strengthening of cement mortar by natural fibers. *Mater Res* 2015;18:177–83.

- <https://doi.org/10.1590/1516-1439.305314>.
- [79] Silva F de A, Zhu D, Mobasher B, Soranakom C, Toledo Filho RD. High speed tensile behavior of sisal fiber cement composites. *Mater Sci Eng A* 2010;527:544–52. <https://doi.org/10.1016/j.msea.2009.08.013>.
- [80] Alan Strauss Rambo D, Umbinger de Oliveira C, Pícolo Salvador R, Dias Toledo Filho R, da Fonseca Martins Gomes O, de Andrade Silva F, et al. Sisal textile reinforced concrete: Improving tensile strength and bonding through peeling and nano-silica treatment. *Constr Build Mater* 2021;301. <https://doi.org/10.1016/j.conbuildmat.2021.124300>.
- [81] Perry G, Dittel G, Gries T, Goldfeld Y. Mutual Effect of Textile Binding and Coating on the Structural Performance of TRC Beams. *J Mater Civ Eng* 2020;32:04020232. [https://doi.org/10.1061/\(asce\)mt.1943-5533.0003331](https://doi.org/10.1061/(asce)mt.1943-5533.0003331).
- [82] Bielak J, Li Y, Hegger J, Chudoba R. Characterization Procedure for Bond, Anchorage and Strain-Hardening Behavior of Textile-Reinforced Cementitious Composites. *Proceedings* 2018;2:395. <https://doi.org/10.3390/icem18-05224>.
- [83] Silva RMC, Silva FA. On the tensile behavior and interface characteristics of carbon textile reinforced concrete. In: Glinicki MA, Józwiak-Niedźwiedzka D, Leung CKY, Olek J, editors. *Brittle Matrix Compos. 12 - Proc. 12th Int. Symp. Brittle Matrix Compos. BMC 2019, Warsaw: 2019*, p. 88–96.
- [84] Wagner J, Curbach M. Bond fatigue of TRC with epoxy impregnated carbon textiles. *Appl Sci* 2019;9. <https://doi.org/10.3390/app9101980>.
- [85] Yin SP, Xu SL, Wang F. Investigation on the flexural behavior of concrete members reinforced with epoxy resin-impregnated textiles. *Mater Struct Constr* 2015;48:153–66. <https://doi.org/10.1617/s11527-013-0174-6>.
- [86] Raupach M. Epoxy-impregnated textiles in concrete – Load bearing capacity and durability. In: Hegger J, Brameshuber W, Will N, editors. *ICTRC’2006 - 1st Int. RILEM Conf. Text. Reinf. Concr., Aachen: RILEM Publications SARL; 2006*, p. 77–88. <https://doi.org/10.1617/2351580087.008>.
- [87] Schleser M, Walk-Lauffner B, Raupach M, Dilthey U. Application of Polymers to Textile-Reinforced Concrete. *J Mater Civ Eng* 2006;18:670–6. [https://doi.org/10.1061/\(asce\)0899-1561\(2006\)18:5\(670\)](https://doi.org/10.1061/(asce)0899-1561(2006)18:5(670)).
- [88] Gong T, Ahmed AH, Curosu I, Mechtcherine V. Tensile behavior of hybrid

- fiber reinforced composites made of strain-hardening cement-based composites (SHCC) and carbon textile. *Constr Build Mater* 2020;262:120913. <https://doi.org/10.1016/j.conbuildmat.2020.120913>.
- [89] Gong T, Heravi AA, Alsous G, Curosu I, Mechtcherine V. The impact-tensile behavior of cementitious composites reinforced with carbon textile and short polymer fibers. *Appl Sci* 2019;9. <https://doi.org/10.3390/app9194048>.
- [90] Li B, Xiong H, Jiang J, Dou X. Tensile behavior of basalt textile grid reinforced Engineering Cementitious Composite. *Compos Part B Eng* 2019;156:185–200. <https://doi.org/10.1016/j.compositesb.2018.08.059>.
- [91] Zhu D, Peled A, Mobasher B. Dynamic tensile testing of fabric-cement composites. *Constr Build Mater* 2011;25:385–95. <https://doi.org/10.1016/j.conbuildmat.2010.06.014>.
- [92] Briggs A. Carbon fibre-reinforced cement. *J Mater Sci* 1977;12:384–404. <https://doi.org/10.1007/BF00566282>.
- [93] Kromoser B, Preinstorfer P, Kollegger J. Building lightweight structures with carbon-fiber-reinforced polymer-reinforced ultra-high-performance concrete: Research approach, construction materials, and conceptual design of three building components. *Struct Concr* 2019;20:730–44. <https://doi.org/10.1002/suco.201700225>.
- [94] de Felice G, D'Antino T, De Santis S, Meriggi P, Roscini F. Lessons Learned on the Tensile and Bond Behavior of Fabric Reinforced Cementitious Matrix (FRCM) Composites. *Front Built Environ* 2020;6:1–15. <https://doi.org/10.3389/fbuil.2020.00005>.
- [95] Bochmann J, Curbach M, Jesse F. Carbonbeton unter einaxialer Druckbeanspruchung: Ergebnisse systematischer experimenteller Untersuchungen. *Beton- Und Stahlbetonbau* 2017;112:293–302. <https://doi.org/10.1002/best.201700006>.
- [96] Mansur de Castro Silva R, de Andrade Silva F. Carbon textile reinforced concrete: materials and structural analysis. *Mater Struct Constr* 2020;53. <https://doi.org/10.1617/s11527-020-1448-4>.
- [97] Barhum R, Mechtcherine V. Effect of short, dispersed glass and carbon fibres on the behaviour of textile-reinforced concrete under tensile loading. *Eng Fract Mech* 2012;92:56–71.

- <https://doi.org/10.1016/j.engfracmech.2012.06.001>.
- [98] Yao Y, Silva FA, Butler M, Mechtcherine V, Mobasher B. Tension stiffening in textile-reinforced concrete under high speed tensile loads. *Cem Concr Compos* 2015;64:49–61. <https://doi.org/10.1016/j.cemconcomp.2015.07.009>.
- [99] Zamir M, Sripada R, Peled A. Hybrid fillers in carbon-fabric-reinforced cement-based composites. *Cem Concr Compos* 2019;98:113–24. <https://doi.org/10.1016/j.cemconcomp.2019.02.005>.
- [100] Zhu D, Liu S, Yao Y, Li G, Du Y, Shi C. Effects of short fiber and pre-tension on the tensile behavior of basalt textile reinforced concrete. *Cem Concr Compos* 2019;96:33–45. <https://doi.org/10.1016/j.cemconcomp.2018.11.015>.
- [101] Hinzen M, Brameshuber W. Influence of short fibres on strength, ductility and crack development of textile reinforced concrete. *Proc. Fifth Int. RILEM Work. High Perform. Fiber Reinf. Cem. Compos., RILEM Proceedings PRO; 2007*, p. 105–12.
- [102] Gong T, Hamza AA, Curosu I, Mechtcherine V. On the synergetic action between strain-hardening cement based composites (SHCC) and carbon textile reinforcement under tensile loading. In: Pijaudier-Cabot G, Grassl P, La Borderie C, editors. *10th Int. Conf. Fract. Mech. Concr. Concr. Struct.*, 2019. <https://doi.org/10.21012/fc10.235471>.
- [103] Hegger J, Voss S. Investigations on the bearing behaviour and application potential of textile reinforced concrete. *Eng Struct* 2008;30:2050–6. <https://doi.org/10.1016/j.engstruct.2008.01.006>.
- [104] Yao Y, Bonakdar A, Faber J, Gries T, Mobasher B. Distributed cracking mechanisms in textile-reinforced concrete under high speed tensile tests. *Mater Struct Constr* 2016;49:2781–98. <https://doi.org/10.1617/s11527-015-0685-4>.
- [105] Nguyen DL, Ryu GS, Koh KT, Kim DJ. Size and geometry dependent tensile behavior of ultra-high-performance fiber-reinforced concrete. *Compos Part B Eng* 2014;58:279–92. <https://doi.org/10.1016/j.compositesb.2013.10.072>.
- [106] Preinstorfer P, Kollegger J. New insights into the splitting failure of textile-reinforced concrete. *Compos Struct* 2020;243:112203. <https://doi.org/10.1016/j.compstruct.2020.112203>.

- [107] Goliath KB, Carlos D, Cardoso T, Silva FDA. Flexural Creep Behavior Of I-Sections Carbon-TRC Beams. FERRO 13, n1–9, 2021.
- [108] Morales Cruz C, Raupach M. Influence of the surface modification by sanding of carbon textile reinforcements on the bond and load-bearing behavior of textile reinforced concrete. MATEC Web Conf 2019;289. <https://doi.org/10.1051/mateconf/201928904006>.
- [109] Banholzer B, Brameshuber W, Jung W. Analytical evaluation of pull-out tests-The inverse problem. Cem Concr Compos 2006;28:564–71. <https://doi.org/10.1016/j.cemconcomp.2006.02.015>.
- [110] Krüger M. Vorgespannter Textilbewehrter Beton 2004.
- [111] D’Antino T, Papanicolaou C. Mechanical characterization of textile reinforced inorganic-matrix composites. Compos Part B Eng 2017;127:78–91. <https://doi.org/10.1016/j.compositesb.2017.02.034>.
- [112] AC434. Acceptance criteria for concrete and masonry strengthening using fabric-reinforced cementitious matrix (FRCM) composite Systems. ICC Eval Serv Whittier, CA 2018.
- [113] Schütze E, Lorenz E, Curbach M. Test methods for textile reinforced concrete. 11th Int Symp Ferroцем Text Reinf Concr 3rd ICTRC 2015:307–18.
- [114] Colombo IG, Magri A, Zani G, Colombo M, Di Prisco M. Erratum: Textile reinforced concrete: Experimental investigation on design parameters (Materials and Structures (2013)). Mater Struct Constr 2013;46:1953–71. <https://doi.org/10.1617/s11527-013-0023-7>.
- [115] Deng M, Dong Z, Zhang C. Experimental investigation on tensile behavior of carbon textile reinforced mortar (TRM) added with short polyvinyl alcohol (PVA) fibers. Constr Build Mater 2020;235:117801. <https://doi.org/10.1016/j.conbuildmat.2019.117801>.
- [116] Larrinaga P, Chastre C, Biscaia HC, San-José JT. Experimental and numerical modeling of basalt textile reinforced mortar behavior under uniaxial tensile stress. Mater Des 2014;55:66–74. <https://doi.org/10.1016/j.matdes.2013.09.050>.
- [117] Hegger J, Will N, Bruckermann O, Voss S. Load-bearing behaviour and simulation of textile reinforced concrete. Mater Struct Constr 2006;39:765–76. <https://doi.org/10.1617/s11527-005-9039-y>.

- [118] Schmidt M, Bielak J, Hegger J. Large-Scale Tests on the Structural and Deformation Behaviour of I-Beams with Carbon Reinforcement. *Proc Fiber Reinf Polym Reinf Concr Struct* 14 2019.
- [119] Bielak J, Schmidt M, Hegger J, Jesse F. Structural behavior of large-scale I-beams with combined textile and CFRP reinforcement. *Appl Sci* 2020;10. <https://doi.org/10.3390/app10134625>.
- [120] Hegger J, Zell DM, Voss DS. Dimensioning of TRC structures. *Grc* 2008 2008.
- [121] Hegger J, Will N, Schneider M. Textilbeton: Tragverhalten-Bemessung-Sicherheit. *6th Colloq Text Reinf Struct* 2011:269–84.
- [122] Voss S. Engineering models for supporting behavior of textile reinforced concrete 2008.
- [123] Kulas C. Zum Tragverhalten getränkter textiler Bewehrungselemente für Betonbauteile. 2013.
- [124] Rempel S, Kulas C, Hegger J. Bearing Behavior of Impregnated Textile. *FERRO-11 – 11th Int Symp Ferrocem 3rd ICTRC - Int Conf Text Reinf Concr* 2015:71–8.
- [125] Molter M. Zum Tragverhalten von textilbewehrtem Beton. Rheinisch-Westfälischen Technischen Hochschule Aachen, 2005.
- [126] Yin S, Xu S, Li H. Improved mechanical properties of textile reinforced concrete thin plate. *J Wuhan Univ Technol Mater Sci Ed* 2013;28:92–8. <https://doi.org/10.1007/s11595-013-0647-z>.
- [127] Rempel S, Ricker M, Hegger J. Safety concept for textile-reinforced concrete structures with bending load. *Appl Sci* 2020;10:1–18. <https://doi.org/10.3390/app10207328>.
- [128] Voss S. Dimensioning of textile reinforced concrete structures 2006:151–60. <https://doi.org/10.1617/2351580087.015>.
- [129] Büttner T, Orłowsky J, Raupach M. Investigation of the durability of textile reinforced concrete-test equipment and modelling the long-term behaviour. *Proc 5th Int RILEM Work (HPFRCC 5)* 2007:335–43.
- [130] Orłowsky J, Raupach M. Durability model for AR-glass fibres in textile reinforced concrete. *Mater Struct Constr* 2008;41:1225–33. <https://doi.org/10.1617/s11527-007-9321-2>.
- [131] Munck Matthias D, Kadi Michael E, Eleni T, Jolien V, Svetlana V, Jan W,

- et al. Durability study of textile reinforced cementitious composites with low fiber volume fraction 2017:189–94.
- [132] Mechtcherine V, Lieboldt M. Permeation of water and gases through cracked textile reinforced concrete. *Cem Concr Compos* 2011;33:725–34. <https://doi.org/10.1016/j.cemconcomp.2011.04.001>.
- [133] Wagner J, Spelter A, Hegger J, Curbach M. Ermüdungsverhalten von Carbonbeton unter Zugschwellbelastung. *Beton- Und Stahlbetonbau* 2020;115:710–9. <https://doi.org/10.1002/best.201900104>.
- [134] De Munck M, Tysmans T, Wastiels J, Kapsalis P, Vervloet J, El Kadi M, et al. Fatigue behaviour of textile reinforced cementitious composites and their application in sandwich elements. *Appl Sci* 2019;9. <https://doi.org/10.3390/app9071293>.
- [135] Mechtcherine V. Novel cement-based composites for the strengthening and repair of concrete structures. *Constr Build Mater* 2013;41:365–73. <https://doi.org/10.1016/j.conbuildmat.2012.11.117>.
- [136] Seidel A, Lepenies I, Engler T, Cherif C, Zastrau BW. Aspects of Creep Behavior of Textile Reinforcements for Composite Materials~!2009-03-04~!2009-10-15~!2009-12-11~! *Open Mater Sci J* 2009;3:67–79. <https://doi.org/10.2174/1874088x00903010067>.
- [137] Soudki K, Alkhrdaji T. Guide for the Design and Construction of Externally Bonded FRP Systems for Strengthening Concrete Structures (ACI 440.2R-02). 2005. [https://doi.org/10.1061/40753\(171\)159](https://doi.org/10.1061/40753(171)159).
- [138] Spelter A, Rempel S, Will N, Hegger J. Testing concept for the investigation of the long-term durability of textile reinforced concrete. *Am Concr Institute, ACI Spec Publ* 2018;2018-June:1–9.
- [139] Botelho Goliath K, Daniel DC, de A. Silva F. Flexural behavior of carbon-textile-reinforced concrete I-section beams. *Compos Struct* 2021;260:113540. <https://doi.org/10.1016/j.compstruct.2021.113540>.
- [140] Donnini J, Corinaldesi V, Nanni A. Mechanical properties of FRCM using carbon fabrics with different coating treatments. *Compos Part B Eng* 2016;88:220–8. <https://doi.org/10.1016/j.compositesb.2015.11.012>.
- [141] Barhum R, Mechtcherine V. Effect of short, dispersed glass and carbon fibres on the behaviour of textile-reinforced concrete under tensile loading. *Eng Fract Mech* 2012;92:56–71.

<https://doi.org/10.1016/j.engfracmech.2012.06.001>.

- [142] Schütze E, Bielak J, Scheerer S, Hegger J, Curbach M. Einaxialer Zugversuch für Carbonbeton mit textiler Bewehrung. Beton- Und Stahlbetonbau 2018;113:33–47. <https://doi.org/10.1002/best.201700074>.
- [143] Arboleda D. Fabric reinforced cementitious matrix (FRCM) composites for infrastructure strengthening and rehabilitation: Characterization methods. Fac Univ Miami 2014:1–224.

3 Flexural behavior of carbon-TRC I-section beams

Article published: January 5, 2021 – *Composite Structures*

3.1. Introduction

Corrosion resistant materials, such as carbon or alkali-resistant glass fibers, to reinforce cement-based matrix have become a considerable alternative to replace conventional steel bars reinforcement. These materials can be used in the form of textile [1-3] or fiber reinforced polymer (FRP) bars [4-6]. It has been proposed as an alternative to overcome some of the deficiencies presented by the conventional reinforced concrete (RC), such as the need for large reinforcement cover, susceptibility to corrosion and heavy weight.

Textile reinforced concrete (TRC) is a relatively new and promising cement-based composite since this material has high tensile strength and high durability, with potential to build thin, modular, low weight structures and slender concrete members [8,9]. This composite has been used for new constructions and load-bearing structural members, as well as precast elements [10], shell structures [11-13], parking slabs [14] and sandwich elements [15-18]. Many applications in combination with FRP bars can also be found in the literature, e.g. prestressed elements [19], foot and cycle-bridges [20,21] and precast slabs [22].

Design models to predict load-bearing behavior of full TRC beams under bending have already been reported in the literature, [8,9,23-33], but these usually reduce to the well-known cross-section analysis (moment-curvature) commonly adopted for the design of conventional RC. This model, however, is not able to provide information on the tension-stiffening and cracking behavior of TRC beams. Models based on moment-rotation behavior, on the other hand, may be used to incorporate influence of the bond and concrete softening mechanisms, but their use has been limited to RC beams [34-41]. For such comprehensive evaluation, it is important to obtain adequate constitutive relations for the materials and interface

through mechanical characterization [42], that affect serviceability and load-carrying capacity of TRCs [43]. It is worth mentioning that TRCs exhibit a crack formation stage, followed by crack growth with strain-hardening behavior. For flexural members, this results in high deflection values and significant crack openings prior to failure [44], which is a problem for the serviceability limit state.

To model TRC behavior, different efficiency factors are usually adopted to account for the characteristics of the fiber textile, e. g. the number and length of the fibers strands and the shear lag effect associated to late activation of inner filaments comprising the textile yarn. The factors k_f and k_c describe the efficiency of the fabric [26, 33, 45, 46] and the fiber inside the composite [23-27, 46,47], respectively. On the other hand, [48] showed that these factors do not lead to a clear understanding of the tensile behavior due to the stress distribution profile in a roving for different coating or impregnation degrees. Design approaches were proposed by these authors and took into account the coaxial ring model, differentiating the sleeve and core filaments level of stress. Other aspects, such as tension stiffening effect and material adherence were included. In addition, it was suggested a bond-lag effect in the roving filaments. Some authors reported greater efficiency for plates tested under bending, which has been associated to the resulting yarn curvature, producing friction that ends up improving the transference of force from outer to inner filaments [25-29]. In their analysis of TRC beams, to account for the shear lag effect, Valeri et al. [33] also considered a stiffness factor k_e , defined as the ratio between effective textile modulus and the expected yarn modulus obtained from uniaxial test [25, 49-51].

In order to improve the handling of fabrics when manufacturing the elements, to protect and keep the dry fibers together to form complex structures, stiffer coatings such as epoxy and polyacrylate or flexible system like styrene-butadiene rubber (SBR) resins [52-62] may be used, which also improves the bond of the inner filaments and load transmission. In opposition to epoxy, SBR laminated textiles are flexible and provides easy transportation and application. On the other hand, SBR coatings usually exhibit a poor adherence and frictional bond to the concrete matrix, resulting in a composite unable to form a multiple fine cracking pattern, ultimately leading to a tensile behavior characterized by complete pullout of the yarns.

One alternative to improve bond performance is to impregnate the textile with epoxy resin and sand. Some studies have found that the use of sand-epoxy

impregnation can enhance mechanical bond strength, frictional resistance and stiffness [63-70], thus improving member bearing. This is due to the increased surface roughness introduced by sand, reducing the slip between fibers and matrix [71] and making the forces between constituents to be transferred more effectively. Moreover, crack pattern is improved by reducing crack spacing and openings. However, the strong bond strength may lead to a simultaneous abrupt fracture of all filaments comprising the textile, which characterizes a brittle failure [72].

Hybrid fiber reinforced composites consisting of strain-hardening based-cement composite (SHCC) matrices and continuous textile reinforcement yield a better crack control with a pronounced multiple cracking behavior [73-80]. Research papers [44, 71, 78] have reported an increase in composite strain capacity and mechanical properties when simultaneously applying textiles and short fibers as reinforcement in cementitious matrices in comparison to ordinary TRC. Conversely, other authors [74, 79] have reported no gain in ultimate strain. In addition, the use of the SHCC matrices results in high inelastic deformations, making the composites to exhibit ductile behavior along with higher energy dissipation [75, 76].

The main goal of this research is to investigate the performance of carbon-TRC I-beams made with SBR laminated textile and considering three different material conditions: plain TRC, sand-coated TRC and hybrid TRC-SHCC. An experimental investigation consisting in four-point bending tests is carried out and the results such as failure modes, load-deflection curves, moment-curvature relations and cracking patterns are reported. For a comprehensive analysis, the results of a full mechanical characterization for materials and interface are also presented. Digital Image Correlation (DIC) technique was used to monitor displacement field and crack patterns. Finally, the experimental results are compared to an analytical approach incorporating the influence of material and interface properties.

3.2. Experimental Program

3.2.1. Materials and Mechanical Characterization

3.2.1.1. Carbon Textile

A flexible carbon textile coated with styrene-butadiene rubber (SBR) resin supplied by the company V.FRASS denominated SITgrid017KB was used in the study. It is a bidirectional mesh with openings of 8.5 and 10 mm and widths of 4.2 and 2.7 mm in the warp and weft directions, respectively. Details of the warp yarns that form the textiles were observed using a Nikon stereo microscope model SMZ800N and a cross-sectional area of 3.32 mm² and a perimeter of 9.1 mm were measured. Uniaxial tension tests in the same carbon warp yarn used in the present work were performed by Santos [81], indicating a tensile strength (f_t) of 1140 MPa and an average modulus of elasticity of (E_f) 189 GPa, referred to the measured cross-section area. This modulus of elasticity is within the range of values reported in literature [8, 9, 32, 50] and slightly lower than the reference value provided by the manufacturer (250 GPa). On the other hand, the strength obtained by Santos seems to be lower than expected; an ultimate strain of approximately $\epsilon_{fu} = 0.010$ to 0.015 has been reported in literature [8, 9, 32, 50].

To improve the bond between the textile and the cementitious matrix, which is usually poor for SBR laminated textiles, an extra impregnation with epoxy resin and sand – hereafter referred as rigid impregnation – was applied over the yarns. The textile was not stretched before manually application of the rigid impregnation. The enhancement in the bond performance after sand-epoxy impregnation has already been shown elsewhere in literature by means of pullout and tensile tests [67, 69, 71, 72, 76]. In the present investigation, the epoxy resin used was Sikadur[®]-32 and the natural sand had the same grain size as the sand used as fine aggregate in the matrix (1.18 mm). A period of at least 24 hours was adopted for curing of resin before the sand-coated textile was applied. Throughout the work, the specimens made with textile with and without a rigid impregnation were denominated ST (Sand-epoxy impregnation) and RT (SBR-laminated Reference textile), respectively.

3.2.1.2. Matrix

Two different types of matrices were used in this study, the plain concrete and the strain-hardening cement-based composite (SHCC) with 2% in volume of PVA (Polyvinyl Alcohol) microfibers, designed M1 and M2 respectively. The Kuralon® REC15 fibers used, supplied by Kuraray™, had a length of 12 mm and an average diameter of 40 μm .

The plain concrete was designed for a cement-based composite reinforced with textile. The combination of high amount of cement with fly ash and micro silica provides a high compressive strength matrix. In its composition, a fine aggregate natural sand with 1.18 mm maximum diameter was used, along with a water-to-binder ratio of 0.3, adapted from previous studies [74]. The SHCC matrix was chosen based on its ability to improve ductility of TRC [44, 73-76]. For the composition of the SHCC matrix, an adaptation of the mix design adopted by Curosu [77] was used. To obtain this behavior and ensure the initiation of cracks, a restricted particle size distribution is necessary, obtained with fine-grained material (finer sand, fly ash and CP V) [77]. The compositions used for both matrices are presented in Table 3.1.

Table 3.1 - Composition for cementitious matrices per m³ and main compressive properties.

Material	M1	M2
CP2 cement	632	-
CPV cement	-	505
Sand (1.18 mm)	947	-
Sand (0.06-0.2 mm)	-	536
Fly ash	265	621
Micro silica	50.5	-
Water	266	338
Super plasticizer (Glenium)	25	11.3
Viscosity modifying agent	-	1.2
PVA fibers	-	26
Water-to-binder ratio	0.3	0.3
Mechanical Properties	M1	M2
Compressive strength (MPa)	76.0 \pm 2.6	37.8 \pm 1.5
Compressive strain at peak (mm/mm)	0.0033	0.0038
Young's Modulus (GPa)	28.4 \pm 0.8	23.1 \pm 0.4

To evaluate the mechanical properties of the studied matrices, compression tests were performed using a servo hydraulic testing machine MTS 810 with load capacity of 500 kN (Figure 3.1a). The compressive strength and Young's modulus

of each matrix were evaluated at 28 days of age and can be seen in Table 1. Modulus of elasticity was determined as the slope of the chord between stresses corresponding to 25 and 50% of the peak strength, according [82]. Properties were obtained with average of three samples with 50 mm in diameter and 100 mm of height. The tests were conducted at a constant displacement rate of 0.2 mm/min up to failure. Figure 1 shows average stress-strain curves for the two matrices studied. It is important to highlight the behavior after peak of the M2 matrix (Figure 3.1b). The SHCC shows a smooth decay in resistance after the peak load, which may contribute to the ductility of TRC beams failure mode governed by compression.

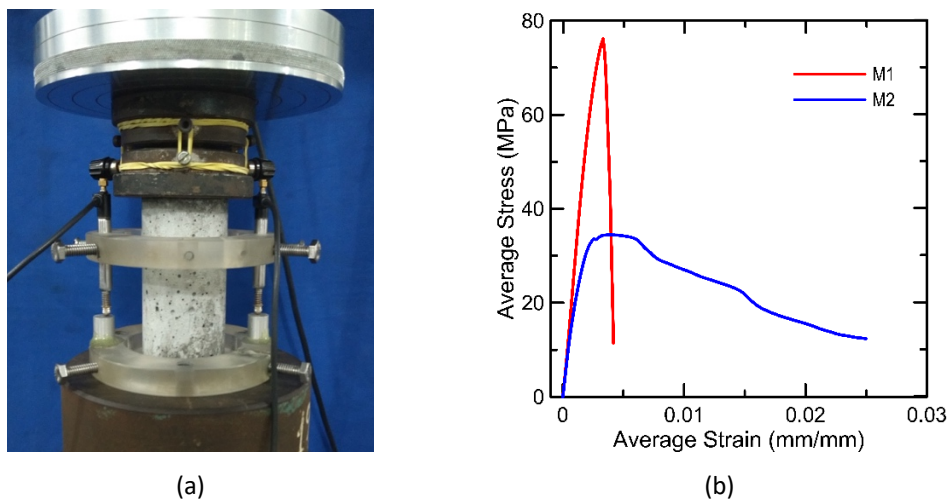


Figure 3.1 – (a) Compression test set up and (b) Mechanical response of the concrete matrices in compression test.

3.2.1.3. Pullout Test

In order to characterize the interface, pullout tests consisting in pulling the embedded yarn out from the matrix were performed. The influences associated to the use of a sand-epoxy coating and a SHCC matrix were evaluated.

The pullout specimens were prepared using a cylinder mold with 25 mm x 20 mm (diameter x height) and the embedded length of the yarns was 20 mm. A single warp yarn was positioned in center of mold and filled with matrix. All the samples were tested on a servo hydraulic MTS 810 Universal Machine with a load capacity of 250 kN at a vertical displacement rate of 1.5 mm/min. A 2.5 kN load cell was used to improve accuracy of load acquisition. The test set up used can be seen in Figures 3.2a and 3.2b. The average bond stress was calculated dividing the pullout force by the yarn surface area (perimeter multiplied by nominal embedded length).

Figure 3.2c presents bond stress versus slip curves from pullout tests obtained as the average result from five specimens tested for each condition. It can be noted that the average bond strength obtained for the sand-epoxy impregnated yarn (2.87 ± 0.02 MPa) is up to 2.7 times greater than that obtained for the reference yarn without impregnation (1.10 ± 0.04 MPa). For RT-M1 specimens, the weak bond between textile-SBR coating-matrix led to a complete pullout of the yarns, while the interlock produced by the sand-coating in ST-M1 specimens reduced considerably the relative slip between the yarn and the matrix, as expected [71]. Such improvement makes the reinforcement to be more efficiently activated in structural members [27]. Another interesting comparison can be done between RT-M1 and RT-M2. Usually, the bond-slip response increases with the concrete compressive strength and, therefore, a lower bond strength would be expected for the RT-M2 case. However, the confinement provided by PVA fibers in M2 as the yarn is pulled out mobilizes a greater friction force along the interface, ultimately increasing the bond strength and making the peak bond stresses for RT-M1 and RT-M2 to be nearly the same – 1.10 ± 0.04 MPa and 1.0 ± 0.04 MPa, respectively. In previous studies performed by [75], the peak forces for SBR-carbon yarn from plain matrix and PE-SHCC were nearly identical in the pullout tests; however, it was observed that PBO fibers led to an increase of about 20% of the pullout force. In both cases where the pullout behavior was improved (ST-M1 and RT-M2), an abrupt drop in the bond-slip curve was seen after the peak.

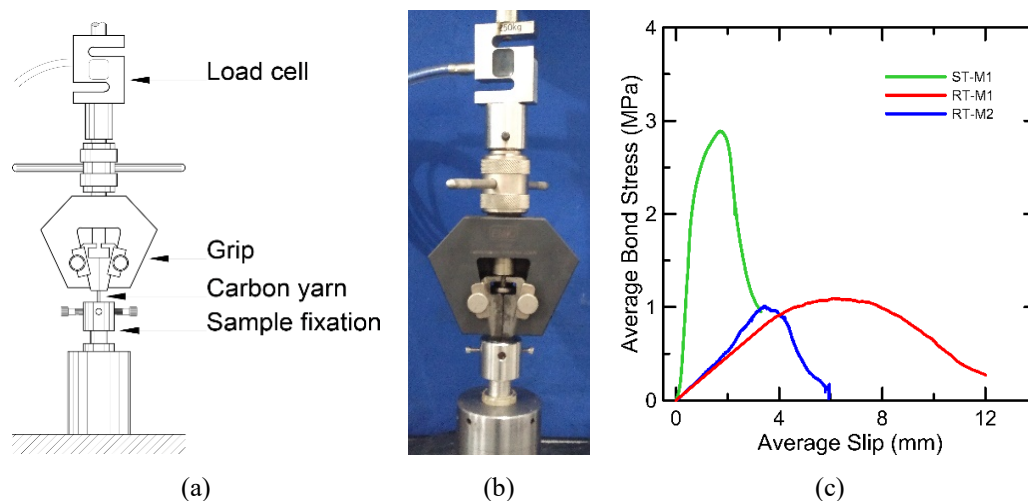


Figure 3.2 - Pullout test: (a) Set up scheme; (b) overview of test setup; (c) average bond stress versus average slip.

On the other hand, specimens with SHCC (RT-M2) exhibited smaller slip values when compared to the plain concrete. The RT-M1 provided bond stress–slip relationships with a pronounced softening branch, i.e. smooth yarn pullout. Considering the bond stiffness K_b as the slope of the secant line from origin to a bond stress equivalent to 40% of the bond strength, the following values can be obtained for RT-M1, ST-M1 and RT-M2, respectively: 0.21, 4.08 and 0.30 MPa/mm. It can be seen that the stiffness for the sand-coated specimens is about twenty times that obtained for the plain textile, which basically have their linear response governed by adhesion mechanism. It is worth highlighting that the aforementioned pullout behavior does not include the mechanical anchorage at the cross (weft) yarn junctions [83-85].

3.2.1.4. Four Point Bending Test

Carbon-TRC beams were tested in four-points bending test to assess their flexural performance in three different conditions: with reference textile and plain matrix (RT-M1), with sand-epoxy impregnation and plain matrix (ST-M1) and with reference textile and SHCC (RT-M2). Three 2000 mm long beams having I-sections with 80 mm of flange width, 180 mm of depth and 12.5 mm of thickness for both web and flange were fabricated, one sample for each aforementioned condition.

The beams were cast using a steel I-shape formwork with the desired final dimensions (Figure 3.3a). The assembled cage reinforcement was placed in the formwork before the beam was cast horizontally as shown in Figure 3.3b. Along the junction between web and flanges, a nylon line was used to keep the layers of the reinforcement together. In the Figure 3.3c it is possible to observe the simple connection between web and the flange, i.e. the junction of the assemble cage. Care was taken to place the textile in the middle of the specimen thickness. Beams were removed from the formwork after 48 hours and kept in a humid chamber until the test day, at 28 days of age.

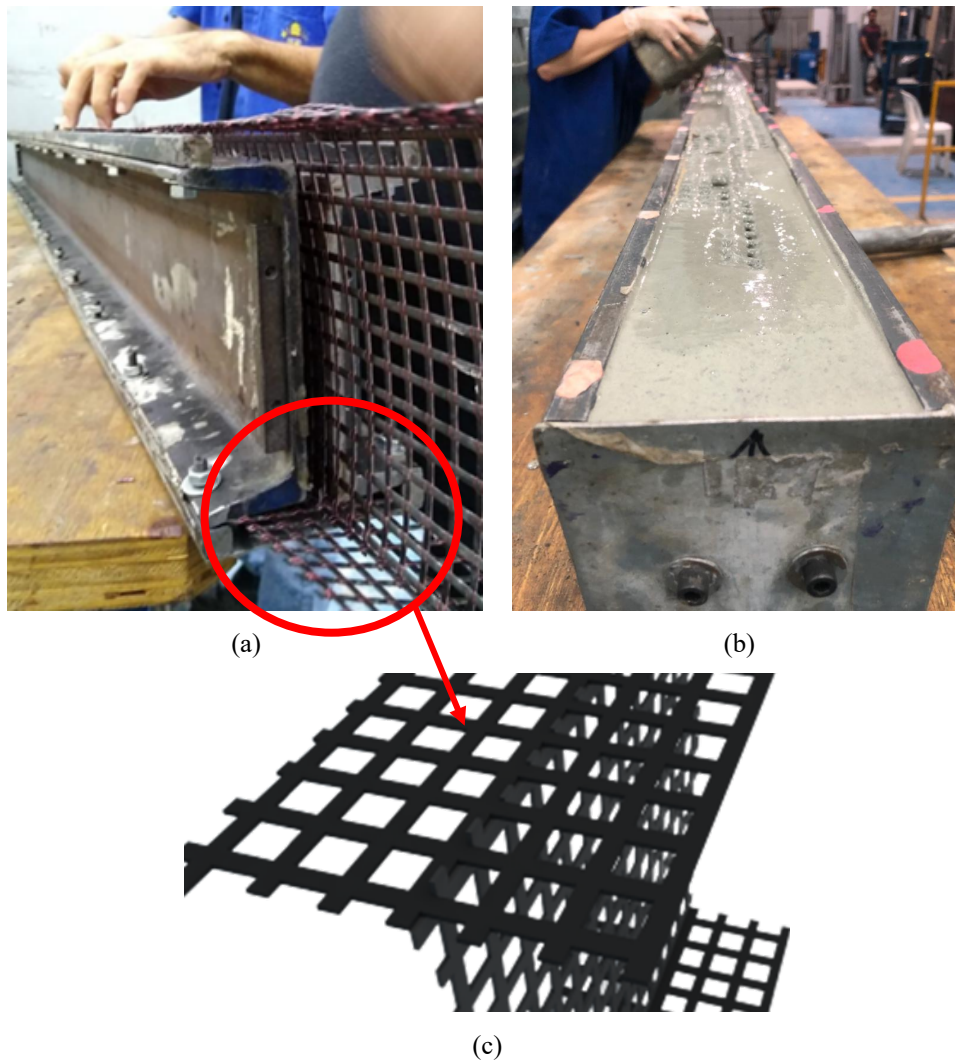


Figure 3.3 - (a) Positioning of the reinforcement in the form and (b) concrete being cast in the form.

The beams were tested in a four-point bending configuration over an 1800 mm span and with a shear span of 750 mm. A hinge was placed over the load distribution beam to ensure equal forces to be applied at the loading points. Testing was conducted using a servo-controlled hydraulic actuator with load capacity of 500 kN under displacement control at a rate of 1 mm/min. The deflection was measured with a displacement transducer placed at the mid-span and a strain gage was installed at the top of the beam mid-span to capture the compressive strain evolution throughout the test. The curvature and crack propagation were monitored by DIC technique over a web area of 300 x 155 mm at the constant moment region. To validate the DIC analysis, the displacements obtained using this technique with the aid of software GOM [86] were compared with the transducer displacement,

showing good agreement. An overview of the test setup is presented in Figure 3.4a, whereas a detailed scheme is shown in Figure 3.4b.

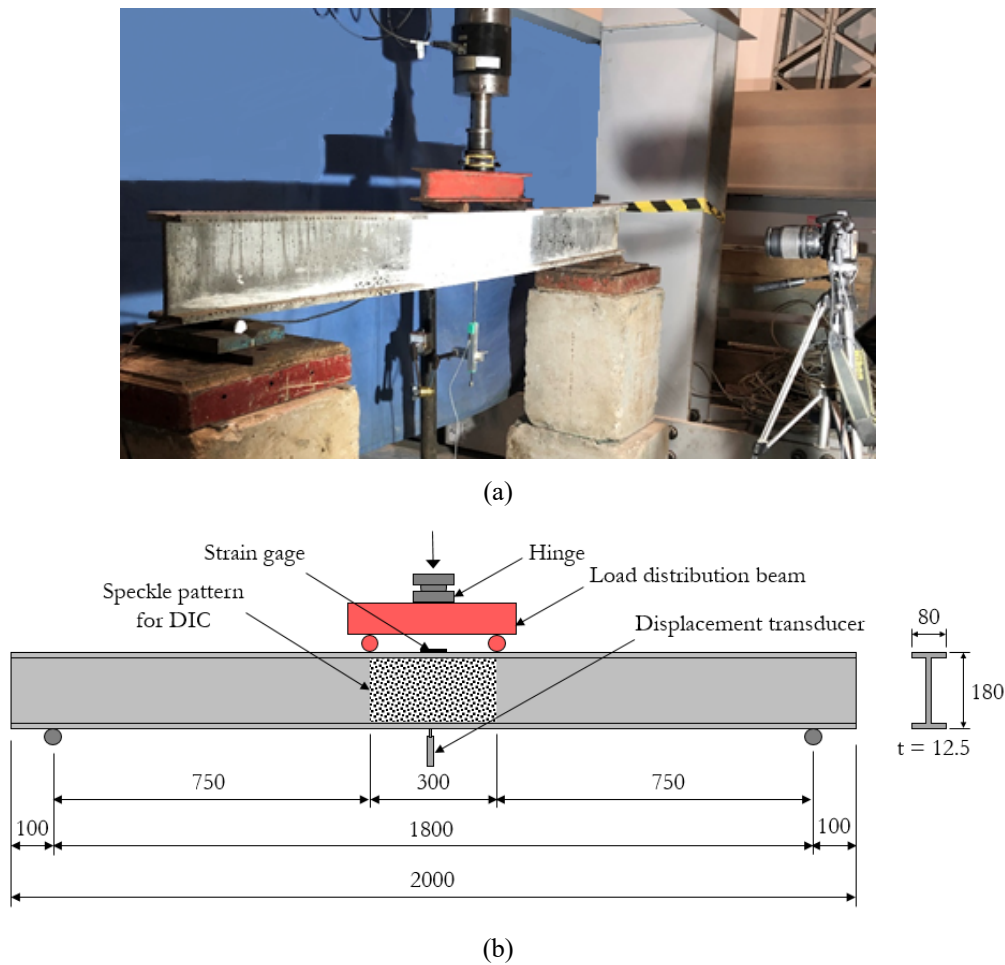


Figure 3.4 - Four-point Bending Test: (a) overview of test setup; (b) scheme of test and cross-section (dimensions in mm).

3.3. Results and Discussions

In this Section, the flexural behavior of the analyzed carbon-TRC I-beams obtained experimentally are reported, discussed and compared to analytical predictions. Table 3.2 summarizes the main results obtained experimentally.

The tested beams presented different failure modes, as reported in Table 3.2. Figure 3.5 shows the failure mode of the beams. RT-M1 exhibited three macro-cracks along the constant moment region. However, its failure was governed by shear between support and load application, without mobilization of its maximum flexural capacity. The shear failure was characterized by the formation of a critical diagonal crack and flange detachment along web-to-flange junction, as shown in Figure 3.5a. This failure mode was induced by the weak type of connection used

between the web and flanges reinforcement, which consisted in simply crossing the web weft yarns with the flange mesh, as shown in Figure 3.3c. The uncoated weft yarns have low penetration into the flange and poor adherence to the matrix, resulting in a low ability to transfer forces along the junction. In the case of the RT-M2 beam, the PVA fibers helped to transfer the forces between web and flange and, for the ST-M1 beam, the sand-coated weft yarns have better adherence and were able to transfer forces between web and flange. In the case of the beam with surface treated textile (ST-M1), the failure mode was characterized by rupture of longitudinal yarn in the tension zone. The improvement in bonding between matrix and fabric modified the rupture shape, making ST-M1 fail by bending, as presented in Figure 3.5b. Finally, the beam with SHCC matrix (RT-M2) exhibited a local failure, characterized by crushing of concrete near the load application point, with spalling of concrete cover at the web and formation of wedge sliding mechanism at the flange (Figure 3.5c). This failure may be dependent upon the size of the load introduction region.

Table 3.2 - Summary of experimental results.

Result	Specimen			
	Description	Units	RT-M1	ST-M1
Failure mode	-	Shear	Flexural (tension)	Flexural (compression)
Maximum load (F_{max})	kN	13.45	16.06	12.70
Maximum moment (M_{max})	kN.m	5.04	6.02	4.76
Deflection at failure (δ_u)	mm	26.89	25.48	31.64
Curvature at peak moment (Φ_{peak})	1/m	0.077	0.076	0.125
Load at first crack (F_{cr})	kN	1.17	1.76	2.27
Mean crack spacing (s_m)	mm	110.16	25.64	21.46
Service crack spacing ($s_{2.5}$)	mm	110.20	31.10	33.50
Mean crack opening (w_m)	mm	0.87	0.15	0.09
Service crack opening ($w_{2.5}$)	mm	0.41	0.06	0.03

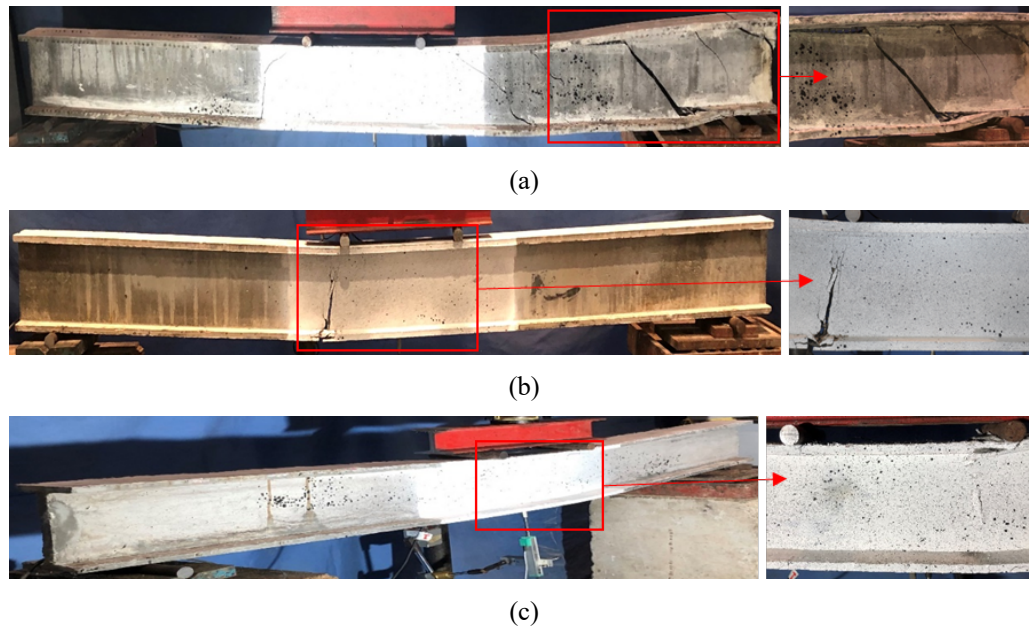


Figure 3.5 - Failure mode of beams: (a) RT-M1; (b) ST-M1; (c) RT-M2 beams.

The load-deflection curves of TRC beams, which were measured with displacement transducers, are shown in the Figure 6. It can be noticed that the ST-M1 presented the highest peak load, i.e. an increase of 19.5 % with respect to RT-M1, which failed prematurely due to shear. An essentially linear elastic behavior was obtained for both beams, with a similar mid-span deflection at failure of 25 mm, followed by an abrupt failure (Table 3.2). The results therefore show there was an improvement in the flexural behavior in terms of strength and stiffness after sand-coating. The RT-M2 presented a behavior similar to ST-M1 at initial loading stages before the first crack load and during the beginning of crack formation (Figure 3.6b), confirming the positive influence of the fibers to the behavior. For beam RT-M2, there was a loss of linearity between 10 and 20 mm of deflection and the final load was 5.6 % smaller than RT-M1, but with a failure deflection of 31.64 mm, i.e. 17.7 % greater than RT-M1. Although the lower compressive properties of SHCC matrix, its ability to transfer tensile stresses through cracks contributed to enhance the crack control and to improve the stiffness in the cracked state. The ductility of RT-M2 is associated to the so-called concrete softening mechanisms, namely cover spalling and wedge-sliding with friction, as well as to a possible decay in the capacity of transferring tensile stresses after significant increases in crack width.

Figure 3.6b presents a detail of the load-deflection curve for low deflections to obtain information about the pre-cracked stage. The exact cracking load (F_{cr}) cannot

be clearly obtained directly from this plot. Therefore, DIC analysis was conducted to identify the instant of time associated to the first crack formation at the constant moment region and the corresponding load (Table 3.2). It can be seen that the cracking load for ST-M1 and RT-M2 increased with respect to RT-M1. It was noticed that the use of the SHCC matrix was more efficient than surface treatment. The improvement for each was respectively 1.94 and 1.50 times greater than the reference textile with plain matrix value (1.17 kN). This can be explained by the fact that, due to the low adhesion of the uncoated textile, the cross yarn (weft) acts like a defect, making the tensile stress trajectory to deviate and inducing a stress concentration in the vicinity, as shown in Figure 3.7. This effect was partially mitigated with the improvement of adherence (ST-M1) or through the fiber-bridge mechanism (RT-M2). For the case of specimen ST-M1, the enhanced interface allows a small portion of the stresses to be transferred through the transverse yarn, despite its lower stiffness when compared to the surrounding concrete, leading to a slightly higher cracking stress when compared to the uncoated specimen.

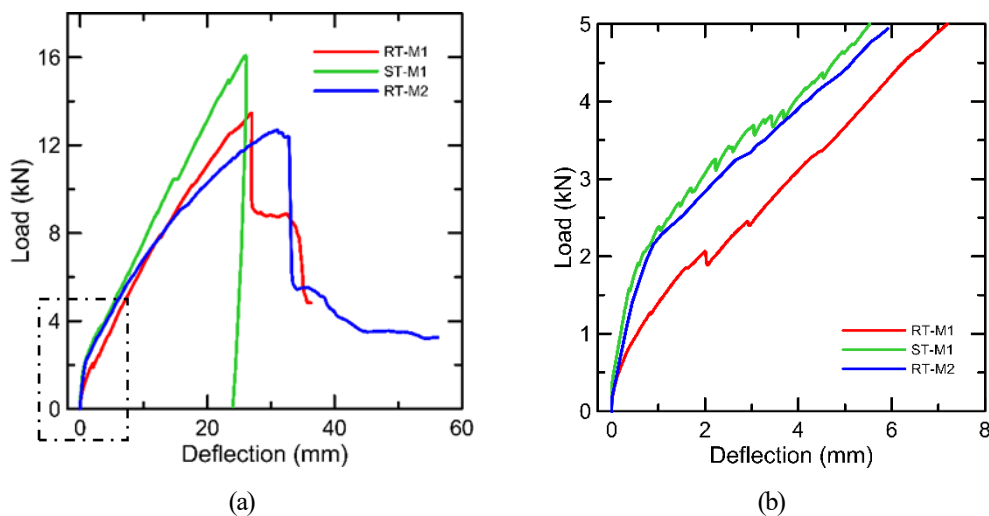


Figure 3.6 - Load-deflection curves: (a) for full test; (b) detail for low deflections.

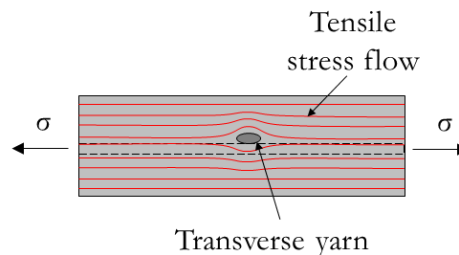


Figure 3.7 - Tensile stress trajectory.

Moment-curvature relations are presented in Figure 8a, derived using DIC and a procedure similar to that described by [87]. It is important to highlight that these relations were obtained over the constant moment region and, therefore, include the contribution of concrete between cracks (tension stiffening). From these relations, the cracking moments can be clearly identified, as shown in Figure 3.8b. In the initial part of the curves (Figure 3.8b), it is observed the transition from stage I, where concrete still resists to tension, to stage II, where multiple cracks are formed. Beams RT-M1 and ST-M1 presented a similar slope at stage II, only shifted upwards for ST-M1 due to a greater tension stiffening effect. For RT-M2, a lower stiffness was seen for stage I, which is associated to the lower modulus of M2. On the other hand, the stiffness at stage II is similar to the beam reinforced with sand-coated fabric. According to [72], the improvement in stiffness after the cracking is due to a delay in crack expansion as a result of the bridge effect caused by the short fibers. A similar curvature at failure of approximately 0.076 m⁻¹ was obtained for beams RT-M1 and ST-M1 (Table 3.2). For RT-M2, an increase of 64 % in curvature at failure was obtained with respect to RT-M1 (Figure 3.8a). According [41], the major contribution of fibers in tension region is not in flexural capacity but through the tension stiffening mechanism allowing the development of more and finer cracks (as will be seen later). In addition, there were opposing effects for this specimen: while the fibers were able to improve the crack pattern (Figure 3.9c), the porosity of the matrix might have increased [46, 74, 76], affecting negatively the matrix response for compressive stresses.

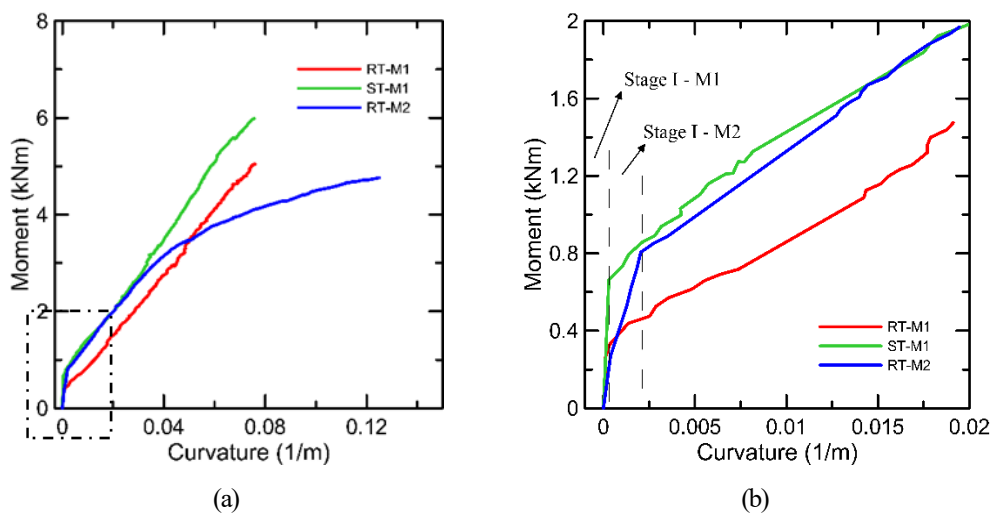


Figure 3.8 - Moment-curvature relations (a) and initial moment stages in detail (b).

Figure 3.9 shows the details about crack spacing and crack opening with loading gathered with the DIC technique using an approach similar to that reported by [87]. Table 2 shows the mean crack spacing and mean crack opening, evaluated with the average cracks at the maximum moment, and the properties at the service moment of 2.5 kNm. To measure the average crack spacing, four load stages set to 0.4, 0.6, 0.8 and 1 of the maximum moment were used and are shown in Figure 3.9e. It can be clearly seen that ST-M1 and RT-M2 beams (Figures 3.9b and 3.9) had their cracking behavior greatly improved with respect to the reference condition (RT-M1, Figure 3.9a), respectively due to enhanced bonding associated to the interlock effect from sand-coating and due to fiber-bridging mechanism. The beam with uncoated textile and plain matrix presented crack widths of 82.8 % and 89.7 % higher than ST-M1 and RT-M2, respectively. The mean spacing crack decreased with increasing curvatures for ST-M1 and RT-M2. For RT-M1, after the appearance of the cracks (Figure 3.9d) is it followed by a stabilized cracking stage characterized by the widening of cracks up to sudden failure (Figure 3.9e). In the case of ST-M1 and RT-M2 beams, new cracks are formed as the curvature increases until it reaches saturation (Figure 3.9e). The use of the SHCC matrix was very efficient in controlling crack opening, keeping it below 0.1 mm, as show in Figure 3.9d. As seen in Section 2.3, M2 presented a peak bond stress peak nearly identical to the plain matrix. However, the addition of discontinuous PVA fibers to the matrix resulted in a network of fine cracks (Figure 3.9c) and increased the rate of reinforcement.

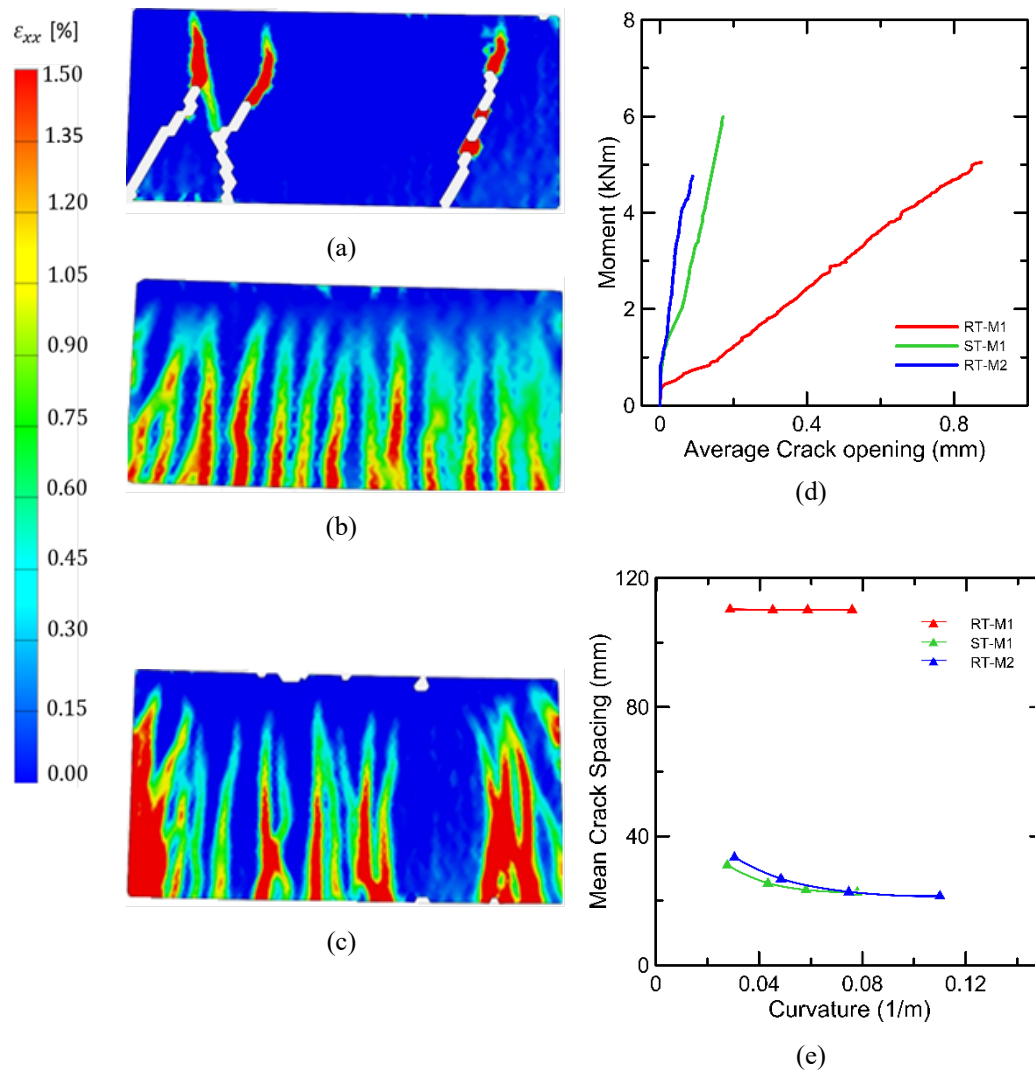


Figure 3.9 -DIC analysis of the (a) RT-M1, (b) ST-M1 and (c) RT-M2 beams; (d) Moment vs average crack opening; (e) mean crack spacing vs curvature.

To evaluate the influence of material and interface properties and geometry to the beam response, a mechanical model based on the tension stiffening approach presented in the Model Code 2010 [86] for conventional RC is adopted. Based on the assumption that the bond stress developed along the reinforcement-matrix interface is constant along the length over which transference of forces occurs (Figure 3.10), it can be easily shown that the average stress, σ , calculated as the total force necessary to produce an average strain $\epsilon_{av} = \Delta L/L$ in the composite divided by the reinforcement area is given as:

$$\sigma = \epsilon_{av} E_f k_e + \frac{1}{2} \frac{(f_{ctm} + f_{ctr})}{\rho_f} \quad \text{Eq. 3.1}$$

where $\varepsilon_{av} = \Delta L/L$ is the average strain, E_f is the modulus of elasticity of the reinforcement, k_e is stiffness factor due to shear lag effect, f_{ctm} is the mean concrete cracking strength, f_{ctr} is the concrete residual tensile stress transferred across crack and ρ_f is the reinforcing geometric ratio. Other tension stiffening models for TRC members subject to tension are available in literature [81, 82, 87], but these usually adopt more complex bond-slip laws.

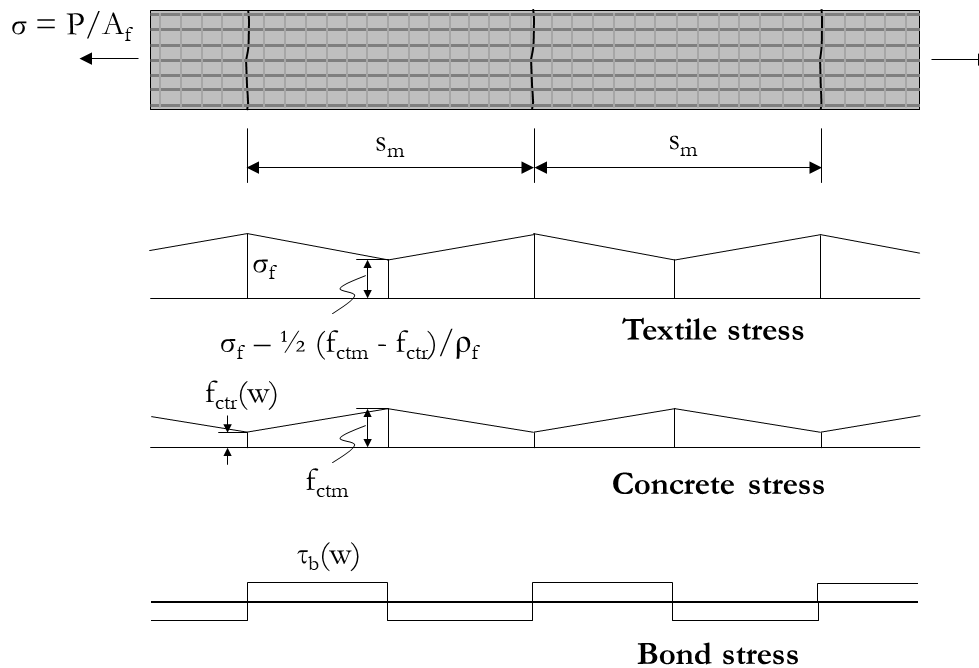


Figure 3.10 - Tension stiffening model adopted for TRC with fiber reinforced concrete.

To obtain the response of a beam considering the tension-stiffening effect, the neutral axis position and the bending moment acting on the beam can be determined from balance of forces and moments for a given average curvature Φ_{av} , assuming the usual plane section hypothesis. Two additional considerations are adopted in the present work: i) the stresses throughout the tension (cracked) zone are determined according to Eq. 3.1, assuming a homogeneous material; and ii) the compressive stresses are determined neglecting the contribution of the textile in compression. Although the contribution of the textile may be effective up to a certain level of compressive strain, it is strongly dependent on the ability of concrete to provide lateral restraint, which is compromised as the concrete enters its non-linear regime characterized by significant lateral expansion. Moreover, the constitutive relationships adopted are presented in Figure 11 and the parameters are

summarized in Table 3.3. In these relations, it is important to highlight the following features: i) a constant residual stress $f_{ctr} = 0.9 f_{ctm}$ is adopted in the post-cracked condition for the SHCC matrix; ii) stiffness and effectivity factors are adopted for the textile, for an appropriate correlation between experimental and theoretical slopes during the cracked stage; and iii) the concrete tensile strength at cracking was assumed equal to the elastic stress at first crack obtained experimentally from data presented in Table 3.2.

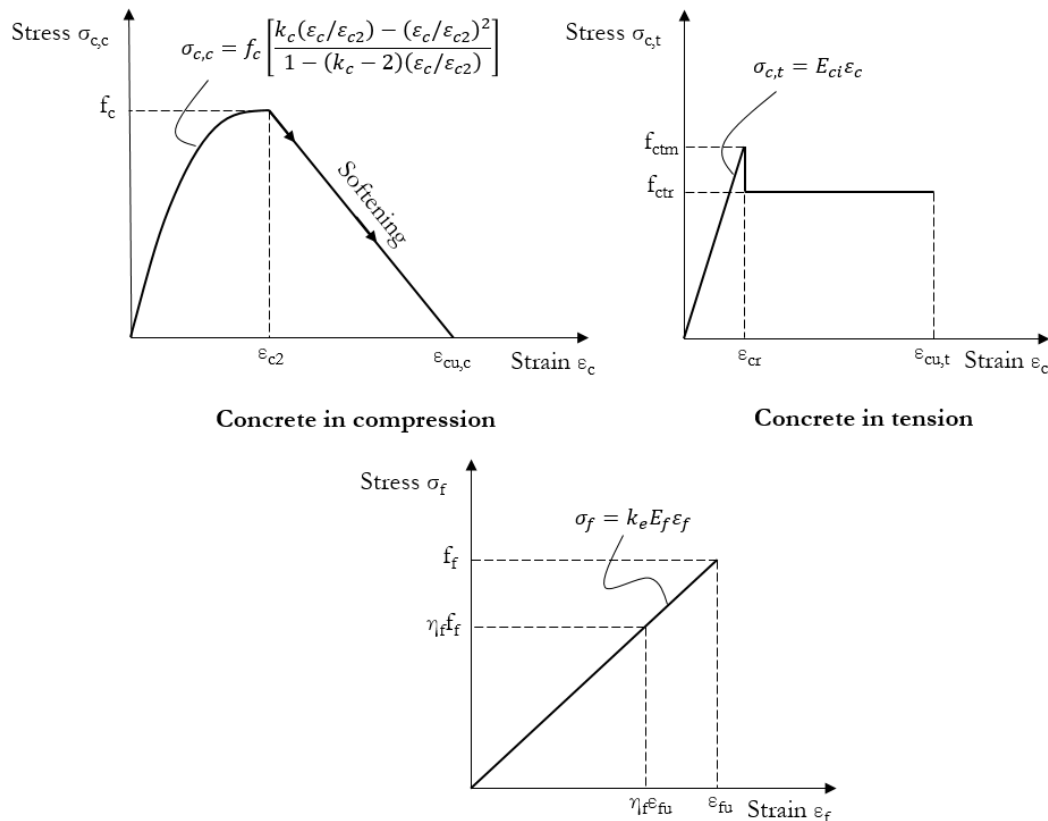


Figure 3.11– Constitutive relationships assumed in the model.

In Figure 3.12, the moment-curvature relations determined with the theoretical approach are compared to those obtained experimentally. For the RT-M1 and ST-M1 specimens, curves neglecting the concrete contribution (without tension stiffening, ‘No TS’) are also plotted. A good agreement between experiment and theory was obtained and the model is able to capture the greater tension-stiffening for the ST-M1 specimen, although the strength seems to be overestimated if $\eta_f = 1.0$ is assumed. It must be noted that the stiffness factors k_e were selected to obtain a similar slope between experiment and test. For the RT-M2 beam, a good agreement was also achieved for the linear range of the experimental curve. However, it seems that the beginning of local failure made the actual response

deviates from the expected behavior, similar to what was observed by Preinstorfer et al. [8]. For a more rational approach incorporating local mechanisms such as that presented by Barros et al. [88], further tests and analyses are required.

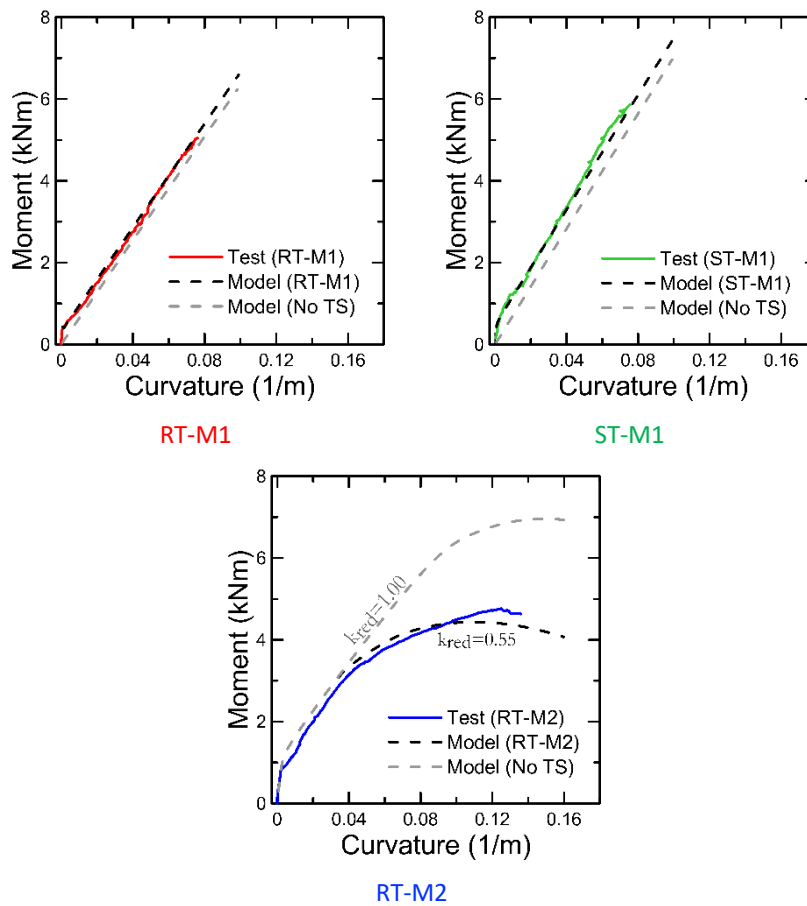


Figure 3.12 – Comparison between moment-curvature relations obtained theoretically and experimentally.

The model can also be extended to provide information about crack opening and spacing. Using the model presented in Figure 3.13, the crack spacing and opening can be written respectively as:

$$s_c = 2 \frac{(f_{ctm} - f_{ctr})}{\tau_b (U_f / A_f) \rho_f} \quad \text{Eq. 3.2}$$

$$w = \frac{s_c}{E_f k_e} \left[\sigma - \frac{1}{2} \frac{(f_{ctm} + f_{ctr})}{\rho_f} \left(1 + \frac{k_e E_f \rho_f}{E_{ci}} \right) \right] \quad \text{Eq. 3.3}$$

where U_f is the perimeter of the reinforcement and τ_b is the nominal bond stress, assumed equal to the bond strength obtained experimentally and reported in Section 3.2.2. As mentioned previously, the bond behavior does not include the presence of the transverse yarns, which improve the bond behavior [8, 52, 89, 90]. To account for the additional pullout strength provided by the cross yarns, a second condition

with nominal bond strength taken as $2\tau_b$ was considered. In Figure 3.13, the crack openings obtained with DIC are compared to those computed according to Eq. 3.3. In general, the correlation between model and experiment was satisfactory for design purposes, but the following important remarks must be made: i) the condition of $2\tau_b$ (considering influence of cross yarn) for beam RT-M1 resulted in excessive underprediction of crack openings; and ii) the condition of τ_b (neglecting influence of cross yarn) for beam ST-M1 resulted in much greater values of crack opening. These observations suggest that the influence of the cross yarn is strongly dependent on the textile surface configuration. For the case of RT-M2 beam, the cracking response is mostly affected by the concrete residual tensile strength the cross yarns seem to have lesser influence to the response.

Table 3.3– Properties adopted in theoretical model.

Parameter	Specimen		
	RT-M1	ST-M1	RT-M2
f_c (MPa)	76	76	37.7
k_c	1.3	1.3	2
ε_{c2}	0.0033	0.0033	0.0033
$\varepsilon_{cu,c}$	0.0042	0.0042	0.0330
$\varepsilon_{cu,t}$	-	-	0.015
f_{ctm} (MPa)	2.20	3.31	4.27
f_{ctr} (MPa)	0	0	3.5
E_{ci} (GPa)	33	33	20.6
E_f (GPa)	189	189	189
η_f	1.0	1.0	1.0
k_e	0.4	0.45	0.4
ε_{fu}	0.015	0.015	0.015
τ_b (MPa)	1.1	2.9	1.1

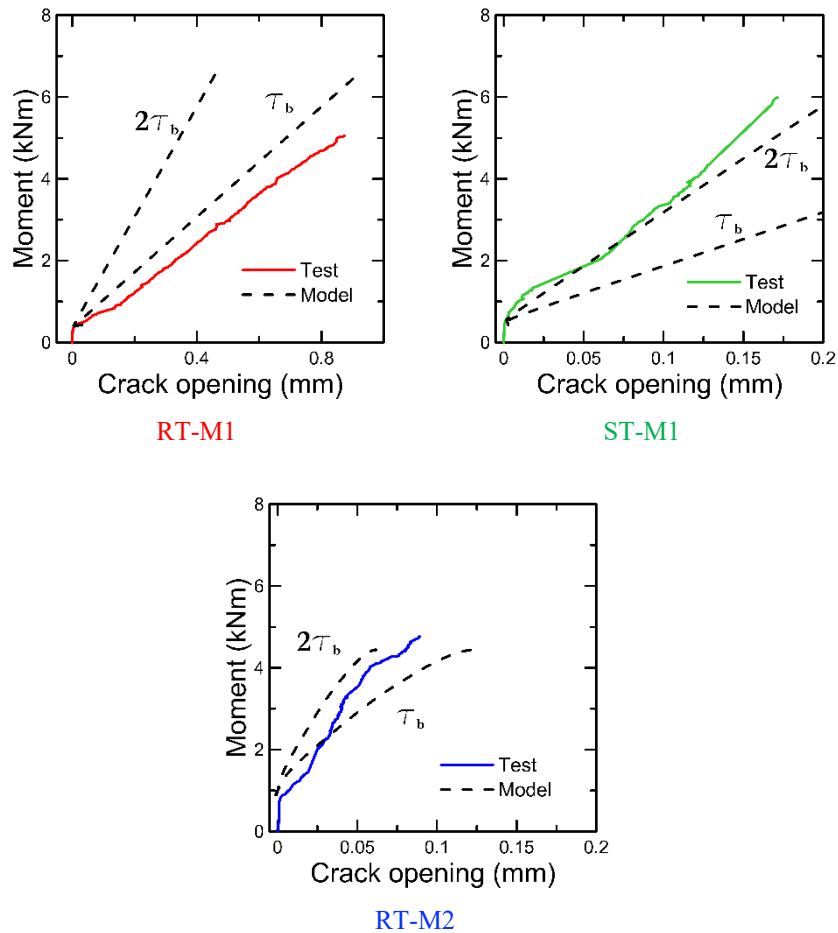


Figure 3.13– Comparison between moment vs crack opening relations obtained theoretically and experimentally.

In order to evaluate the applicability of proposed approach, comparison was made to experimental results available in literature, considering beams failing in bending: i) beam BV1 from Valeri et al. [33]; and ii) specimen D95 E38 tested in four-point bending from Preinstorfer et al. [8]. For appropriate comparison, cross-section geometry and material properties were adopted as reported by the authors. In both studies, $k_e = 0.8$ was adopted and cracking tensile strength was assumed equal to 2.5 MPa, obtained indirectly from the cracking moment. It can be seen, in Figure 14, that a good agreement was achieved in both cases, although the response obtained by Preinstorfer et al. [8] has been also influenced by local failure (spalling). Finally, using Eqs. 2 and 3 along with an estimated bond strength of 2.0 MPa (halfway between specimens RT-M1 and ST-M1), crack spacing and opening of 100 mm and 0.22 mm, respectively, were obtained for specimen D95 E38 for an applied moment of 30 kN.m, in comparison to the values of 66 mm and 0.19 mm obtained experimentally by Preinstorfer et al. [8]. Again, the theoretical predictions

would reduce and approach experimental results if the bond strength is increased to account for the influence of cross yarns.

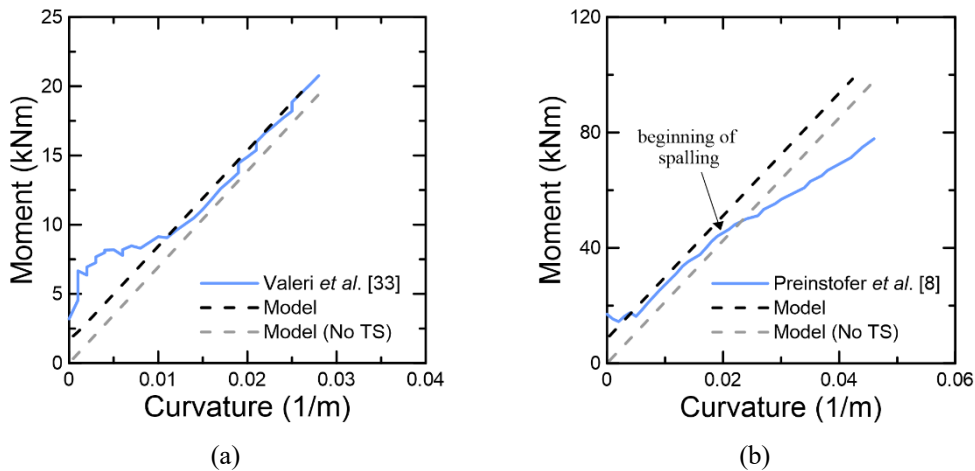


Figure 3.14 - Figure 3.14 – Comparison with experimental moment vs average curvature relations available in literature: a) Valeri et al. [33]; b) Preinstorfer et al. [8].

3.4. Conclusions

In the present work, the bending behavior of carbon-reinforced textile concrete I-beams for structural applications was studied and compared to the analytical model. From the experimental and theoretical results, the following conclusions can be drawn:

- 1) the effectiveness of the surface treatment in comparison to SBR laminated was confirmed by the stiffer and stronger interface obtained with sand-epoxy coating. The bond stress was 2.7 times greater than the reference yarn without extra impregnation. In addition, the impregnation improves the junction behavior, i. e., the connection between warp and weft yarns;
- 2) the use of SHCC matrix did not affect significantly the bond performance between carbon-textile and concrete. The addition of fibers in matrix was able to improve ductility and cracking load in carbon-TRC elements, yet it has not increased their load-bearing behavior. Slight changes during the uncracked stage was observed.
- 3) premature failure due to weak junction and the poor adhesion with the matrix in the RT-M1 beam was observed. The extra impregnation and the SHCC matrix changed the failure mode from shear to flexure-governed and crushing of

concrete, respectively. Wedge-sliding mechanism and cover spalling it was observed in RT-M2;

4) after cracking the use of sand-coating and SHCC were able to improve tension stiffening and crack control of structural members. They contributed to reduce crack spacings and openings, which were about 1/10 of the openings measured for the RT-M1 beam;

5) finally, a design model is proposed to evaluate the bending performance of the TRC beams based on RC-beam flexural-strength design including tension stiffening and cracking pattern response. Moment-curvature experimental and theoretical relations present good agreement for M1 beams. For the M2 beam, it is necessary to consider the premature softening mechanism through of a reduction factor. To measure crack opening in ST specimen, it is necessary to take into account the influence of the cross yarn. For M2 specimen, the cracking response it was more affected more the concrete residual tensile strength.

3.5. References

- [1] I. A. Peled, A. Bentur, B. Mobasher, Textile Reinforced Concrete, first ed., CRC Press (2017).
- [2] T. Triantafillou, Textile Fibre Composites in Civil Engineering, first ed., Woodhead Publishing (2016).
- [3] Brameshuber W, editor. Textile reinforced concrete – state of the art report, RILEM Technical Committee 201-TCR (2006).
- [4] B. Mobasher, Mechanics of Fiber and Textile Reinforced Cement Composites, CRC Press (2011). <https://doi.org/10.1201/b11181>.
- [5] A. Nanni, A. De Luca, H. J. Zadeh, Reinforced concrete with FRP bars: mechanics and design. CRC Press (2014).
- [6] ACI Committee 440, Guide for the Design and Construction of Structural Concrete Reinforced with Fiber-Reinforced Polymer Bars, Technical Report, American Concrete Institute, 2015.

- [7] P. Preinstorfer, B. Kromoser, J. Kollegger, Flexural behaviour of filigree slab elements made of carbon reinforced UHPC. *Constr. Build. Mater.* 199, (2019) 416–423. <https://doi.org/10.1016/j.conbuildmat.2018.12.027>.
- [8] J. Bielak, M. Schmidt, J. Hegger, F. Jesse, Structural Behavior of Large-Scale I-Beams with Combined Textile and CFRP Reinforcement, *Appl. Sci.*, 10 (13), (2020) 4625. <https://doi.org/10.3390/app10134625>.
- [9] S. Rempel, C. Kulas, J. Hegger, Extremely light and slender precast pedestrian bridge made out of textile-reinforced concrete (TRC). *High tech concrete: where technology and engineering meet*. Switzerland (Cham): Springer Verlag, (2017) 2530–2537. https://doi.org/10.1007/978-3-319-59471-2_288.
- [10] A. Scholzen, R. Chudoba, J. Hegger, Thin-walled shell structures made of textile-reinforced concrete: Part I: Structural design and construction, *Struct. Concr.* 16, (2015) 106–114. <https://doi.org/10.1002/suco.201300071>.
- [11] A. Scholzen, R. Chudoba, J. Hegger, Thin-walled shell structures made of textile-reinforced concrete: Part II: Experimental characterization, ultimate limit state assessment and numerical simulation, *Struct Concr.* 16, (2015) 106–114. <https://doi.org/10.1002/suco.201400046>.
- [12] E. Sharei, A. Scholzen, J. Hegger, R. Chudoba, Structural behavior of a lightweight, textile-reinforced concrete barrel vault shell, *Compos. Struc.* 171 (2017) 505-514. <http://dx.doi.org/10.1016/j.compstruct.2017.03.069>.
- [13] A. Schumann, H. Michler, F. Schladitz, M. Curbach, Parking slabs made of carbon reinforced concrete, *Struct. Conc.* 19 (2018) 647–655. <https://doi.org/10.1002/suco.201700147>.
- [14] N. W. Portal, L. N. Thrane, K. Lundgren, Flexural behaviour of textile reinforced concrete composites: experimental and numerical evaluation,

- Materials and Structures (2017) 50:4. <https://doi.org/10.1617/s11527-016-0882-9>.
- [15] A. Junes, A. Si Larbi, An experimental and theoretical study of sandwich panels with TRC facings: Use of metallic connectors and TRC stiffeners, *Eng. Struct.* 113, (2016) 174–185. <http://dx.doi.org/10.1016/j.engstruct.2016.01.042>
- [16] V. Dey, G. Zani, M. Colombo, M. Di Prisco, B. Mobasher, Flexural impact response of textile-reinforced aerated concrete sandwich panels, *Materials and Design* 86, (2015) 187–197. <http://dx.doi.org/10.1016/j.matdes.2015.07.004>.
- [17] I. G. Colombo, M. Colombo, M. di Prisco, Bending behaviour of Textile Reinforced Concrete sandwich beams, *Constr. Build. Mater.* 95, (2015) 675–685. <http://dx.doi.org/10.1016/j.conbuildmat.2015.07.169>.
- [18] O. Steinbock, S. May, M. Curbach, Vorgespannte Deckenelemente aus Carbonbeton Experimentelle Untersuchungen und Konzeption werkstoffgerechter Bauteile, *Beton- und Stahlbetonbau*, 114 (11), (2019) 817-826. <https://doi.org/10.1002/best.201900042>.
- [19] J. Hegger, C. Kulas, H. N. Schneider, W. Brameshuber, M. Hinzen, M. Raupach, T. Büttner, TRC pedestrian bridge-design, load-bearing behavior and production processes of a slender and light-weight construction, in: *Int. RILEM Conf. Mater. Sci., SARL*, (2010) 353–364.
- [20] T. Helbig, S. Rempel, K. Unterer, C. Kulas, J. Hegger, Pedestrian bridge made from carbon-concrete in Albstadt-Ebingen – First entirely carbon-reinforced concrete bridge worldwide, *Beton- und Stahlbetonbau* 111 (10), (2016) 676–685. <https://doi.org/10.1002/best.201600058>.
- [21] S. May, O. Steinbock, H. Michler, M. Curbach, Precast Slab Structures Made of Carbon Reinforced Concrete, *Structures* 18, (2019) 20–27.

<https://doi.org/10.1016/j.istruc.2018.11.005>.

- [22] M. Molter, Zum Tragverhalten von textilbewehrtem Beton. PhD thesis. Aachen, RWTH Aachen (2005).
- [23] S. Voss, Ingenieurmodelle zum Tragverhalten von textilbewehrtem Beton. PhD. Thesis, Aachen, RWTH Aachen (2008).
- [24] C. Kulas, Zum Tragverhalten getränkter textiler Bewehrungselemente für Betonbauteile. PhD Thesis, Aachen, RWTH Aachen (2013).
- [25] S. Voss, J. Hegger, Dimensioning of textile reinforced concrete structures. In: 1st Int. RILEM Symposium on Textile Reinforced Concrete, RILEM Publications, Aachen, Germany, (2006) 151–160. J. Hegger, M. Zell, M. Horstmann, Textile reinforced concrete—realization in applications. In: International fib Symposium Tailor Made Concrete Structures: New Solutions for our society, (2008) 357–362.
- [26] J. Hegger, N. Will, M. Schneider, Textilbeton: Tragverhalten—Bemessung—Sicherheit. Textilbeton in Theorie und Praxis. Tagungsband zum 6, (2011) 269–284.
- [27] J. Hegger, S. Voss, Investigations on the bearing behaviour and application potential of textile reinforced concrete. Eng. Struct. 30, (2008) 2050–2056.
- [28] S. Rempel, Zur Zuverlässigkeit der Bemessung von Biegebeanspruchten Betonbauteilen mit Textiler Bewehrung. PhD. Thesis, Aachen, RWTH Aachen (2018).
- [29] I. Giorgia Colombo, M. Colombo, M. di Prisco¹, F. Pouyaei, Analytical and numerical prediction of the bending behaviour of textile reinforced concrete sandwich beams, J. of Build. Eng. 17, (2018) 183–195. <https://doi.org/10.1016/j.jobbe.2018.02.012>.

- [30] B. Kromoser, P. Preinstorfer, J. Kollegger, Building lightweight structures with carbon-fiber-reinforced polymer-reinforced ultra-high-performance concrete: Research approach, construction materials, and conceptual design of three building components, *Struct. Concr.* 20 (2), (2019) 730-744. <https://doi.org/10.1002/suco.201700225>.
- [31] P. Valeri, M. F. Ruiz, A. Muttoni, Modelling of Textile Reinforced Concrete in bending and shear with Elastic- Cracked Stress Fields, *Eng. Struct.* 215, (2020) 110664. <https://doi.org/10.1016/j.engstruct.2020.110664>.
- [32] R. Muhamad, M. S. M. Ali. D. Oehlers, A. H. Sheikh, Load-slip relationship of tension reinforcement in reinforced concrete members, *Eng. Struct.* 33, (2011) 1098–1106. doi:10.1016/j.engstruct.2010.12.022.
- [33] H. Aydin, R. J. Gravina, P. Visintin, A partial-interaction approach for extracting FRP-to-concrete bond characteristics from environmentally loaded flexural tests, *Comp. Part B* 132, (2018) 214-228. <http://dx.doi.org/10.1016/j.compositesb.2017.09.018>
- [34] M. Haskett, D. J. Oehlers, M.S. M. Ali, Local and global bond characteristics of steel reinforcing bars, *Eng. Struct.* 30, (2008) 376–383. <https://doi.org/10.1016/j.engstruct.2007.04.007>.
- [35] J. A.O. Barro, M. Taheri, H. Salehian, A model to simulate the moment–rotation and crack width of FRC members reinforced with longitudinal bars, *Eng. Struct.* 100, (2015) 43–56. <http://dx.doi.org/10.1016/j.engstruct.2015.05.036>.
- [36] D. J. Oehlers, P. Visintin, J. F. Chen, T. J. Ibell, Simulating reinforced concrete members. Part 1: partial interaction properties. *Proceedings of the Institution of Civil Engineers-Structures and Buildings*, 167 (11), (2014) 646-

653. <https://doi.org/10.1680/stbu.13.00071>.
- [37] D. J. Oehlers, P. Visintin, J. F. Chen, T. J. Ibell, Simulating reinforced concrete members. Part 2: Displacement-based analyses. *Proceedings of the Institution of Civil Engineers-Structures and Buildings*, 167 (12), (2014) 718-727. <https://doi.org/10.1680/stbu.13.00072>.
- [38] D. J. Oehlers, P. Visintin, M. Haskett, W. M. Sebastian, Flexural ductility fundamental mechanisms governing all RC members in particular FRP RC, *Constr. Build. Mater.* 49, (2013) 985–997. <http://dx.doi.org/10.1016/j.conbuildmat.2013.02.018>.
- [39] P. Visintin, D. J. Oehlers, Fundamental mechanics that govern the flexural behaviour of reinforced concrete beams with fibre-reinforced concrete, *Adv. in Struct. Eng.* 21 (7), (2018) 1088-1102. <https://doi.org/10.1177/1369433217739705>.
- [40] S. De Santis, H.A. Hadad, F. De Caso y Basalo, G. De Felice, A. Nanni, Acceptance criteria for tensile characterization of fabric-reinforced cementitious matrix systems for concrete and masonry repair, *J. Compos. Constr.* 22 (6), (2018) 04018048. [https://doi.org/10.1061/\(ASCE\)CC.1943-5614.0000886](https://doi.org/10.1061/(ASCE)CC.1943-5614.0000886).
- [41] F. Jesse, N. Will, M. Curbach, J. Hegger, Load-bearing behavior of textile-reinforced concrete. *ACI Structural Journal* (250), (2008) 59-68.
- [42] M. Hinzen, W. Brameshuber, Improvement of Serviceability and Strength of Textile Reinforced Concrete by Using Short Fibres. In *Proceedings of the 4th Colloquium on Textile Reinforced Structures*, (2009) 261–272.
- [43] I. G. Colombo, A. Magri, G. Zani, M. Colombo, M. di Prisco, Erratum to: Textile Reinforced Concrete: experimental investigation on design parameters.

- Materials and structures, 46 (11), (2013) 1953-1971.
<http://dx.doi.org/10.1617/s11527-013-0017-5>.
- [44] M. C. Rampini, G. Zani, M. Colombo, M. di Prisco, Mechanical Behaviour of TRC Composites: Experimental and Analytical Approaches, *Appl. Sci.* 9, (2019) 1492. <https://doi.org/10.3390/app9071492>.
- [45] A. Peled, Z. Cohen, Y. Pasder, A.s Roye, T. Gries, Influences of textile characteristics on the tensile properties of warp knitted cement based composites, *Cem. and Conc. Compos.* 30, (2008) 174–183.
<https://doi.org/10.1016/j.cemconcomp.2007.09.001>.
- [46] P. Valeri, M. F. Ruiz, A. Muttoni, Tensile response of textile reinforced concrete, *Constr. Build. Mater.* 258, (2020) 119517.
<https://doi.org/10.1016/j.conbuildmat.2020.119517>.
- [47] P. Valeri, M. F. Ruiz, A. Muttoni, Experimental research on textile reinforced concrete for the development of design tools, *Proceedings of the 12th fib international PhD symposium in civil engineering*, (2018) 169-176.
- [48] P. Valeri, M. R. Fernández, A. Muttoni, New perspectives for design of lightweight structures by using textile reinforced concrete, in: *Proceedings of the Fib Symposium Fédération Internationale du Béton (fib)*, (2019) 73–80.
- [49] D. Arboleda, F. G. Carozzi, A. Nanni, C. Poggi, Testing Procedures for the Uniaxial Tensile Characterization of Fabric-Reinforced Cementitious Matrix Composites, *J. Compos. Constr.* 20 (3), (2016) 04015063.
[https://doi.org/10.1061/\(ASCE\)CC.1943-5614.0000626](https://doi.org/10.1061/(ASCE)CC.1943-5614.0000626).
- [50] M. Krüger, H. W. Reinhardt, M. Fichtlscherer, Bond behaviour of textile reinforcement in reinforced and prestressed concrete. *Otto-Graf-Journal* (12), (2001) 33-50.

- [51] M. Raupach, J. Orłowski, T. Büttner, U. Dilthey, M. Schleser, J. Hegger, Epoxy-impregnated textiles in concrete-load bearing capacity and durability. In 1st International RILEM Conference on Textile Reinforced Concrete (ICTRC), RILEM Publications SARL, (2006) 77-88. <https://doi.org/10.1617/2351580087.008>.
- [52] U. Dilthey, M. Schleser, J. Hegger, S. Voss, Load-bearing behaviour of polymer-impregnated textiles in concrete. In Proceedings of the fifth international RILEM workshop (HPFRCC5 PRO53), RILEM Publications SARL, Mainz (2007) 183-192
- [53] J. Wagner, M. Curbach, Bond Fatigue of TRC with Epoxy Impregnated Carbon Textiles, Appl. Sci. 9, (2019) 1980. <https://doi.org/10.3390/app9101980>.
- [54] J. Bielak, Y. Li, J. Hegger, R. Chudoba, Characterization Procedure for Bond, Anchorage and Strain-Hardening Behavior of Textile-Reinforced Cementitious Composites, Proceedings 2, (2018) 395. <https://doi.org/10.3390/ICEM18-05224>.
- [55] M. Schleser, B. W. Lauffer, M. Raupach, U. Dilthey, Application of Polymers to Textile-Reinforced Concrete, J. Mater. Civ. Eng. 18 (5), (2006) 670-676. [https://doi.org/10.1061/\(ASCE\)0899-1561\(2006\)18:5\(670\)](https://doi.org/10.1061/(ASCE)0899-1561(2006)18:5(670)).
- [56] D. Dvorkin, A. Poursaeed, A. Peled, W.J. Weiss, Influence of bundle coating on the tensile behavior, bonding, cracking and fluid transport of fabric cement-based composites, Cem. and Conc. Compos 42, (2013) 9–19. <http://dx.doi.org/10.1016/j.cemconcomp.2013.05.005>.
- [57] D. Dvorkin, A. Peled, Effect of reinforcement with carbon fabrics impregnated with nanoparticles on the tensile behavior of cement-based

- composites, *Cem. Conc. Research* 85, (2016) 28–38.
<http://dx.doi.org/10.1016/j.cemconres.2016.03.008>.
- [58] M. Halvaei, M. Latifi, M. Jamshidi, Study of the microstructure and flexural behavior of cementitious composites reinforced by surface modified carbon textiles, *Constr. Build. Mater.* 158, (2018) 243–256.
<https://doi.org/10.1016/j.conbuildmat.2017.10.044>.
- [59] K. Schneider, A. Michel, M. Liebscher, L. Terreri, S. Hempel, V. Mechtcherine, Mineral-impregnated carbon fibre reinforcement for high temperature resistance of thin-walled concrete structures, *Cem. and Conc. Compos.* 97, (2019) 68–77.
<https://doi.org/10.1016/j.cemconcomp.2018.12.006>.
- [60] G. Perry, G. Dittel, T. Gries, Y. Goldfeld, Mutual Effect of Textile Binding and Coating on the Structural Performance of TRC Beams, *J. Mater. Civ. Eng.* 32 (8), (2020) 04020232. [https://doi.org/10.1061/\(ASCE\)MT.1943-5533.0003331](https://doi.org/10.1061/(ASCE)MT.1943-5533.0003331).
- [61] S. Sueki, C. Soranakom, B. Mobasher, A. Peled, Pullout-Slip Response of Fabrics Embedded in a Cement Paste Matrix, *J. Mater. Civ. Eng.* 19 (9), (2007) 718-727. [https://doi.org/10.1061/\(ASCE\)0899-1561\(2007\)19:9\(718\)](https://doi.org/10.1061/(ASCE)0899-1561(2007)19:9(718)).
- [62] N. W. Portal, I. F. Perez, L. N. Thrane, K. Lundgren, Pull-out of textile reinforcement in concrete, *Constr. Build. Mater.* 71, (2014) 63–71.
<http://dx.doi.org/10.1016/j.conbuildmat.2014.08.014>.
- [63] A. Dalalbashia, B. Ghiassib, D. V. Oliveira, A. Freitas, Effect of test setup on the fiber-to-mortar pull-out response in TRM composites: Experimental and analytical modeling, *Comp. Part B* 143, (2018) 250–268.
<https://doi.org/10.1016/j.compositesb.2018.02.010>.

- [64] C. M. Cruz, M. Raupach, Influence of the surface modification by sanding of carbon textile reinforcements on the bond and load-bearing behavior of textile reinforced concrete, *MATEC Web of Conferences* 289, 04006 (2019). <https://doi.org/10.1051/mateconf/201928904006>.
- [65] J. Donnini, V. Corinaldesi, A. Nanni, Mechanical properties of FRCM using carbon fabrics with different coating treatments, *Comp. Part B* (88), (2016) 220-228, <https://doi.org/10.1016/J.COMPOSITESB.2015.11.012>.
- [66] Bielak J, Li Y, Hegger J, Chudoba R., Characterization procedure for bond, anchorage and strain-hardening behaviour of textile-reinforced cementitious composites. *ICEM Proc* 2 (8), (2018) 395. <https://doi.org/10.3390/ICEM18-05224>.
- [67] R. M. de C. Silva, F. de A. Silva, Carbon textile reinforced concrete: materials and structural analysis. *Materials Structures* (530), (2020) 1-17. <https://doi.org/10.1617/s11527-020-1448-4>.
- [68] S. L. Xu, M. Krüger, H. W. Reinhardt, J. Ožbolt, Bond characteristics of carbon, alkali resistant glass, and aramid textiles in mortar, *J. Mater. Civ. Eng.* 16 (4) (2004) 356–364. [https://doi.org/10.1061/\(ASCE\)0899-1561\(2004\)16:4\(356\)](https://doi.org/10.1061/(ASCE)0899-1561(2004)16:4(356)).
- [69] Q. Li, S. Xu, Experimental research on mechanical performance of hybrid fiber reinforced cementitious composites with polyvinyl alcohol short fiber and carbon textile, *J. Compos. Mater.* 45 (1), (2011) 5–28. <https://doi.org/10.1177/0021998310371529>.
- [70] S. P. Yin, S. L. Xu, H. D. Li, Improved mechanical properties of textile reinforced concrete thin plate, *J. Wuhan Univ. Technol. -Mater. Sci. Ed.* 28 (1), (2013) 92–98. <https://doi.org/10.1007/s11595-013-0647-z>.

- [71] R. Barhum, V. Mechtcherine, Effect of short, dispersed glass and carbon fibres on the behaviour of textile-reinforced concrete under tensile loading. *Eng Fract Mech* (92), (2012) 56–71. <https://doi.org/10.1016/j.engfracmech.2012.06.001>.
- [72] Y. Yao, F.A. Silva, M. Butler, V. Mechtcherine, B. Mobasher, Tension stiffening in textile-reinforced concrete under high speed tensile loads, *Cem. and Concr. Compos.* 44, (2015) 49-61, <http://dx.doi.org/10.1016/j.cemconcomp.2015.07.009>.
- [73] T. Gong, A. A. Heravi, G. Alsous, I. Curosu, V. Mechtcherine, The impact-tensile behavior of cementitious composites reinforced with carbon textile and short polymer fibers, *Appl. Sci.* 9 (19), (2019) 4048, <https://doi.org/10.3390/app9194048>.
- [74] T. Gong, A. Hamza, I. Curosu, On the synergetic action between strain-hardening cement-based composites (SHCC) and carbon textile reinforcement. In: 10 th International Conference on Fracture Mechanics of Concrete and Concrete Structures FraMCoS-X, (2019) 23–26.
- [75] I. Curosu, Influence of Fiber Type and Matrix Composition on the Tensile Behavior of Strain-Hardening Cement-Based Composites (SHCC) under Impact Loading. Ph.D. Thesis, Technische Universität Dresden (2017).
- [76] D. Zhu, S. Liu, Y. Yao, G. Li, Y. Du, C. Shi, C., Effects of short fiber and pre-tension on the tensile behavior of basalt textile reinforced concrete. *Cem. and Concr. Compos.* 96, (2019) 33-45. <https://doi.org/10.1016/j.cemconcomp.2018.11.015>.
- [77] F. de A. Silva, M. Butler, V. Mechtcherine, D. Zhu, B. Mobasher, Strain rate effect on the tensile behaviour of textile-reinforced concrete under static and

- dynamic loading. *Mater Sci Eng A* 528, (2011) 1727–1734.
<https://doi.org/10.1016/j.msea.2010.11.014>.
- [78] R. Barhum, V. Mechtcherine, Influence of short dispersed and short integral glass fibres on the mechanical behaviour of textile-reinforced concrete. *Materials and Structures* (46), (2013) 557–572. <https://doi.org/10.1617/s11527-012-9913-3>.
- [79] ASTM C39 / C39M-18, Standard Test Method for Compressive Strength of Cylindrical Concrete Specimens, ASTM International, West Conshohocken, PA, 2018, www.astm.org.
- [80] B. Mobasher, J. Pahilajani, J., A. Peled, Analytical simulation of tensile response of fabric reinforced cement based composites. *Cem. and Conc. Comp.* 28 (1), (2006) 77-89. <https://doi.org/10.1016/j.cemconcomp.2005.06.007>.
- [81] C. Soranakom, B. Mobasher, Modeling of tension stiffening in reinforced cement composites: Part I. Theoretical modeling. *Materials and Structures*, 43 (9), (2010) 1217-1230. <https://doi.org/10.1617/s11527-010-9594-8>.
- [82] C. Soranakom, B. Mobasher, Modeling of tension stiffening in reinforced cement composites: Part II. Simulations versus experimental results. *Materials and Structures*, 43 (9), (2010) 1231-1243. <https://doi.org/10.1617/s11527-010-9593-9>.
- [83] GOM Correlate. GOM—Precise Industrial 3D Metrology. Braunschweig, Germany Available at: <https://www.gom.com/index.html>. (Accessed: 30th September 2019).
- [84] F. C. A. Santos, Behavior of Textile Reinforced Concrete (TRC) Slender Columns Subject to Compression. Pontificia Universidade Católica do Rio de Janeiro (2018).

- [85] D. C. Cardoso, G. B. Pereira, F. de A. Silva, J. J. Silva Filho, E. V. Pereira, Influence of steel fibers on the flexural behavior of RC beams with low reinforcing ratios: Analytical and experimental investigation. *Compos. Struct.* 222, (2019) 110926. <https://doi.org/10.1016/j.compstruct.2019.110926>.
- [86] fib, fib Model Code for Concrete Structures 2010, Wiley-VCH Verlag GmbH & Co. KGaA, Weinheim, Germany (2013). <https://doi.org/10.1002/9783433604090>.
- [87] F. Focacci, T. D'Antino, C. Carloni, Analytical modelling of the tensile response of PBO-FRCM composites. In Conference of the Italian Association of Theoretical and Applied Mechanics, (2019) 527-536. https://doi.org/10.1007/978-3-030-41057-5_43.
- [88] J. A.O. Barros, M. Taheri, H. Salehian, A model to simulate the moment–rotation and crack width of FRC members reinforced with longitudinal bars, *Eng. Struct.* 100, (2015) 43–56. <http://dx.doi.org/10.1016/j.engstruct.2015.05.036>.
- [89] C. Soranakom, B. Mobasher, Geometrical and mechanical aspects of fabric bonding and pullout in cement composites, *Materials and Structures* 42, (2009) 765–777. <https://doi.org/10.1617/s11527-008-9422-6>.
- [90] A. Peled, A. Bentur, D. Yankelevsky, Effects of Woven Fabric Geometry on the Bonding Performance of Cementitious Composites, *Adv. Cement Bas. Mat.* (7), (1998) 20–27. [https://doi.org/10.1016/S1065-7355\(97\)00012-6](https://doi.org/10.1016/S1065-7355(97)00012-6).

4 Material characterization of carbon-TRC composites

4.1. Introduction

Textile Reinforced Concrete (TRC) composites consist of one or more layers of fabric reinforcement embedded in an inorganic matrix. This is a mixture made of fine-grained concrete with a high dosage of cementitious and fly ash that could be enriched with short fibers. Comparing to conventional reinforced concrete structures, TRC has become attractive due to the use of a high-strength and corrosion-resistant reinforcement [1,2], leading to reduced maintenance costs. This composite material also allows the fabrication of thin-walled structures and components, reducing costs of transportation and erection. Another advantage is related to the possibility of building more climate-friendly constructions due to the smaller concrete cover required for TRC members. In addition, low clinker content cement may be used, since the fabric does not need passivation by the concrete, thus reducing CO₂ emissions [3].

Fabrics are usually composed of synthetic fibers (e.g., carbon, aramid, basalt, AR-glass, PBO) that can be impregnated for protection and durability. The coating or impregnation also leads to a better activation of inner filaments within the yarn and to an improved bond between textile and cement matrix, playing a substantial role in mechanical response of the composite [4,5]. Another important factor that could influence the mechanical response of the composite is the mesh opening and the cross section of the roving [6,7].

Since there is no specific standard or code for the mechanical characterization or design of TRC composites, different material characterization methods, specimens' geometries and procedures to measure the deformation and crack pattern have been used for different research groups, with variations in results. Since the release of the state-of-art report prepared by RILEM Technical Committee TC 201-TRC [1], many other techniques and approaches have been proposed by researchers worldwide. Currently, a new report is being prepared by

the Technical Committee 292-MCC: Mechanical Characterization and Structural design of Textile Reinforced Concrete.

TRC presents a unique behavior and the design of structural elements depends on the complete characterization of the constituent materials, as well as of their interface. The fabric and the matrix can be characterized by simple uniaxial tensile and compressive tests, respectively, whereas pullout and tensile tests can be adopted to characterize the interface and the composite, respectively. Although the presence of the fabric within matrix may affect composite's compressive strength, few works have addressed this topic [3,8–11].

Besides the constituents properties, there are several factors that influence the tensile performance of the TRC such as load introduction, specimen geometry and fabrication [5,12–16]. Important parameters can be derived from this test for the design of the TRC structures, such as the composite strength and deformation at failure, effective modulus and cracking pattern (e.g., first crack stress, crack width and spacing with loading). Other important variables that affect the tensile response are the anchorage and gauge lengths [17,18].

Regarding the compressive characterization of the textile reinforced concrete, little information can be found in the literature [3, 9-12]. Valeri et al. [3] performed uniaxial compression tests in TRC plates with 60x60x30 mm (length x width x thickness). On the other hand, Hawkins et al. [10] investigated the influence of load application eccentricity in TRC specimen with two layers of textiles with 200x15/30x15/30. Santos [11] analyzed the compression behavior of I-section columns and it was proposed the adaptation of a combined loading compression (CLC) test setup. Finally, Pinheiro [19] used CLC test to analyze the compression behavior of TRC with curaua fibers.

The fabric characteristics have a strong influence on the bond behavior and the results obtained from single yarns may not correspond to the actual fabric response. Thus, new yarn pullout test configurations are constantly proposed [20–22]. Traditionally, the bond behavior between matrix-fiber is characterized through pullout tests and several authors performed this test to better understand the interface behavior of fiber-reinforced cementitious matrix composites. Despite this, there is still a lot of divergence in the literature regarding the most appropriate test setup. The more traditional pullout test consists in a single yarn test [23–25], but

some studies also performed tests with pullout of yarn from textile to evaluate the influence of textile structure [20,21].

For successful application of TRC as a structural material, validated design methods based on appropriate values of mechanical and bond properties determined through experimental tests are required. Nevertheless, there is still a gap in the knowledge regarding this correlation between characterization techniques and structural design approaches. Thus, the objective of the present research is to compare the constitutive laws obtained through different techniques for various carbon-TRC materials. Finally, the parameters obtained from tests are used to predict the response of carbon-TRC beams flexural and the predictions are validated against experimental results.

4.2. Experimental program

4.2.1. Materials

The fine-grained cement matrix adopted in the present work has been detailed in a previous work [26]. It was composed by the Brazilian Portland cement CII F-32, fly ash, micro silica and a fine aggregate natural sand with 1.18 mm maximum diameter. This mixture composition leads to a matrix with a flow table spreading of 345 mm and cylinder compression tests revealed a compressive strength of 76 ± 2.6 MPa and a modulus of elasticity of 28.4 ± 0.8 GPa at 28 days. The characterization was performed using a servo hydraulic testing machine MTS 810 with load capacity of 500 kN.

Four carbon fabrics were used in the study, with differences in mesh dimensions, yarn shape and type of coating or impregnation. Regarding the impregnation, fabrics with styrene-butadiene rubber (SBR), acrylate (ACR), epoxy resin (EPX) were used, as well as an SBR textile with extra sand-coating (SND) manually applied. Figure 4.1 shows the different configurations for the bidirectional textiles considered. Table 4.1 reported the nominal properties for EPX fabric was provided by manufacturers and for SBR and ACR were reported by [39]. In addition, the measured properties by authors were added, i.e, warp and weft area and warp perimeter.

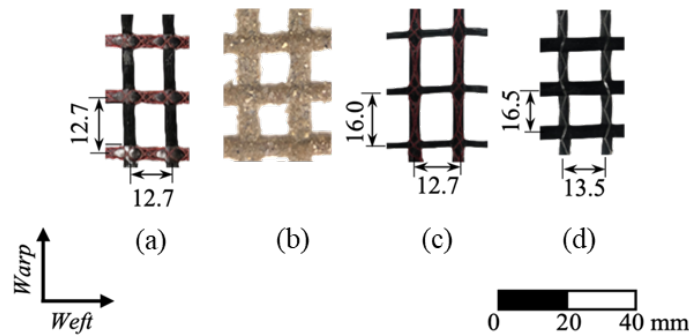


Figure 4.1 -Carbon fabrics with different coating conditions: a) SBR, b) SND, c) ACR and d) EPX.

Table 4.1 - Carbon fabric properties.

	SBR	ACR	EPX
Tensile strength (MPa)	1638	2911	2700
Modulus of Elasticity (GPa)	126	162	250
Warp Yarn area (mm ²)	3.34	1.80	5.44
Weft Yarn area (mm ²)	3.30	0.45	3.85
Warp Perimeter (mm)	3.24	2.81	9.06

4.2.2. Composite characterization

4.2.2.1. Bond properties

To obtain the nominal bond stress (τ_b) and to characterize the interface of different carbon fabrics, pullout tests with the single warp yarn embedded in the matrix were performed. A servo hydraulic MTS 810 Universal Machine with a load capacity of 250 kN was used and tests were conducted at a displacement rate of 1.5 mm/min. A 2.5 kN load cell was used to improve accuracy of load acquisition. The specimens consist in small cylinder having 25 mm x 20 mm (diameter x height) made of cement matrix and a carbon yarn embedded 20 mm. Figure 4.2 presents the test setup used and the specimen dimensions. The average bond stress was calculated dividing the pullout force by the yarn surface area (perimeter multiplied by nominal embedded length). Ten samples were tested for each type of textile.

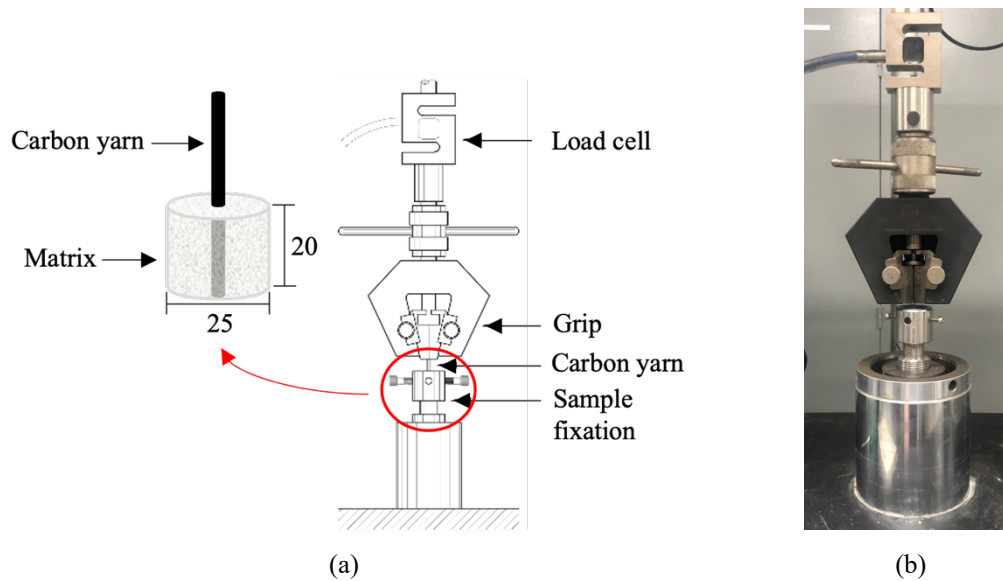


Figure 4.2 - Pullout test: (a) Set up scheme and dimensions (in mm) and (b) overview of test setup.

4.2.2.2. Compression Test

To evaluate the influence of the textile on the compressive strength of the matrix, compressive tests on TRC prisms with one fabric layer having two longitudinal yarns were performed. Prismatic samples were considered and three different testing conditions were considered: i) direct compression on samples cut from undamaged portions of the web of I-section tested in a previous work [26]; ii) directed compression on specimens extracted from plates; and iii) combined loading compression (CLC) tests on specimens extracted from plates. For conditions (ii) and (iii), only SBR textile was studied, whereas all types of textiles were considered in condition (i). The second condition was performed to analyze the influence of the casting process on the compressive strength of the matrix, while the latter to analyze the influence of test setup.

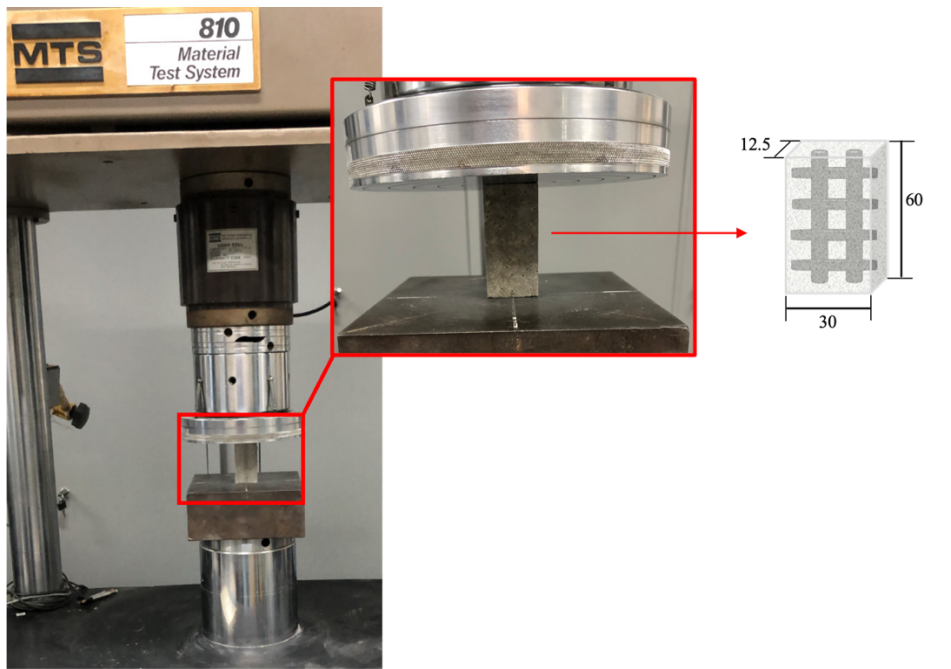
Figure 4.3a shows an overview of setup test for (i) and (ii) conditions, where specimens having 12.5x30x60 mm (thickness x width x length) were tested. The mean compressive strength in each case was obtained from an average of five samples. CLC tests adapted from the ASTM D6641 [30] and illustrated in Figure 4.3b were performed on samples of extracted from 10-mm thick plates with a single textile layer in the middle. Two different unsupported lengths were adopted for the TRC samples tested in the present research: 30 and 40 mm. In all, six specimens were tested, three for each aforementioned condition. For control, three additional

samples of plain matrix and unsupported length of 30 mm were also adopted. Table 4.2 summarizes the tests, number of specimens and geometries considered in the study.

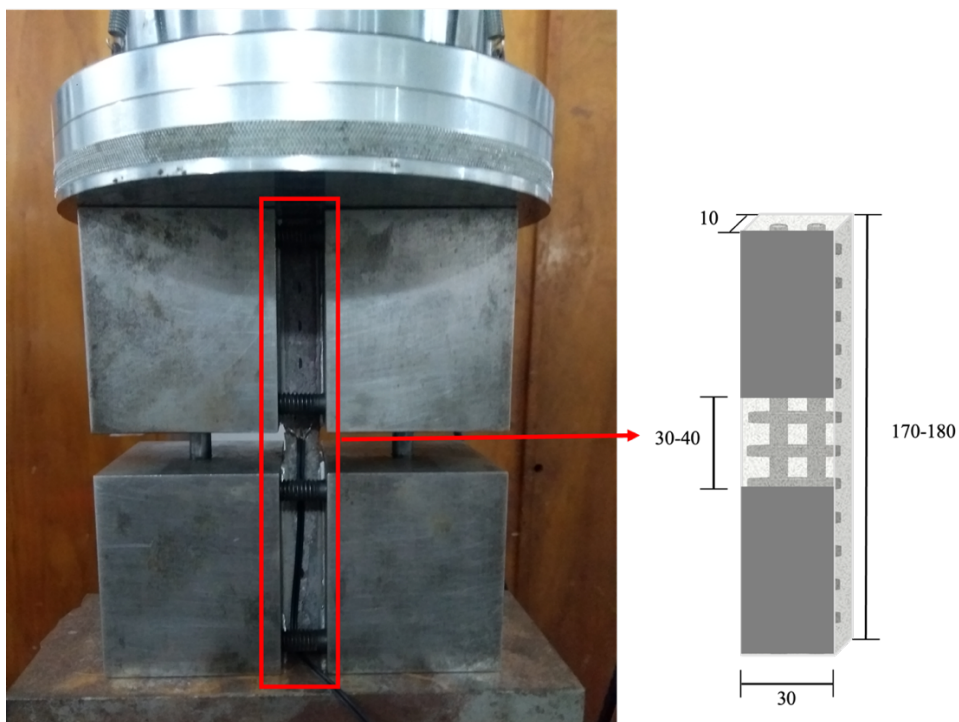
All tests were conducted at a constant displacement rate of 0.3 mm/min up to failure in a servo hydraulic testing machine MTS 810 with load capacity of 500 kN. Table 4.2 shows the nomenclature adopted, which includes the type of coating (SBR, SND, ACR or EPX) and type of specimen (B- prisms cut out from beams, P- prisms cut from plates and C- prisms for CLC tests). For TRC samples, the yarn in the direction of compressive force direction was distinguished, e.g. longitudinal - L (warp) and transversal - T (weft). The specimens of CLC test also were distinguished by unsupported lengths for the TRC samples tested: 30 or 40 mm. For example, specimen SBR-C-30-L refers to the composite with SBR-fabric tested, CLC setup, unsupported lengths of 30 mm and longitudinal yarn parallel to compressive force; and ACR-B-T refers to the composite with ACR-fabric prisms cut of beams in transversal yarn in the direction of compressive force.

Table 4.2 - Summary of specimen tested in the compression test.

Specimen ID	Specimen	Set-up Test	Yarn Direction	Width (mm)	Thickness (mm)	Length (mm)
M-P	Plain Matrix	Uniaxial compression	-	30	12.5	60
M-C-30			-	30	10	170
SBR-C-30-L	SBR-TRC	CLC	Warp	30	10	170
SBR-C-40-L			Warp	10	10	180
SBR-P-L			Warp	30	12.5	60
SBR-B-L			Warp	30	12.5	60
SBR-P-T			Weft	30	12.5	60
SBR-B-T			Weft	30	12.5	60
SND-B-L			SND-TRC	Uniaxial compression	Warp	30
SND-B-T	Weft	30			12.5	60
ACR-B-L	ACR-TRC		Warp	30	12.5	60
ACR-B-T			Weft	30	12.5	60
EPX-B-L	EPX-TRC		Warp	30	12.5	60
EPX-B-T			Weft	30	12.5	60



(a)



(b)

Figure 4.3 - Overview of test setup of (a) compression test and specimen dimensions (in mm) and (b) CLC test and specimen dimensions (in mm).

4.2.2.3. Tensile Test

Direct tensile tests were carried out to derive the composite constitutive relationship in tension. First, all specimens having 120 mm of width and 1000 mm

long were produced with a single textile layer in the middle of the thickness using a hand-lamination technique. All textiles described in Section 4.2.1 were considered. To ensure that the material rupture occurred in the central section, i.e. avoiding premature failure near grips, the samples had their thickness reduced at this region, using two aluminum plates of 500 x 120 x 2 mm on each side. Therefore, samples were 14-mm thick in the central region and 18-mm thick at the ends. In the gauge area, considering the longitudinal yarns, volume fractions of 1.99, 1.08, 2.29 % were ensured for SBR/SND, ACR and EPX, respectively.

The tensile tests were performed on a universal mechanical testing machine model MTS 311 with a loading capacity of 1000 kN. Clevis grip load introduction method was adopted at the ends, according to ACI434.13 [27]. The samples were pressed over an area of 120 x 250 mm with torques defined according to the fabric adopted, as shown in Table 4.3. A rough surface was introduced on the clamping area to increase friction and prevent slippage of the plates. Before the test, specimens were aligned and a preload of 0.2 kN was applied. The test was conducted under displacement control at a rate of 0.5 mm/min, up to failure. A pair of displacement transducers was coupled to the specimen to measure its deformation over the 450-mm gage length. Figure 4.4 shows the test setup and the dimensions adopted.

To assess the crack formation and growth over the gage length, in addition to the visual control, the digital image correlation (DIC) technique was adopted. The setup consisted in a Canon camera model EOS Rebel T6, positioned with direct framing for the tests and configured to record an image every 10 seconds, together with a LED light source to provide uniform lighting during the test, as shown in Figure 4b. The images were analyzed using GOM Correlate [28] software, with the purpose of obtaining information about the crack formation and evolution with the applied load.

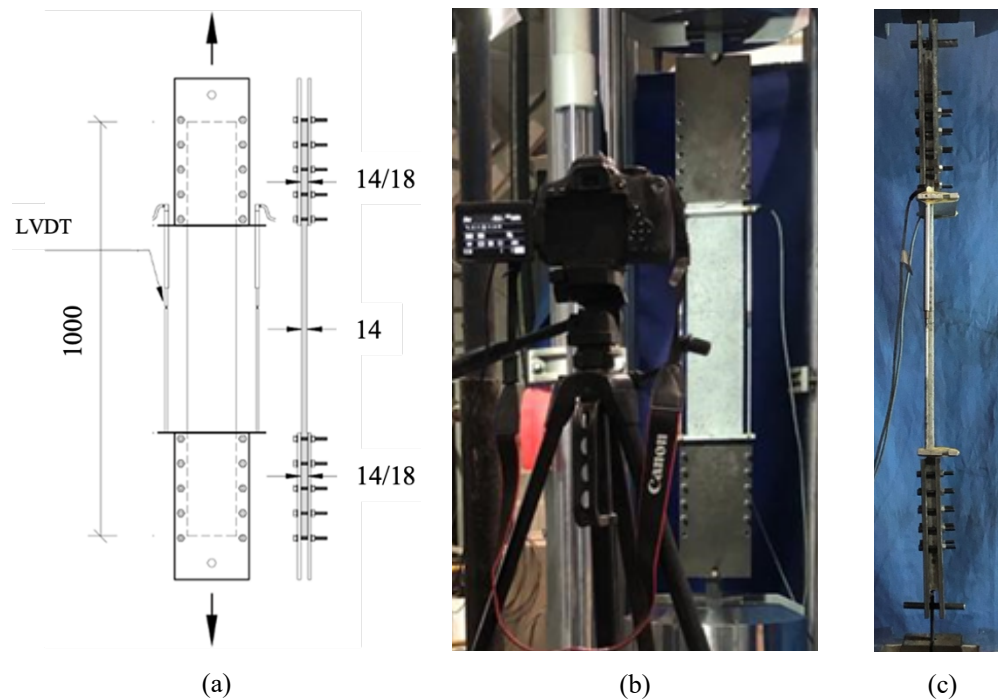


Figure 4.4 - Tensile Test: (a) dimensions (in mm), (b) DIC scheme and (c) clevis grip detail.

In order to analyze the influence of the different testing configurations on TRC properties, SBR specimens were tested in three additional conditions, as shown in Table 3. In these cases, specimens were fabricated with a width of 80 mm, with little influence of the reinforcing ratio. The three conditions are characterized by: i) bolted ends with anchorage and gauge lengths of 250 and 400 mm; ii) glued ends with anchorage and gauge lengths equal to condition (i); and iii) glued ends with anchorage and gauge lengths of 400 and 100, respectively (Figure 5).

Table 3 summarizes the specimens tested in this study. The nomenclature adopted includes the type of coating (SBR, SND, ACR or EPX), type of clamp grip (S - screws or G - tabs glued), width (120 or 80), and the gauge length. For example, SBR-S-80-400 specimen refers to the composite with SBR-fabric tested, screws clamping, dimensions of 80 x 14 mm and gauge length of 400 mm.

Table 4.3 - Summary of specimens tested under direct tension.

Specimen ID	Coating	Clamp grip	Torque (Nm)	Width (mm)	Thickness (mm)	L _{anch} (mm)	Gauge Length (mm)	Fiber strands (FS)	ρ_f (%)
SBR-S-120-450		Screws	13	120	14	250	450	10	1.99
SBR-S-80-400	styrene	(S)	13	80	14	250	400	7	2.09
SBR-G-80-100	butadiene	tabs	-	80	14	400	100	7	2.09
SBR-G-80-400	rubber	Glued (G)	-	80	14	250	400	7	2.09
SND-S-120-450	sand-epoxy	Screws (S)	15	120	14	250	450	10	1.99
ACR-S-120-450	acrylate		15	120	14	250	450	10	1.07
EPX-S-120-450	epoxy		18	120	14	250	450	10	2.29

**Figure 4.5 - Tensile test with steel tabs glued with different gauge lengths.**

4.3. Results and Discussions

4.3.1. Pullout Test

Representative bond stress vs slip curves obtained from pullout tests for all materials considered are shown in Figure 4.6. Table 4.4 summarizes the results for this test, including the maximum pullout load (P_{max}), the corresponding bond strength (τ_b) and the bond stiffness (κ_b), defined as the slope of the secant line from origin to a bond stress equivalent to 40% of the bond strength.

Table 4.4 - Results obtained from pullout test.

	SBR	SND	ACR	EPX
P_{\max} (N)	198.9 ± 8.3	533.4 ± 22.9	1118.7 ± 63.8	1230.6 ± 160.9
τ_b (MPa)	1.10 ± 0.04	2.94 ± 0.11	17.26 ± 0.98	21.90 ± 2.86
κ_b (MPa/mm)	0.21 ± 0.04	4.08 ± 0.26	31.49 ± 14.52	55.33 ± 18.03

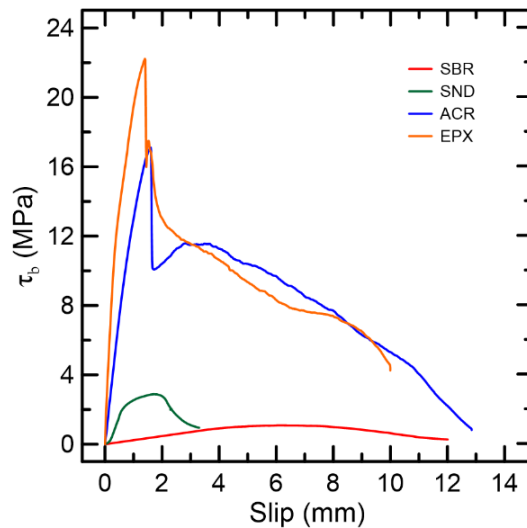


Figure 4.6 - Representative bond stress versus slip curves.

Results show that the surface coating has a significant influence on the bond stress-slip response. The lower bond stress of 1.104 MPa for SBR confirms the weak adhesion of the styrene butadiene rubber with the cementitious matrix, already described in previous studies [24,26,29]. When the sand-epoxy impregnation was adopted, an enhanced interfacial behaviour was achieved and the bond strength was 2.7 times greater than that for plain SBR. For ACR and EPX materials, the higher bond strengths confirm the superior adhesion between these materials and the matrix. The bond strengths of ACR and EPX are respectively 15.7 and 19.9 times greater than that obtained for the plain SBR, respectively.

Regarding the bond stiffness κ_b , it can be seen that there is large difference between the specimens. In the case of SBR, ACR and EPX, κ_b is governed by adhesion mechanism of bond, while for SND there is an additional interlock mechanism. It is worth highlighting that the connection between warp and weft yarns plays an important role at stiffness response of the TRC and the pullout results discussed in this Section do not account for the contribution of this mechanism [30–33].

4.3.2. Compression Test

Table 4.5 presents a summary of results for compression tests, showing the compressive strength $f_{c,TRC}$ for each condition studied, as well as the normalized values, taking the mean plain matrix cylinder strength as reference ($f_{c,cyl}$). To compare the influence of textile of different carbon textile condition and sample dimensions on compressive strength is also presented in Table 4.5. This properties was also normalized with the mean plain matrix for each dimensions condition, where prism compressive strength ($f_{c,prism}$) and CLC compressive strength ($f_{c,clc}$). The influence of warp and weft yarn of different carbon textile condition on compressive strength is graphically shown in Figure 4.7a, whereas Figure 4.7b presents the comparison between SBR and plain matrix samples.

Table 4.5 - Results of compressive strength for different compression tests.

Specimen	Compressive strength (MPa)	$f_{c,TRC}/f_{c,cyl}$	$f_{c,TRC}/f_{c,prism}$	$f_{c,TRC}/f_{c,clc}$
Cylinder	76.0 ± 2.6	1.00	-	-
M-P	57.8 ± 9.9	0.76	1.00	-
M-C-30	84.1 ± 4.7	1.10	-	1.00
SBR-C-30-L	73.2 ± 3.8	0.96	-	0.87
SBR-C-40-L	70.6 ± 5.9	0.92	-	0.84
SBR-P-L	47.5 ± 9.9	0.62	0.82	-
SBR-B-L	42.4 ± 8.6	0.56	0.73	-
SBR-P-T	62.1 ± 6.0	0.81	1.07	-
SBR-B-T	46.8 ± 6.7	0.61	0.81	-
SND-B-L	37.2 ± 6.9	0.49	0.64	-
SND-B-T	39.4 ± 6.1	0.52	0.68	-
ACR-B-L	57.4 ± 5.0	0.75	0.99	-
ACR-B-T	27.0 ± 5.9	0.35	0.47	-
EPX-B-L	28.5 ± 7.7	0.37	0.49	-
EPX-B-T	48.0 ± 6.5	0.63	0.83	-

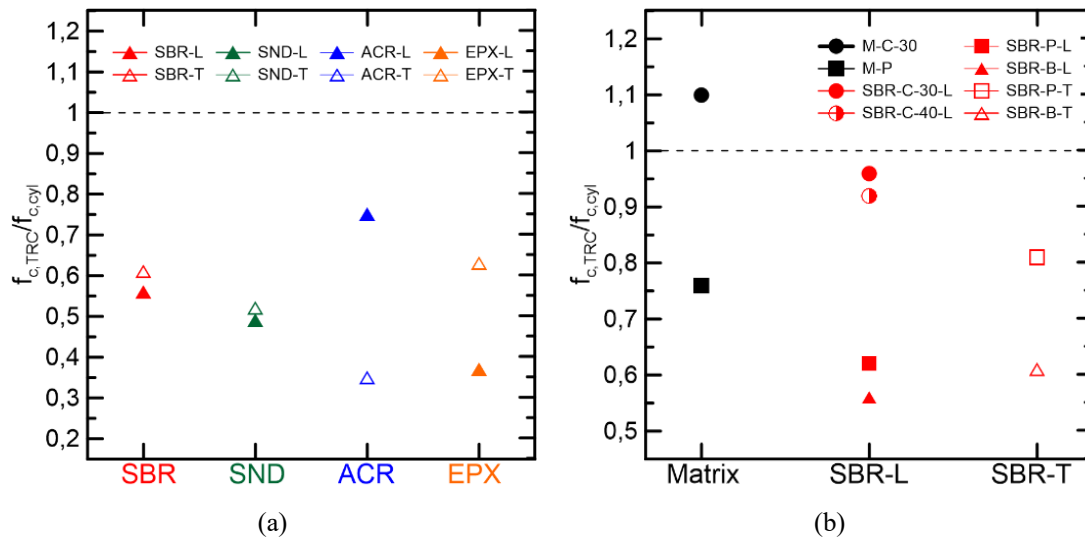


Figure 4.7 - Results of compression tests for (a) different carbon textiles and (b) SBR samples under different testing conditions.

Analyzing the plain matrix compressive strength (Figure 4.7b), an increase of 10 % and a decrease of 24 % were respectively observed for CLC and direct compression on prismatic samples with respect to cylinder tests (76.0 MPa). These results indicate a significant influence of shape and scale effect on the results. As presented in Figure 4.8, the CLC tests allow limited space for crack propagation and may have also contributed for a higher capacity.

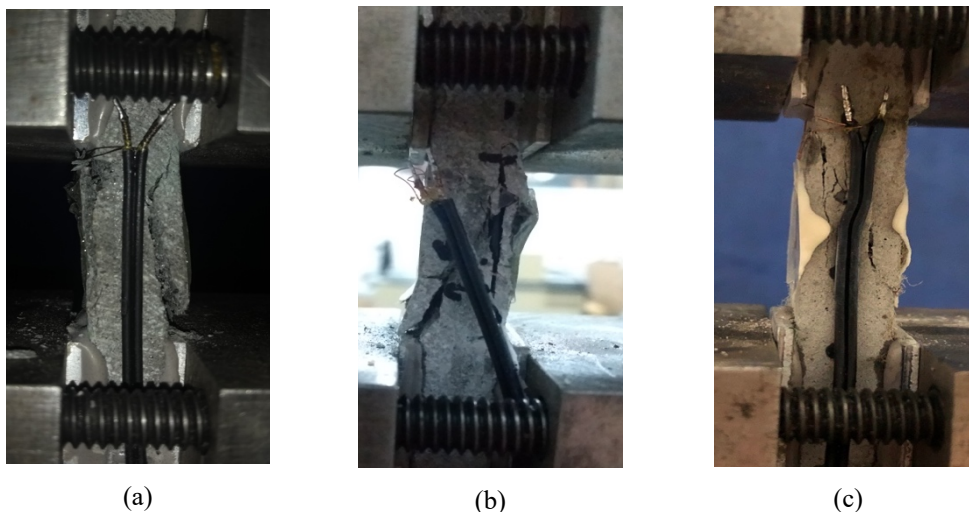


Figure 4.8 - Failure mode of CLC specimens: (a) M-C-30 (b) SBR-C-30-L and (c) SBR-C-40-L.

For TRC samples, a slight decrease on compressive strength was observed for specimens cut from beams in comparison to specimens extracted from plates. It is possible that the process of producing TRC-beams resulted in a poorer compaction

of the matrix. Comparing the results of specimens cut out from plates for SBR-TRC with those for plain matrix with the same geometry, a reduction of 17.9 % (47.5 MPa) and an improvement of 7.4 % (62.1 MPa) on compressive strength were observed for longitudinal and transverse yarn directions, respectively.

When comparing the influence of test setup, the best results were found for CLC tests. However, it is possible to observe that, even in this case, the presence of fabric led to a decrease in compressive strength. In fact, strength of TRC samples when tested in CLC was reduced by roughly 13 - 16 % and no significant difference was noticed between specimens with 30 and 40 mm of unsupported length.

Comparing the results for different types of carbon textile, reductions on compressive strength were seen for all TRC specimens with respect to plain matrix, as discussed in previous studies [3,34–36]. A more pronounced difference on compressive strength was observed for ACR and EPX samples. It is important to highlight that SBR yarns in warp and weft directions have similar cross-sectional areas and sizes, whereas a significant difference can be found for ACR and EPX (Table 1). In addition, as already mentioned, a more rigid connection between yarn for ACR and EPX is proven due to the stiff impregnation of the textiles, providing greater transverse yarn stiffness. According to Bochman [9] the parameters that can influence the behavior of the TRC material under compression are: “reinforcement ratio (number of weakness planes); yarn size (size of individual weakness); effective area (transverse tensile stress load paths), soft or stiff impregnation type of yarn (transverse yarn stiffness); and textile reinforcement orientation (inclination of weakness planes) with respect to the loading direction”. In all cases, failure was initiated by a longitudinal crack formed in the fabric region.

As aforementioned, the results obtained for TRC with respect to the plain matrix tested to the same setup, the reduction of compressive strength was of about 13-18 % for CLC test and for the plain prism. Ortlepp et al. [34] proposed a design model with a reduction factor of 0.6 for TRC under compression due to the observed disintegration when RC columns with TRC confinement was tested. A compression strut failure at about 60% of the predicted load was reported by Molter [35] and Voss [36] proposed a reduction factor of about 0.30 on compressive strength for TRC composites.

4.3.3. Tensile Test

Table 4.6 summarizes the average tensile properties for specimens of 120 x 14 cross-section area for different carbon-TRC composites and Figure 4.9 shows the representative stress-strain curves for each type of carbon-TRC. The composite stress was calculated dividing the applied force by the cross-sectional area of longitudinal yarns, as suggested in previous works [13,18]. The theoretical tensile response can be described by a trilinear curve, where the main stages are: 1) uncracked; 2) crack formation; and 3) crack widening up to failure, as presented in Figure 4.9. In the figure, the stress and strain corresponding to matrix cracking and that define the transition from Stage 1 to Stage 2 are defined as σ_{cr} and ε_{cr} , respectively. The ultimate stress (σ_u) and strain (ε_u) correspond to the curve peak load and an efficiency factor k_f can be defined as the ratio between σ_u and the nominal textile strength f_{tu} . The slope of third branch of the curve corresponds to the effective modulus of elasticity of the textile, defined in this work as $E_{f,eff}$.

The idealized behavior described in the previous paragraph follows the model proposed by Goliath *et al.* [26] and accounts for the tension stiffening effect and for the textile efficiency, which depends mainly on the bond between yarn and matrix, as well as on the type of impregnation and its ability to activate inner filaments [4, 16, 37, 38]. The application of the model along with a regression technique to the experimental results allows the determination of the following parameters: i) the effective stiffness factor that is defined as the ratio between effective and nominal textile moduli ($k_e = E_{f,eff}/E_f$); and the effective concrete tensile strength (f_{ct}). Figure 4.10 presents the model applied to the representative tensile curves.

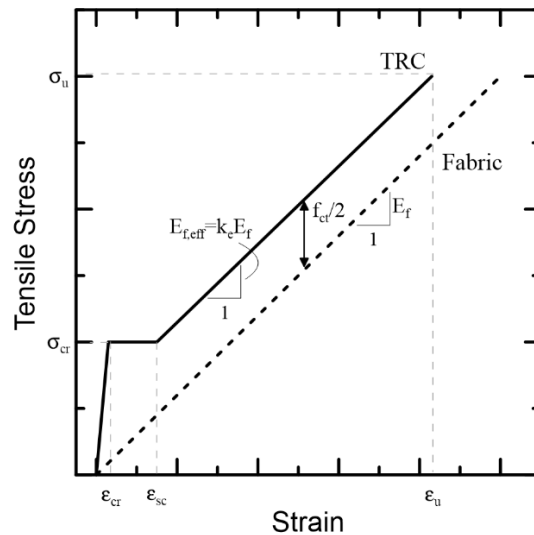


Figure 4.9 - Representative curve for tensile test.

Table 4.6 - Average results of tensile test for different carbon fabrics.

Specimen	SBR-S-120-450	SND-S-120-450	ACR-S-120-450	EPX-S-120-450
n_{cr}	1.33 ± 0.57	12.67 ± 1.53	15.50 ± 0.71	19.33 ± 1.53
S_m (mm)	-	40.33 ± 5.07	33.18 ± 1.87	28.32 ± 4.21
N (mm ⁻¹)	0.30 ± 0.13	2.8 ± 0.33	3.40 ± 0.15	4.20 ± 0.33
$w_{m,u}$ (mm)	0.52 ± 0.17	0.14 ± 0.05	0.38 ± 0.16	0.22 ± 0.12
$w_{max,u}$ (mm)	-	0.24 ± 0.08	0.58 ± 0.18	0.47 ± 0.16
σ_{cr} (MPa)	101.11 ± 34.98	107.29 ± 22.48	225.07 ± 65.64	116.58 ± 11.38
ϵ_{cr} (%)	0.008 ± 0.005	0.007 ± 0.004	0.007 ± 0.001	0.008 ± 0.002
F_u (kN)	11.30 ± 2.01	23.11 ± 1.37	45.80 ± 7.61	45.84 ± 2.26
σ_u (MPa)	318.33 ± 47.82	694.17 ± 41.00	2242.81 ± 422.48	1190.71 ± 58.80
ϵ_u (%)	0.88 ± 0.21	0.84 ± 0.19	1.03 ± 0.32	1.40 ± 0.14
k_f	0.18	0.41	0.87	0.45
Results obtained by the model				
$w_{m,u,mod}$	0.87	0.47	0.14	0.38
$\tau_{b,ind}$ (MPa)	1.92	9.96	9.29	23.36
f_{ct} (MPa)	2.90	3.58	1.74	4.46
$E_{f,eff}$ (GPa)	33.1	64.3	208.7	70.6
k_e	0.19	0.38	1.23	0.42

n_{cr} – average number of cracks within gauge length;
 N – crack density = number of cracks related to the gauge length;
 w_m – average crack width at ultimate tensile strength;
 w_{max} – maximum crack width at ultimate tensile strength;
 $w_{m,u,mod}$ – average crack width obtained with the model;
 $\tau_{b,ind}$ – nominal bond stress determined indirectly with the model.

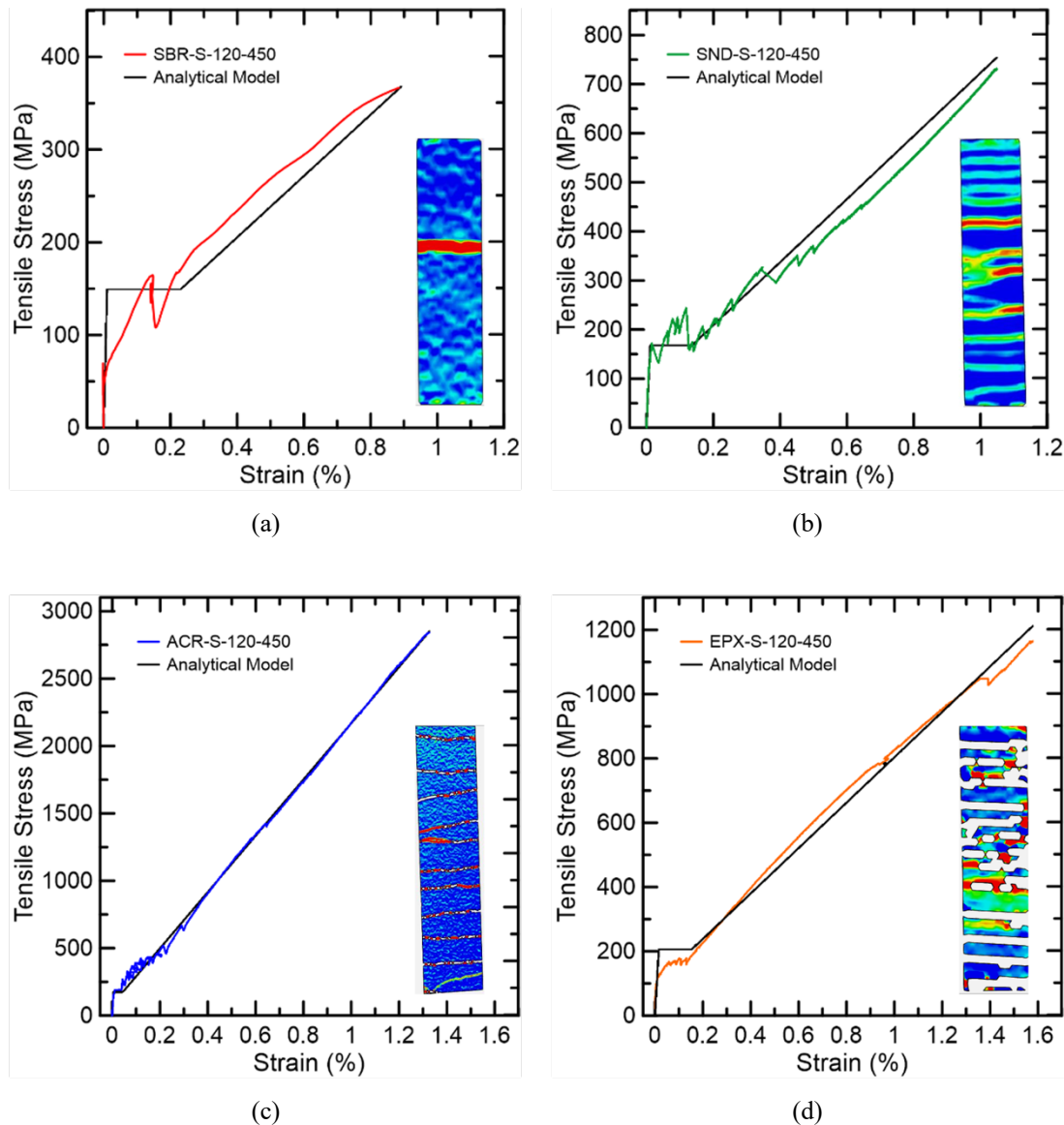


Figure 4.10 - Tensile stress vs strain curve for (a) SBR-S-1-450, SND-S-1-450, ACR-S-1-450 and (d) EPX-S-1-450.

As reported in previous studies [24, 39], the SBR coating over the dry fibers leads to poor adherence to the concrete matrix, ultimately leading to low tensile load-capacity (318.2 MPa) and low stiffness after the crack formation stage, as shown in Figure 4.10. In this case, dissipation of energy occurs due to slippage and SBR-coated TRC specimens exhibit pseudo-ductility [38, 40-42]. When the sand-epoxy coating is added, the sand improves the friction at the interface between matrix and fabric reinforcement and an increase in the tensile strength can be observed – 694.2 MPa, i.e. 2.2 times the capacity of plain SBR samples.

Superior tensile response was observed for the ACR specimens, despite having the lowest reinforcement ratio, with a tensile strength of 2243 MPa. On the other hand, EPX samples did not reach the high tensile strength expected values for this fabric, with a tensile strength of 1191 MPa. After the tests, EPX specimens exhibited microcracks in the grip area. This may have led to inefficient activation of the inner filaments, making both strength and stiffness to be lower than expected. The crack parameters were obtained using DIC technique. Table 4.6 shows larger crack widths at ultimate strength for SBR (0.52 mm) and a reduction of 73% was seen when sand-epoxy impregnation was used. It is possible to note a better response of SND, ACR and EPX with respect to crack control, confirming that the greater bond leads to a denser cracking pattern. In addition, the number of cracks of SND, ACR and EPX specimens were about 13, 16 and 19, with average spacings of the 40.3, 33.2 and 28.3 mm (Table 4.6) at the failure, respectively.

To compare the tensile response of different carbon-TRC, the nominal bond stress ($\tau_{b,ind}$) was determined indirectly through the model proposed by Goliath *et al.* [139]. The parameter was evaluated with the values obtained experimentally in tensile test. The values of $\tau_{b,ind}$ are reported in Table 4.6 and it can be confirmed that highest and lowest values of nominal bond strength of 23.4 MPa and 1.92 MPa were seen for EPX and SBR, respectively. Both values agree with the results obtained in pullout test (Table 4.3). On the other hand, values for ACR and SND were near and respectively equal to 9.29 and 9.96 MPa. For ACR specimens, this result was half of the peak bond strength observed in pullout test, suggesting that the bond capacity was not mobilized due to reduced crack values and limited yarn slip during tests. For the SND specimens, the higher bond strength determined indirectly (3.4 times the peak bond strength from pullout tests) may be related to the positive influence of transverse yarns.

Regarding the influence of different geometries and setups adopted for SBR samples, a significant variation in the strength, strain at failure, stiffness and crack width values was observed, as shown in Table 4.7. Using the same approach adopted previously, indirect properties can also be obtained and are presented in the table. Figure 4.11 shows the stress vs strain curves to assess the influences of cross section (Figure 4.11a), setup (Figure 4.11b) and gauge length (Figure 4.11c).

Table 4.7 - Average results of tensile test for SBR specimens for different set up conditions.

Specimen	SBR-S-120-450	SBR-S-80-400	SBR-G-80-100	SBR-G-80-400
n_{cr}	1.33 ± 0.57	1.67 ± 0.57	1.00 ± 0.00	3.67 ± 0.58
N (%)	-	0.40 ± 0.14	1.00 ± 0.00	0.90 ± 0.35
$w_{m,u}$ (mm)	0.30 ± 0.13	0.71 ± 0.16	-	3.33 ± 2.81
$w_{max,u}$ (mm)	0.52 ± 0.17	0.74 ± 0.03	3.74 ± 0.69	7.37 ± 4.25
σ_{cr} (Mpa)	101.10 ± 25.19	103.30 ± 14.90	158.00 ± 27.10	92.50 ± 37.68
ϵ_{cr} (%)	0.008 ± 0.005	0.013 ± 0.003	0.002 ± 0.0004	0.021 ± 0.035
F_u (kN)	11.30 ± 2.01	8.00 ± 0.75	13.50 ± 0.82	10.30 ± 0.77
σ_u (Mpa)	318.2 ± 47.82	344.3 ± 32.22	580.10 ± 34.66	453.20 ± 33.35
ϵ_u (%)	0.880 ± 0.210	0.355 ± 0.191	2.993 ± 0.523	2.193 ± 0.692
k_f	0.18	0.20	0.34	0.27
Results obtained by the model				
$w_{m,mod}$	0.87	0.34	4.69	3.70
$\tau_{b,ind}$ (MPa)	1.52	0.52	0.64	0.91
f_{ct} (MPa)	2.90	1.42	2.98	2.80
$E_{f,eff}$ (GPa)	33.1	62.2	13.5	15.6
k_e	0.19	0.37	0.08	0.09

The reduction of 33 % in the width from 120 to 80 mm led to a slight improvement in the tensile strength of about 8 %. According [7], the width depends on the mesh dimensions, with a minimum number of fiber strands in the width, making possible this reduction for SBR fabric with no loss in tensile strength. However, a major difference was observed in the strain capacity, which decreased from 0.88 to 0.30 % when reducing the sample width. Consequently, stiffness increased significantly and stiffness factors of 0.37 and 0.19 were respectively obtained for SBR-S-80-400 SBR-S-120-450, respectively. Since the reinforcing ratios are near, the stiffer behavior observed for narrower specimens may be explained by crack formation outside the measurement area in all specimens tested for the sample SBR-S-80-400. Once the crack forms outside the LVDT measurement area, the material behavior becomes apparently stiffer, as can be seen in Figure 11a for a strain of about 0.4 %. In addition, an increase of 0.45 to 0.74 mm was observed for average crack width for these specimens in ultimate tensile strength. Comparing the nominal bond stress determined indirectly, smaller values for SBR-S-80-400 were obtained (0.52 MPa) compared to SBR-S-120-450 (1.52

MPa). The SBR-S-80-400 lower bond performance may be associated with the smaller amount of fiber strand observed for this specimen and the relationship between the number and width of cracks.

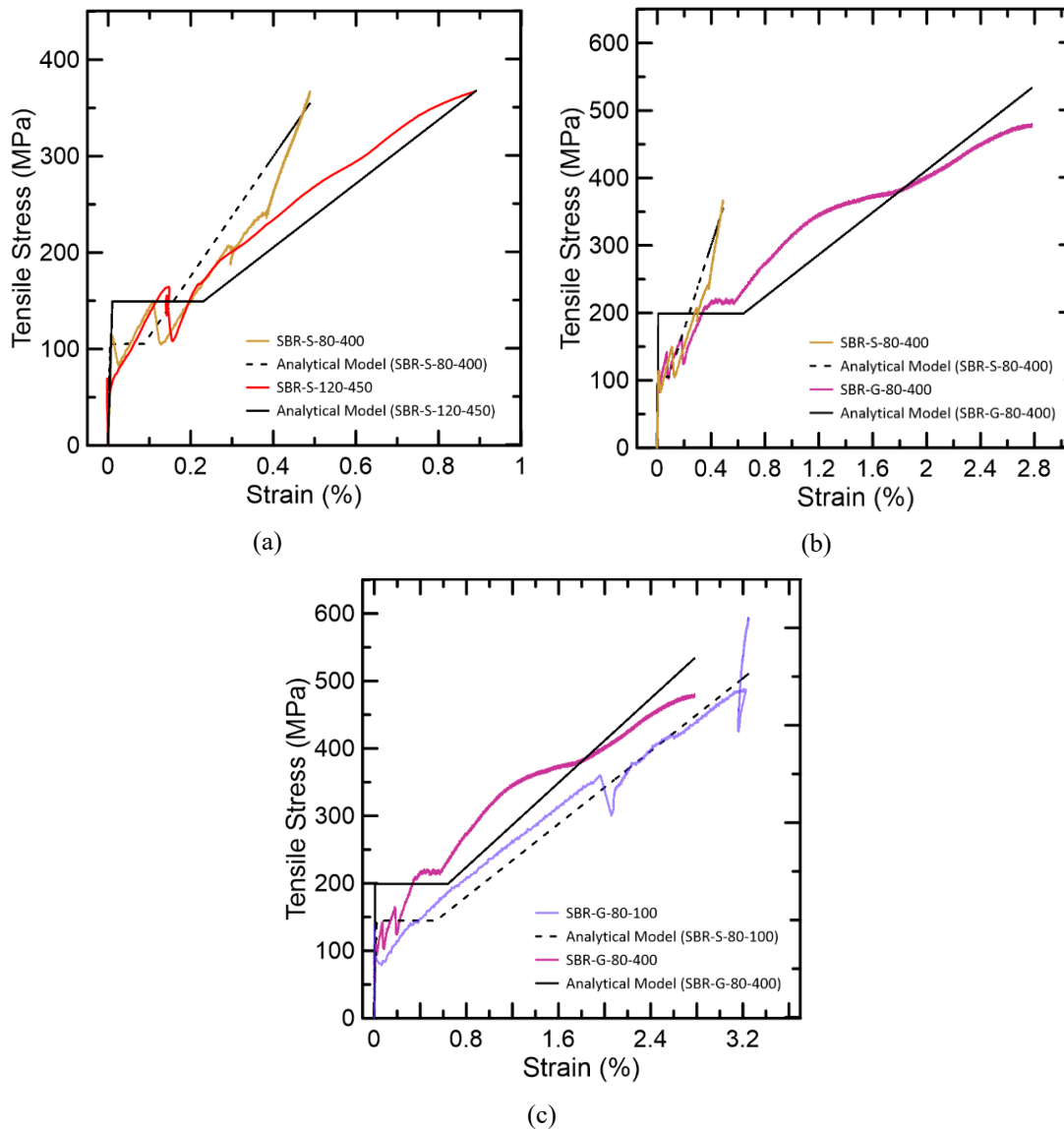


Figure 4.11 - Representative tensile stress vs strain curve for SBR specimens: (a) effect of cross section, (b) effect of testing setup and (c) effect of gauge length.

The setup and the gauge length effect is presented in Figure 4.11b. Comparing the influence of the grip used, increases of about 30 % in tensile strength and 518 % in strain capacity were observed for glued tabs in comparison to the screw clamped condition. The major influence of the setup was in terms of cracking pattern, with an increase of average crack number formed in the specimen from 1.67 to 3.67 mm and crack width from 0.75 to 7.37 mm for SBR-S-80-400 and SBR-G-80-400, respectively. However, in relation to the different setup and

dimensions used, it was observed that the variability in the strain measured at the end of each phase is mainly related to the location of the cracks within the gauge length. Thus, this fact will directly affect the effective modulus and, consequently, the stiffness factor. No studies were found that compare results between the same techniques analyzed in this study.

With respect the gauge length, the reduction of gauge length from 400 to 100 mm led to a significant increase in tensile strength (30 %) and decrease in strain capacity (36.5 %), as can be seen observed in Figure 4.11c. This is a consequence of the increase in the anchorage length from 250 to 400 mm. However, the effective modulus is the similar in both cases ($k_e = 0.08\sim 0.09$) as well as the crack density (1 – 0.9 %). A similar behavior was observed in literature [17, 43, 44]. Arboleda *et al.* [37] also observed that increasing the contact length between the metal tabs and the specimens the TRC apparent tensile strength increases. According to [17], the shorter the gauge length, the greater tensile strength.

4.4. Influence of Material Parameters on Beam Response

In this Section, the constitutive laws derived from the experimental program are adopted in a moment-curvature analysis of TRC beams tested by the authors. The experimental program and results are reported in Goliath *et al.* [26].

A typical cross-section analysis was carried out, using idealized constitutive laws for matrix and reinforcement as presented in Figure 4.12. It is important to highlight that an effective response in tension is considered for concrete, to account for the influence of textile and tension stiffening effect. Different combinations of material parameters were considered for comparison, as summarized in Table 4.7. Figure 4.13 presents comparisons between experiments and models adopted, based on experimental tensile properties of specimens having 120 mm of width and 400 mm of anchorage length.

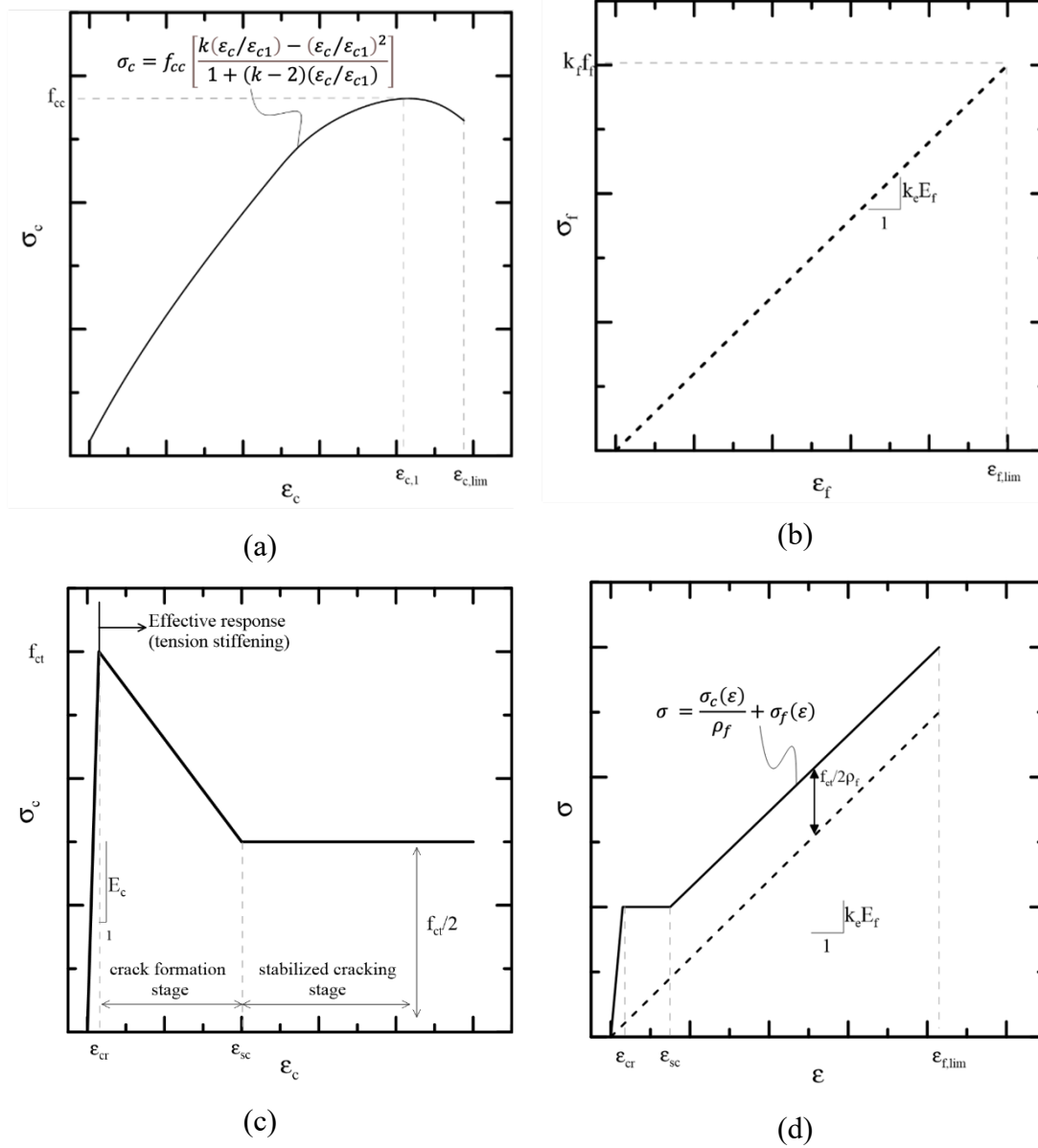


Figure 4.12 - Idealized constitutive laws.

Table 4-8 - Different combinations of material parameters.

Specimen	Parameters					
	k_e	k_f	f_{ct} (MPa)	ρ_f	η	
SBR-S-120-450	0.18	0.19	2.90	0.6	0.8	1.0
SBR-S-80-400	0.37	0.20	1.42	-	-	1.0
SBR-G-80-100	0.08	0.34	2.98	-	-	1.0
SBR-G-80-400	0.09	0.27	2.80	-	-	1.0
SND-S-120-450	0.38	0.41	3.58	0.6	0.8	1.0
ACR-S-120-450	1.23	0.87	1.74	0.6	0.8	1.0
EPX-S-120-450	0.28	0.42	4.46	0.6	0.8	1.0

With respect to the reduction factors (η) applied to concrete strength to account for the influence of textile on the compressive strength of concrete, it can be seen from Figure 4.13 that this parameter did not play a major role on the response. It is worth mentioning that in all cases the failure did not occur by crushing the concrete, but by shear failure or yarn rupture. Thus, the reduction used had no impact on the flexural response of the beams.

In terms of overall response, a poorer agreement was observed for SBR beams, indicating that the properties adopted from the reference tests are not appropriate – this difference will be better discussed in the next paragraph. For SND and EPX specimens (Figures 4.13b and 4.13d), the models underestimated the flexural capacity and stiffness of the beams, but a reasonable agreement with the initial part of the curve (up to a moment of 2.5 kNm). For ACR (Figure 4.13c), a better agreement was reached when using the parameters derived from the tensile tests. However, a shear failure was reported for ACR beam, making the model to overestimate the capacity.

The influence of cross-section, setup and gauge length for SBR can be evaluated from Figure 4.14. The best agreement was presented for model with properties derived from SBR-S-80-400 tests (model by Goliath *et al.* [26]), despite the lower flexural capacity observed. The greater bending capacity of the specimens may be related to the higher transversal stresses acting on the yarn, improving the textile effectivity [103]. The SBR-S-120-450, SBR-G-80-400 and SBR-S-80-400 produced similar effectiveness factor of 0.19, 0.27 and 0.20, respectively.

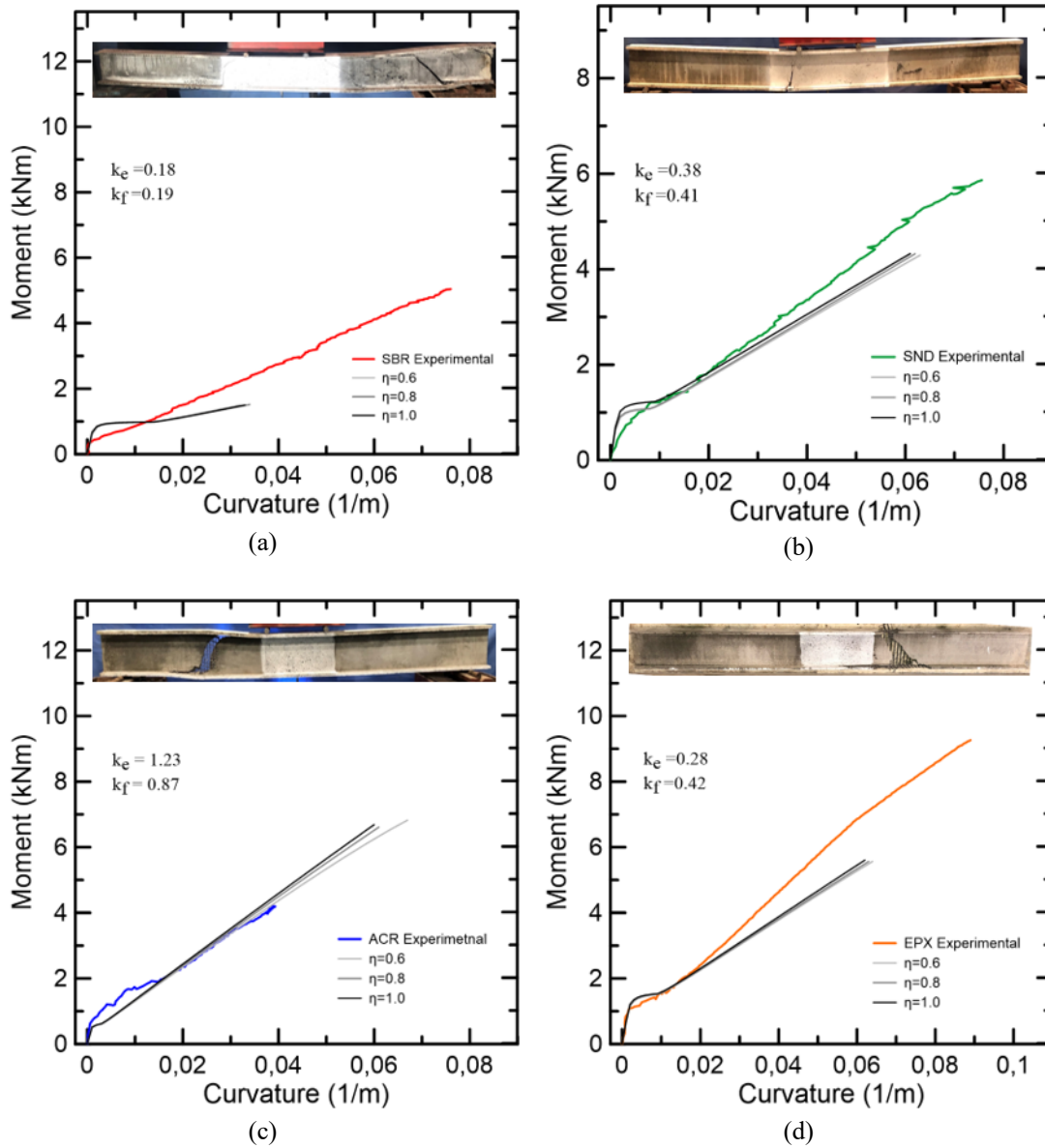


Figure 4.13 - Influence of different parameters on the flexural response of TRC beams.

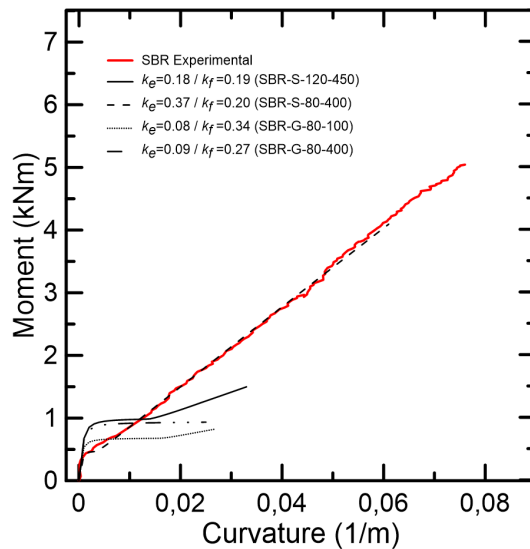


Figure 4.14 - Influence of different tensile test on flexural response of SBR-carbon TRC.

4.5. Conclusions

In the present work, the mechanical characterization of different carbon-TRC composite is investigated and the results used in an analytical model to evaluate the flexural response of carbon-TRC I-section beams. Based on the results of the experimental investigation carried out in this paper, the following conclusions can be drawn:

- 1) The characterization of the interface between matrix and yarn indirectly measured in tensile test was comparable to the same properties obtained in single yarn pullout test for SBR and EPX. In case of SND, the nominal bond strength is enhanced in tensile test due the strong connection between warp and weft yarn. On the other hand, for ACR specimens, the consideration of the weft yarn leads a decrease of bond strength due to the smaller yarn cross-section area in this direction and less rigidity in the connection between the yarns.
- 2) The compressive strength of the matrix is reduced due to the incorporation of the textile, as well as to the manufacturing process of the TRC elements. However, this reduction does not affect the flexural response of tension-governed carbon-TRC beams.
- 3) Tensile tests for different carbon textiles showed the great influence of coating, mesh dimensions and stiffness of the fabric in tensile properties. The best behaviors were observed for ACR, EPX and SND, respectively, in terms of tensile strength, crack pattern and effectiveness modulus of elasticity. The results obtained in this test were used to determine indirectly the parameters be used in analytical models.
- 4) The characterization results for SBR fabric revealed that there was a strong influence of dimensions and setup test on the TRC composite response. The gauge length has more impact on crack pattern and tensile strength, but slight difference in terms of effective modulus of elasticity.

When comparing analytical results from the models, a major parameter of influence is the stiffness factor. It was seen that the test setup consisting of screws and a cross section area of 80 x 14 mm led to the better agreement between model and experiments.

4.6. References

- [1] Brameshuber W. Report 36: textile reinforced concrete-state-of-the-art report of RILEM TC 201-TRC. Rilem publications; 2006.
- [2] Mobasher B. Mechanics of fiber and textile reinforced cement composites. 2011. <https://doi.org/10.1201/b11181>.
- [3] Valeri P, Ruiz MF, Muttoni A. Modelling of Textile Reinforced Concrete in bending and shear with Elastic-Cracked Stress Fields. *Eng Struct* 2020;215:110664. <https://doi.org/10.1016/j.engstruct.2020.110664>.
- [4] Valeri P, Fernández Ruiz M, Muttoni A. Tensile response of textile reinforced concrete. *Constr Build Mater* 2020;258:119517. <https://doi.org/10.1016/j.conbuildmat.2020.119517>.
- [5] de Felice G, D’Antino T, De Santis S, Meriggi P, Roscini F. Lessons Learned on the Tensile and Bond Behavior of Fabric Reinforced Cementitious Matrix (FRCM) Composites. *Front Built Environ* 2020;6:1–15. <https://doi.org/10.3389/fbuil.2020.00005>.
- [6] Schütze E, Lorenz E, Curbach M. Test methods for textile reinforced concrete. *11th Int Symp Ferrocem Text Reinf Concr 3rd ICTRC* 2015:307–18.
- [7] Schütze E, Bielak J, Scheerer S, Hegger J, Curbach M. Einaxialer Zugversuch für Carbonbeton mit textiler Bewehrung. *Beton- Und Stahlbetonbau* 2018;113:33–47. <https://doi.org/10.1002/best.201700074>.
- [8] Bochmann J, Jesse F, Curbach M. Experimental Determination of the Stress-Strain Relation of Fine Grained Concrete Under Compression 2017:11.
- [9] Bochmann J, Curbach M, Jesse F. Influence of artificial discontinuities in concrete under compression load—A literature review. *Struct Concr* 2018;19:559–67. <https://doi.org/10.1002/suco.201700041>.
- [10] Hawkins W, Orr J, Ibell T, Shepherd P. An Analytical Failure Envelope for the Design of Textile Reinforced Concrete Shells. *Structures* 2018;15:56–65. <https://doi.org/10.1016/j.istruc.2018.06.001>.
- [11] Santos FCA dos. Behavior of Textile Reinforced Concrete (TRC) Slender Columns Subject to Compression. Pontificia Universidade Católica do Rio de Janeiro (PUC-Rio), 2018.
- [12] D’Antino T, Papanicolaou C. Mechanical characterization of textile

- reinforced inorganic-matrix composites. *Compos Part B Eng* 2017;127:78–91. <https://doi.org/10.1016/j.compositesb.2017.02.034>.
- [13] De Santis S, Hadad HA, De Caso y Basalo F, de Felice G, Nanni A. Acceptance Criteria for Tensile Characterization of Fabric-Reinforced Cementitious Matrix Systems for Concrete and Masonry Repair. *J Compos Constr* 2018;22:04018048. [https://doi.org/10.1061/\(asce\)cc.1943-5614.0000886](https://doi.org/10.1061/(asce)cc.1943-5614.0000886).
- [14] HARTIG, J. et al. Influence of experimental setups on the apparent uniaxial tensile load-bearing capacity of textile reinforced concrete specimens. *Materials and structures*, v. 45, n. 3, p. 433-446, 2012.
- [15] Rampini MC, Zani G, Colombo M, di Prisco M. Mechanical behaviour of TRC composites: Experimental and analytical approaches. *Appl Sci* 2019;9. <https://doi.org/10.3390/app9071492>.
- [16] Yao Y, Silva FA, Butler M, Mechtcherine V, Mobasher B. Tension stiffening in textile-reinforced concrete under high speed tensile loads. *Cem Concr Compos* 2015;64:49–61. <https://doi.org/10.1016/j.cemconcomp.2015.07.009>.
- [17] Donnini J, Corinaldesi V. Mechanical characterization of different FRCM systems for structural reinforcement. *Constr Build Mater* 2017;145:565–75. <https://doi.org/10.1016/j.conbuildmat.2017.04.051>.
- [18] Tekieli M, De Santis S, de Felice G, Kwiecień A, Roscini F. Application of Digital Image Correlation to composite reinforcements testing. *Compos Struct* 2017;160:670–88. <https://doi.org/10.1016/j.compstruct.2016.10.096>.
- [19] Doutorado T De, Janeiro R De. Felipe Pinheiro Teixeira Mechanical Behavior of Natural Fiber Cement Based Composites for Structural Applications Felipe Pinheiro Teixeira Mechanical Behavior of Natural Fiber Cement Based Composites for Structural Applications 2020.
- [20] Williams Portal N, Fernandez Perez I, Nyholm Thrane L, Lundgren K. Pull-out of textile reinforcement in concrete. *Constr Build Mater* 2014;71:63–71. <https://doi.org/10.1016/j.conbuildmat.2014.08.014>.
- [21] Xu S, Krüger M, Reinhardt H-W, Ožbolt J. Bond Characteristics of Carbon, Alkali Resistant Glass, and Aramid Textiles in Mortar. *J Mater Civ Eng* 2004;16:356–64. [https://doi.org/10.1061/\(asce\)0899-1561\(2004\)16:4\(356\)](https://doi.org/10.1061/(asce)0899-1561(2004)16:4(356)).
- [22] Peled A, Bentur A. Geometrical characteristics and efficiency of textile

- fabrics for reinforcing cement composites. *Cem Concr Res* 2000;30:781–90. [https://doi.org/10.1016/S0008-8846\(00\)00239-8](https://doi.org/10.1016/S0008-8846(00)00239-8).
- [23] Peled A, Sueki S, Mobasher B. Bonding in fabric-cement systems: Effects of fabrication methods. *Cem Concr Res* 2006;36:1661–71. <https://doi.org/10.1016/j.cemconres.2006.05.009>.
- [24] Mansur de Castro Silva R, de Andrade Silva F. Carbon textile reinforced concrete: materials and structural analysis. *Mater Struct Constr* 2020;53. <https://doi.org/10.1617/s11527-020-1448-4>.
- [25] Banholzer B, Brameshuber W, Jung W. Analytical evaluation of pull-out tests-The inverse problem. *Cem Concr Compos* 2006;28:564–71. <https://doi.org/10.1016/j.cemconcomp.2006.02.015>.
- [26] Botelho Goliath K, Daniel DC, de A. Silva F. Flexural behavior of carbon-textile-reinforced concrete I-section beams. *Compos Struct* 2021;260:113540. <https://doi.org/10.1016/j.compstruct.2021.113540>.
- [27] AC434. Acceptance criteria for concrete and masonry strengthening using fabric-reinforced cementitious matrix (FRCM) composite Systems. ICC Eval Serv Whittier, CA 2018.
- [28] GOM: Precise Industrial 3D Metrology. GOM Correlate n.d.
- [29] Krüger M, Reinhardt H-W, Fichtlscherer M. Bond behaviour of textile reinforcement in reinforced and prestressed concrete. *Otto-Graf-Journal* 2001;12:33–50.
- [30] Mobasher B, Peled A, Pahilajani J. Distributed cracking and stiffness degradation in fabric-cement composites. *Mater Struct Constr* 2006;39:317–31. <https://doi.org/10.1617/s11527-005-9005-8>.
- [31] Soranakom C, Mobasher B. Modeling of tension stiffening in reinforced cement composites: Part I. Theoretical modeling. *Mater Struct Constr* 2010;43:1217–30. <https://doi.org/10.1617/s11527-010-9594-8>.
- [32] Sueki S, Soranakom C, Mobasher B, Peled A. Pullout-Slip Response of Fabrics Embedded in a Cement Paste Matrix. *J Mater Civ Eng* 2007;19:718–27. [https://doi.org/10.1061/\(asce\)0899-1561\(2007\)19:9\(718\)](https://doi.org/10.1061/(asce)0899-1561(2007)19:9(718)).
- [33] Soranakom C, Mobasher B. Geometrical and mechanical aspects of fabric bonding and pullout in cement composites. *Mater Struct Constr* 2009;42:765–77. <https://doi.org/10.1617/s11527-008-9422-6>.
- [34] Ortlepp R, Ortlepp S. Textile reinforced concrete for strengthening of RC

- columns: A contribution to resource conservation through the preservation of structures. *Constr Build Mater* 2017;132:150–60. <https://doi.org/10.1016/j.conbuildmat.2016.11.133>.
- [35] Molter M. Zum Tragverhalten von textilbewehrtem Beton. Rheinisch-Westfälischen Technischen Hochschule Aachen, 2005.
- [36] Voss S. Dimensioning of textile reinforced concrete structures 2006:151–60. <https://doi.org/10.1617/2351580087.015>.
- [37] Arboleda D, Carozzi FG, Nanni A, Poggi C. Testing Procedures for the Uniaxial Tensile Characterization of Fabric-Reinforced Cementitious Matrix Composites. *J Compos Constr* 2016;20:04015063. [https://doi.org/10.1061/\(asce\)cc.1943-5614.0000626](https://doi.org/10.1061/(asce)cc.1943-5614.0000626).
- [38] Donnini J, Corinaldesi V, Nanni A. Mechanical properties of FRCM using carbon fabrics with different coating treatments. *Compos Part B Eng* 2016;88:220–8. <https://doi.org/10.1016/j.compositesb.2015.11.012>.
- [39] Gong T, Ahmed AH, Curosu I, Mechtcherine V. Tensile behavior of hybrid fiber reinforced composites made of strain-hardening cement-based composites (SHCC) and carbon textile. *Constr Build Mater* 2020;262:120913. <https://doi.org/10.1016/j.conbuildmat.2020.120913>.
- [40] Silva F de A, Butler M, Mechtcherine V, Zhu D, Mobasher B. Strain rate effect on the tensile behaviour of textile-reinforced concrete under static and dynamic loading. *Mater Sci Eng A* 2011;528:1727–34. <https://doi.org/10.1016/j.msea.2010.11.014>.
- [41] Barhum R, Mechtcherine V. Effect of short, dispersed glass and carbon fibres on the behaviour of textile-reinforced concrete under tensile loading. *Eng Fract Mech* 2012;92:56–71. <https://doi.org/10.1016/j.engfracmech.2012.06.001>.
- [42] Mechtcherine V. Novel cement-based composites for the strengthening and repair of concrete structures. *Constr Build Mater* 2013;41:365–73. <https://doi.org/10.1016/j.conbuildmat.2012.11.117>.
- [43] Arboleda D. Fabric reinforced cementitious matrix (FRCM) composites for infrastructure strengthening and rehabilitation: Characterization methods. *Fac Univ Miami* 2014:1–224.
- [44] Contamine R, Si Larbi A, Hamelin P. Contribution to direct tensile testing of textile reinforced concrete (TRC) composites. *Mater Sci Eng A*

- 2011;528:8589–98. <https://doi.org/10.1016/j.msea.2011.08.009>.
- [45] Hegger J, Voss S. Investigations on the bearing behaviour and application potential of textile reinforced concrete. *Eng Struct* 2008;30:2050–6. <https://doi.org/10.1016/j.engstruct.2008.01.006>.

5 Flexural creep of carbon-TRC beams

Article submitted: January, 2022 – *Composite Structures*

5.1. Introduction

Research works on Textile Reinforced Concrete (TRC) have been extensively carried out in the past decades and the material's application in load-bearing members is already a reality [1-4]. To date, the main applications for the TRC structures are for pedestrian bridges [5], façade panels [6], TRC-pavilions [7,8] and parking slabs [9]. TRC is also attractive in structural strengthening of RC beams against bending [10-12] and shear [13,14], RC columns [15] and masonry structures [16,17].

Textiles offer superior corrosion resistance and are lightweight materials with high tensile strength, therefore rising as potential candidate for internal reinforcement of cement-based matrices. These textiles are comprised of multifilament yarns in a structured open mesh form. In general, carbon [18-20], alkali-resistant glass [21,22], basalt [23,24], PBO [25,26] and natural [27-30] fibers have been commonly adopted to produce TRC composites. These fibers can be impregnated with a polymer matrix, e.g., styrene-butadiene rubber (SBR) [31,32], epoxy [33-36] or acrylate [37-39] for protection, for durability, to allow a different yarn shape or to improve bond between yarn and cement matrix [40,41]. Among all the fibers used in TRC, carbon is known for its high tensile strength and Young's modulus, superior durability and its effectiveness as reinforcement in cement-based matrix [42,43]. Carbon-TRCs exhibit a strain-hardening behavior with crack formation and growth stages strongly dependent on the coating adopted [32,38]. This will have a significant impact on the serviceability limit states (SLS) of structural members, for which appropriate cracking and deflection control must be ensured [44,45].

The bond behavior between carbon fabric and cement matrix has been largely studied by many authors [19,20, 32, 38, 46-48] and it has been seen that, in

impregnated textiles, this property is highly related to the type of polymer used. Epoxy coating (EPX) results in a rigid textile with good chemical affinity with the cementitious matrices [49]. In contrast to epoxy, styrene butadiene (SBR) impregnation leads to poorer activation of inner filaments and adherence to the concrete matrix. The result is a composite with lower stiffness and characterized by wide largely spaced cracks [50]. The acrylic based polymer (ACR) impregnation is stiffer than SBR and yields moderate adherence to the surrounding cementitious matrix [39]; ACR-fabric reinforced TRCs exhibit multiple fine cracking pattern, higher tensile strength and higher energy absorption compared to those reinforced with SBR-fabric [51]. Despite the relative differences between these impregnations, it is known that polymers exhibit relevant creep deformations even at room temperature, although studies on fiber reinforced polymers have shown that the presence of fibers may reduce significantly the long-term deformation [52,53]. To date, little is known about the time-dependent behavior of TRCs with different impregnations, which is required for an appropriate assessment of SLS in a structural level.

The understanding about TRC flexural creep behavior is essential for the design of structural load-bearing components in terms of serviceability throughout desired lifespan. When subjected to sustained loading, increases in deflections and crack widths are likely to occur and, in addition, creep rupture may occur at higher stresses. This behavior requires a complex understanding of the individual influence of the cementitious matrix, filaments, fiber-matrix interface, and filament-filament interaction for sustained load over time [54]. The properties that affect the fabric behavior under sustained loading are related to the constituents, i.e., fiber mechanical properties and coating characteristics. In fact, the quality of impregnation is fundamental, and the occurrence of flaws or pores increase stress concentration that can result in microcracks [55] that grow under constant loading over time until filament fracture. Moreover, cracks in the coating may lead to fiber exposure [56, 57].

Another parameter that influences creep response is the load ratio – ratio between applied load and material's short-term strength – and environmental conditions [54, 58]. Ortlepp & Jesse [58] performed tensile tests in AR-glass TRC under sustained load for load ratios up to 80% for a time period of six months. None of the specimens failed at load ratios below 60% and they concluded that the time

to failure decreases with increasing load ratios for AR-glass TRC. Interaction between filament and bond failures was also reported.

Freitag et al. [54] carried out tests in pre-cracked plates on a climate chamber at 20°C and relative humidity of 65%. The specimens were manually loaded at load ratios between 30 and 80%. As conclusions of the study, slow strain rates during the primary and secondary creep stages were observed. The deformations increased and time-to-failure decreased with increasing load ratios.

Spelter et al. [59] investigated the long-term durability of the AR-glass TRC under constant load at three different temperatures (20, 40 and 60°C) and load ratios between 70 and 97%. For the purpose of deriving a time to failure curve and determining a reduction factor for the tensile strength of the carbon textile reinforcement, the testing concept described above [59] was used by Spelter et al. [56]. The specimens were exposed to water, temperature and pH solution and pre-cracked up to the final crack pattern. When analyzing the residual capacity, no strength loss was observed for this specimen. In fact, an increase of strength was found after more than 5000 h of testing in comparison to the short-term tests, which was attributed to the alignment of filaments.

The creep behavior of TRC remains a gap in the knowledge, while appropriate comprehension of the phenomenon is relevant for the design of structural members. So far, there is no sufficient experimental data available on the overall behavior of TRC members to allow studying the complex interaction between phases of the composite and developing methodologies for a long-term prediction of the behavior. Current guidelines for TRC establish upper bound limits for TRC service tensile stress when used for external strengthening of existing masonry or concrete structures [59-61].

The objective of the current research is to investigate experimentally the long-term behavior of carbon-TRC I-section structural beams under sustained load and the influence of different coating conditions (SBR, ACR, EPX and SND). The flexural creep tests reported in this work were carried out for three months, during which time-dependent deflections and crack openings were monitored. Then, specimens were unloaded and had their recovery evaluated for ten days. Finally, monotonic tests were performed to assess the members' residual capacity.

5.2. Experimental program

5.2.1. Materials

5.2.1.1. Carbon Textile

Carbon fabrics with three different types of coating were used in this study, namely styrene-butadiene rubber (SBR), acrylate (ACR) and epoxy resin (EPX), resulting in flexible, moderately-stiff and rigid carbon textiles, respectively. Due to the usually poor bond observed for SBR-coated textiles [62], a fourth condition was considered, in which an extra impregnation with sand-epoxy (SND) was manually applied over the SBR-yarns, resulting in a rigid textile. The different conditions for the bidirectional textiles are shown in Figure 5.1 and the properties for each fabric, for EPX fabric was provided by manufacturers and for SBR and ACR were reported by [51]. by manufacturers are reported in in Table 51. The SBR and ACR carbon fabrics were produced by V. FRAAS, Germany, while the EPX-carbon fabric was fabricated by Solidian, Germany.

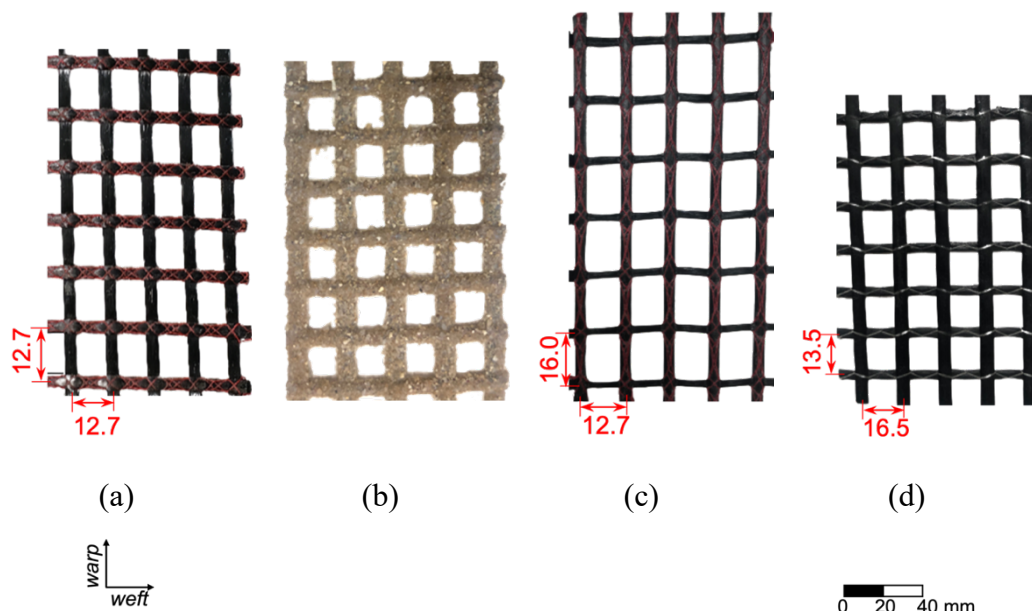


Figure 5.1 - Carbon fabrics with different coating conditions: a) SBR, b) SND, c) ACR and d) EPX.

Table 5.1– Carbon fabric properties reported by manufacturers.

	SBR	ACR	EPX
Tensile strength (MPa)	1638	2911	2700
Modulus of Elasticity (GPa)	126	162	250
Warp Yarn cross-section (mm²)	3.34	1.80	5.44
Weft Yarn cross-section (mm²)	3.30	0.45	3.85
Mesh Geometry (mm)	10 x 8.5	16 x 12.7	11.5 x 10.5

5.2.1.2.Cementitious Matrix

The fine-grained concrete used to produce the TRC beams was composed by the Brazilian Portland cement CII F-32, fly ash, micro silica and a fine aggregate natural sand with 1.18 mm maximum diameter. The compressive strength and the Young's modulus were obtained as the average of three samples having 50 mm in diameter and 100 mm of height. The characterization was carried out according to the ASTM C39 [63], using a servo hydraulic testing machine MTS 810 with load capacity of 500 kN. The mixture composition leads to a matrix with a flow table spreading of 345 mm, compressive strength of 76 ± 2.6 MPa and a modulus of elasticity of 28.4 ± 0.8 GPa at 28 days. More information about the matrix is presented in a previous work [64].

5.2.2.I-section beams production

The I-section structural beams were produced with a total length of 2000 mm, having 80 mm of flange width, 180 mm of depth and 12.5 mm of thickness. Eight beams were fabricated, with two samples for each impregnation condition studied – one for reference monotonic test and another for the flexural creep test. The beams were named according to their respective coating condition, i.e. SBR, ACR, EPX and SND. All beams were manufactured using the same steel formwork with the desired final shape and a single layer of reinforcement was adopted for web and flanges. Along the junction between web and flanges, a nylon line was used to tie together the orthogonal layers of the reinforcement for assembly purposes, as shown in Figure 5.2a. Although preferable, the reinforcement could not be

assembled in C-shape configuration as done in previous works [71, 72, 79, 80], because the fabrics used in the present work were supplied with coating and were relatively rigid. Therefore, bending in such small radius would cause the transverse yarns to break. The I-shape reinforcement was placed in the formwork before casting the concrete with the beam positioned horizontally, as shown in Figure 5.2b. The concrete was manually vibrated on the outside of the formwork. In all cases, the textile warp direction (see Figure 5.1) was placed parallel to the beam axis. While the reinforcement was placed manually, care was taken to keep it in the middle of the wall thickness. The beams were removed from the formwork after 48 hours and cured in a humid chamber until they reached 28 days of age.

As the yarn cross section area of each fabric was different, the geometric reinforcing ratio (ρ_f) for each beam varies, as presented in Table 5.2. The highest and lowest reinforcement ratios were 2.74% and 1.28%, respectively for EPX and ACR beams, while the SBR and SND had a ratio of 2.29%. This parameter was computed using the total yarn cross-sectional within I-section.

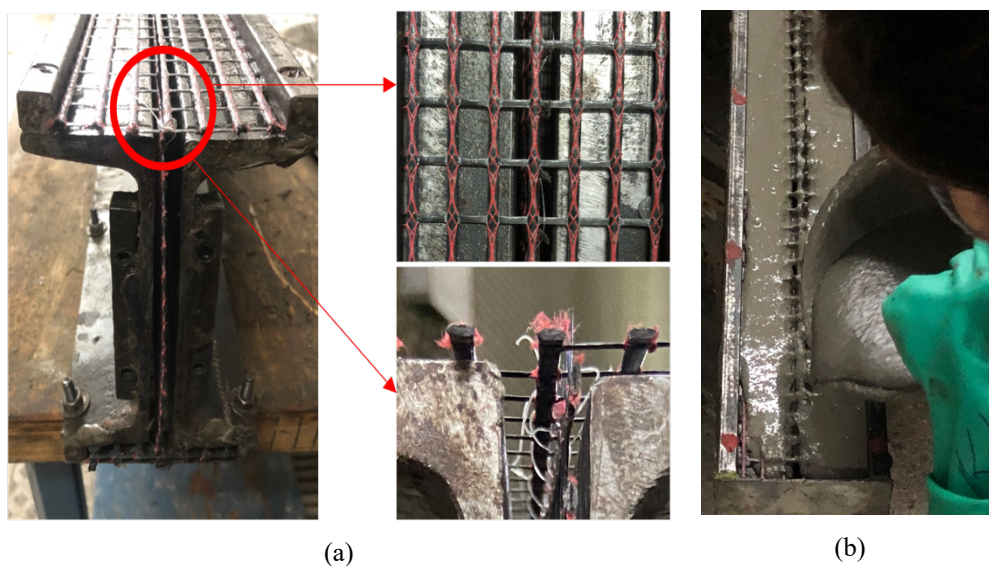


Figure 5.2– (a) Reinforcement assemble cage detail and (b) concrete casting process.

5.2.3. Overview of Experimental Program

The experimental program includes short- and long-term tests, as detailed in the flowchart presented in Figure 5.3. For the short-term reference tests, four beams were loaded monotonically up to failure in a four-point bending configuration, while having their flexural behavior monitored. For the long-term tests, the program comprised the following steps: i) a pre-cracking stage for a total load of 4 kN to

produce an initial cracking pattern; ii) creep tests under a sustained load of 4 kN for 90 days; iii) unloading and recovery for 10 days; and iv) post-creep monotonic tests performed up to failure to assess residual capacity. All tests were initiated with specimens at 28 days of age.

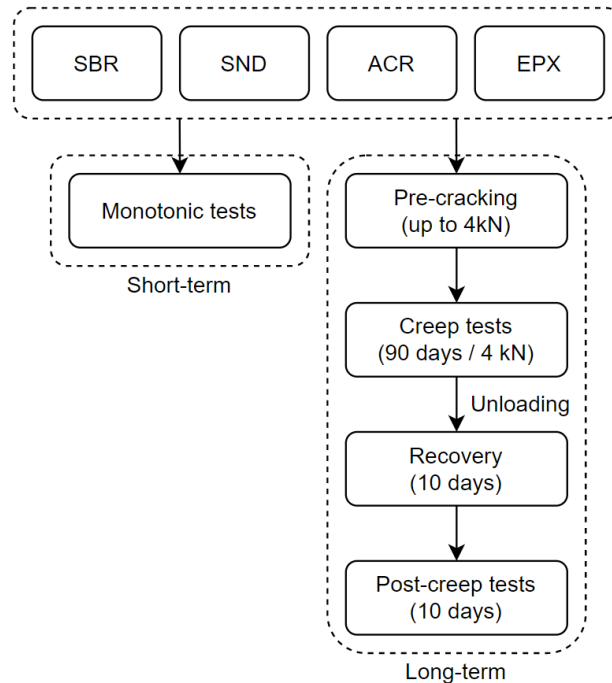
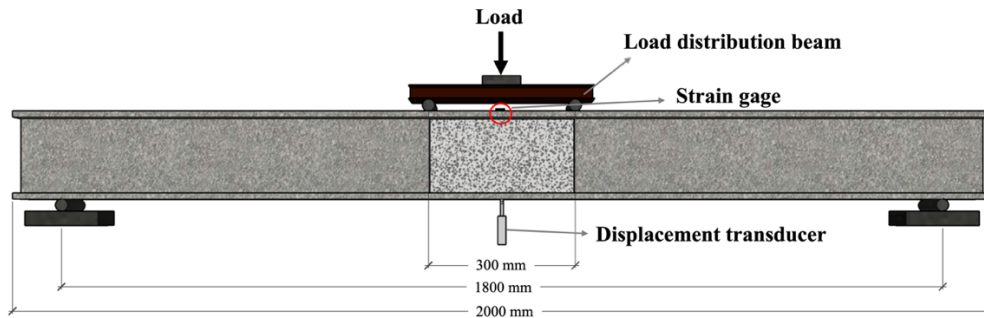


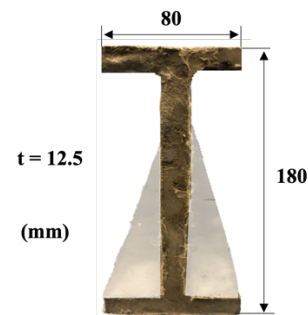
Figure 5.3– Flowchart representation of experimental program process.

5.2.3.1. Monotonic Test

The beams were tested in a four-point bending configuration over an 1800 mm span, with a shear span of 750 mm and constant moment region of 300 mm, as shown in the Figure 5.4a. A hinge was placed over the load distribution beam to ensure equal force distribution to the loading points. The tests were performed at a constant displacement rate of 1 mm/min up to failure using an MTS servo-controlled hydraulic actuator with 500 kN capacity. A displacement transducer was used to monitor the beam mid-span deflection. To measure the crack development, digital image correlation (DIC) technique was used over the constant moment region. In addition, a strain gage was placed on the top of the beam to record the concrete compressive strain at the mid-span. Figure 5.4 shows an overview of the setup test and the instrumentation adopted. The same methodology was adopted for the pre-cracking and post-creep tests, except that, for the former, tests were interrupted at an applied load of 4 kN (roughly 16 – 36 % of the ultimate load) and unloaded at a force rate of 1 kN/min.



(a)



(b)

Figure 5.4– Overview of the (a) scheme of test and (b) four-point bending setup and cross-section beam.

5.2.3.2. Long-term Test

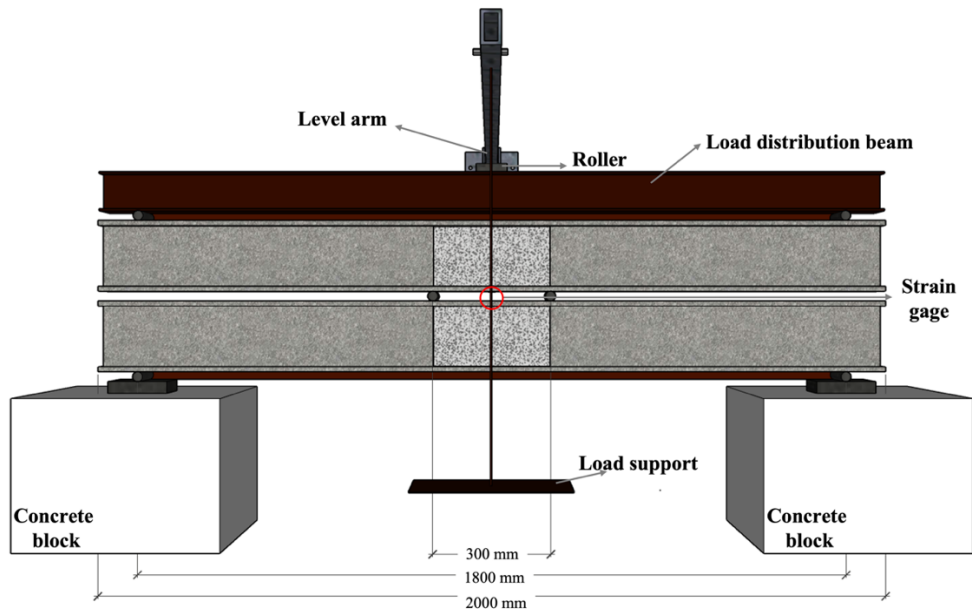
As mentioned previously, the long-term test is divided in four main steps, namely (1) pre-cracking, (2) sustained loading, (3) recovery and (4) post-creep monotonic test, as shown in the flowchart of Figure 5.3. After the pre-loading stage up to 4 kN and subsequent unloading, beams were moved to a room with controlled temperature ($24 \pm 1.5^\circ \text{C}$) and humidity ($55 \pm 5\%$) conditions for the flexural creep tests. Figure 5.5a shows an overview of the test setup adopted, which reproduces a four-point bending configuration with a constant moment region of 300 mm. For reasons of rationalization of laboratory space, only three frames were used to test the beams. The SND and ACR beams were tested in the same frame simultaneously (SND below), while SBR and EPX were tested in a separate frame.

Figure 5.5b shows details about instrumentation and load application. A support was placed in the middle of the beam span to support the displacement transducer, allowing to capture only the mid-span deflection for each beam. As depicted in Figure 5b, some of the rollers were allowed to move to mitigate the development

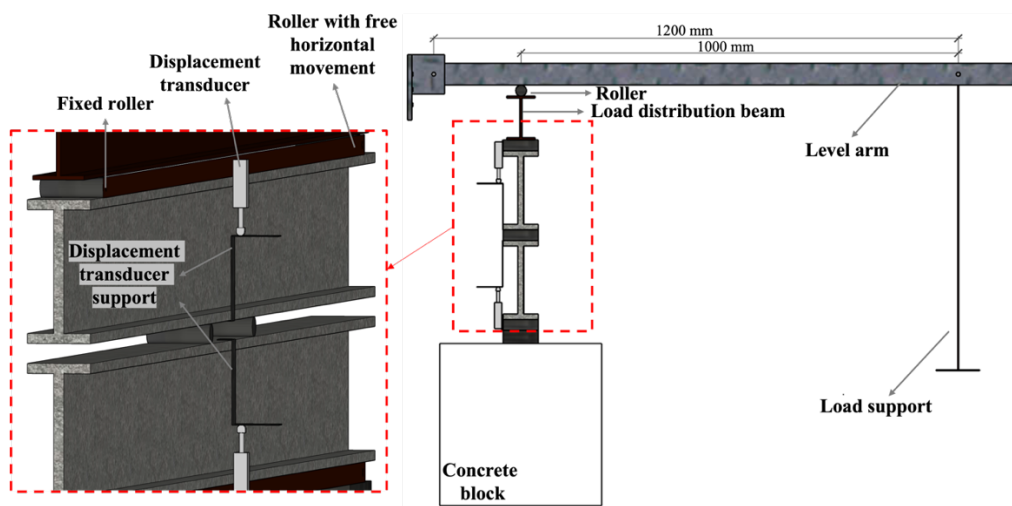
of horizontal forces. The load application system consists of a 1000 mm lever arm pinned at the wall and supported over the loaded structure. Prior to testing, the system was calibrated using load cells and it was concluded that a total dead load of 730 N should be added to the system to achieve an applied load of 4 kN over the beams. The dead weights were gradually applied over a period of approximately 2 min to avoid dynamic overload. It is important to highlight that the weight of the top beam is approximately 350 N, which is lower than 10% of the applied load and is assumed negligible in further analyses.

The same service load of 4 kN was applied for all specimens. The main objective was to analyze the behavior of the beams for a similar applied load. The ratios between applied and ultimate loads P_s/P_u (P_s = applied service load; P_u = ultimate load) for the beams are shown in Table 2. It is worth mentioning that this ratio does not correspond to the textile service-to-failure stress ratio because beams failed in shear (see Section 5.3.1). Therefore, P_u is not directly associated the textile capacity in tension. The mid-span deflection and compressive strain on the top of the beam were continuously monitored with displacement transducer and strain gage, as shown in the Figure 5.5. The crack opening of the widest crack was monitored weekly through pictures taken from the constant moment region, analyzed with Image J software [65].

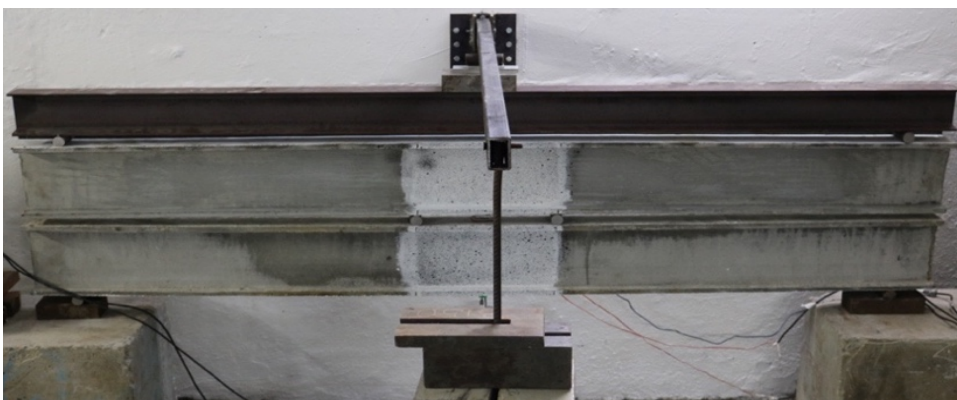
After 90 days, the load was removed and the elastic recovery data acquired. The DIC technique was used during the unloading process to analyze the crack closure and to capture the formation of new cracks. After unloading, the beams were kept in the test setup for another ten days and the creep recovery was monitored. Finally, the specimens were subjected to a post-creep four-point bending test until failure using the same loading system described in Section 5.2.3.1.



(a)



(b)



(c)

Figure 5.5 - (a) Scheme of flexural creep test and (b) details of the instrumentation and load application; (c) flexural creep test setup.

5.3.Results and discussion

5.3.1.Short-term Monotonic Tests

Table 5.2 summarizes the results obtained for the short-term monotonic tests carried out for the reference beams and Figure 5.6 shows the failure mode observed. SND had its failure governed by yarn rupture in the tension zone (Figure 5.6b), whereas SBR (Figure 5.6a) and ACR (Figure 5.6c) exhibited a shear dominated failure, characterized by the formation of a critical diagonal crack as well as longitudinal cracks along the web-to-flange junction, as a consequence of the weak connection used between the web and flange reinforcements (Section 5.2). Sand coating strategy was able to prevent the web weft yarns to be pulled out of the flange, leading to increased shear capacity. In the case of the EPX (Figure 5.6d) concrete cover spalling and yarn rupture of flange and web reinforcements were also observed. This beam also presented a shear dominated failure with a critical diagonal crack, similar to SBR and ACR.

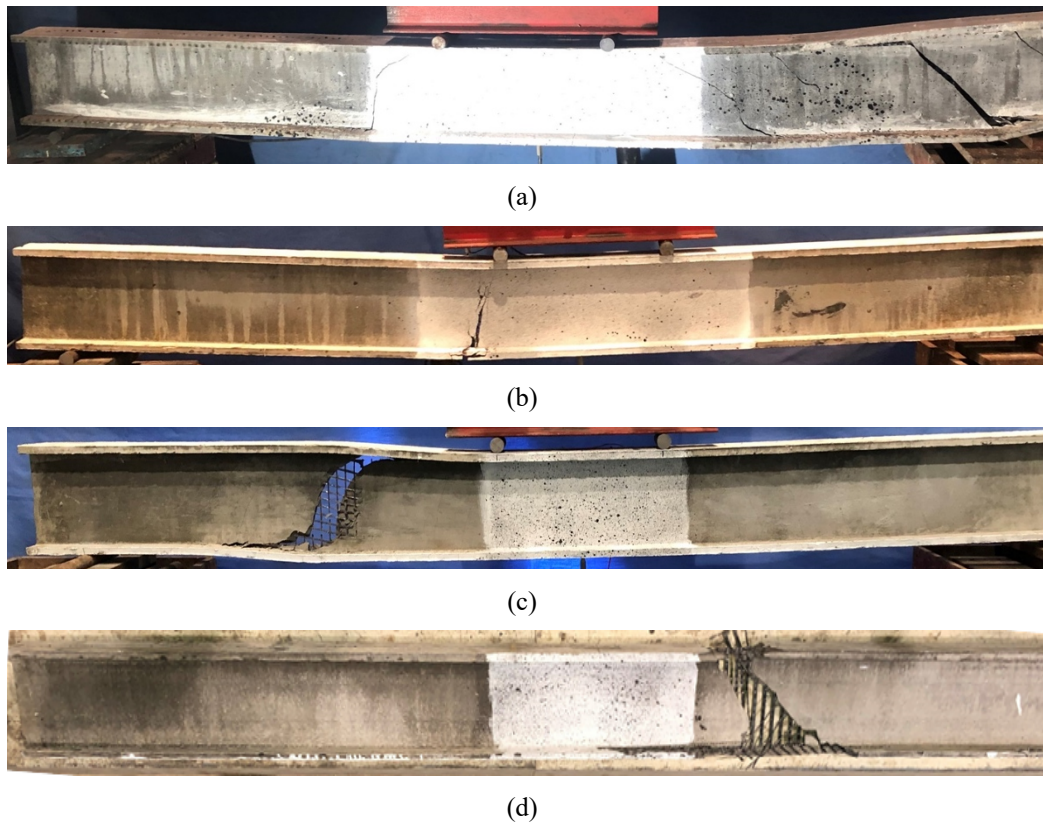


Figure 5.6– Failure mode of beams in monotonic test: a) SBR; b) SND; ACR and EPX.

Table 5.2– Summary of short-term monotonic tests results.

Specimen	SBR	SND	ACR	EPX
ρ_f (%)	2.29	2.29	1.28	2.74
P_{cr} (kN)	1.27	1.59	2.02	2.38
P_u (kN)	13.45	16.06	11.21	24.71
P_s/P_u	0.30	0.25	0.36	0.16
δ_u (mm)	26.89	25.48	18.97	36.06
M_u (kN.m)	5.04	6.02	4.21	9.26
f_{ct} (MPa)	2.26	4.82	5.03	5.89
E_f (GPa)	71.6	76.1	147.8	68.6
$\sigma_{f,s}$ (MPa)	234.8	235.3	422.0	197.1
$\sigma_{c,s}$ (MPa)	13.9	13.7	13.3	13.4
LR	0.14	0.14	0.15	0.07
$w_{m,s}$ (mm)	0.25	0.04	0.02	0.02
$w_{max,s}$ (mm)	0.32	0.09	0.06	0.05
$s_{m,s}$ (mm)	110.32	36.15	49.64	22.00
$s_{m,u}$ (mm)	110.32	25.64	35.42	14.84
τ_b (MPa)	0.36	0.54	4.08	37.6
Failure mode	Shear	Flexural (tension)	Shear	Shear (yarn rupture)

ρ_f – geometric reinforcing ratio;
 P_{cr} – first crack load;
 P_s and P_u – service (4 kN) and ultimate loads, respectively;
 M_u – bending moment at ultimate load;
 δ_u – mid-span deflection at ultimate load;
 $\sigma_{f,s}$ – tensile stresses at outermost yarns for service load;
 $\sigma_{c,s}$ – compressive stress at the outermost concrete fiber for service load
 $w_{m,s}$ and $w_{max,s}$ – mean and widest crack widths at service load;
 $s_{m,s}$ and $s_{m,u}$ – average crack spacing at service and ultimate loads;
 τ_b – nominal bond stress;
 f_{ct} – effective concrete tensile strength;
 E_f – effective textile tensile modulus;
LR – load ratio

Since beam response is highly influenced by coating [64], the effective modulus of elasticity (E_f) and the effective cracking stress (f_{ct}) for each beam were indirectly obtained through regression of experimental results for load interval between 2 kN and 6 kN, considering the approximate linear elastic model described in Appendix A. Values of E_f and f_{ct} are summarized in Table 5.2. Comparing these effective moduli of elasticity with those reported by manufacturer (Table 5.1), efficiency

factors of 0.57, 0.60, 0.91 and 0.27 are found for SBR, SND, ACR and EPX. While efficiency factors for SBR, SND [64] and ACR are in good agreement with literature, EPX value seems quite low. According to Valeri et al. [71], once the fabric is embedded in a cementitious matrix, a reduction in the cracked stage is assumed and the efficiency factor is adopted to take into account the non-uniform profile of stresses. This response depends on many factors related to the type of fabric (mesh opening, manufacturing process, coating, surface treatment, bumpiness) and on its anchorage conditions (length and properties) [71-78].

The stresses mobilized at the outermost yarns in tension can then be obtained from a typical linear cross-section analysis. Based on the reference ultimate strains presented in Table 5.1 for each material (1.3% for SBR and SND; 1.8% for ACR; and 1.1% for EPX), the load ratio (LR) with respect to the textile strength can be estimated for each case, as presented in Table 5.2. It can be seen that the load ratio ranges from 0.07 to 0.15, which indicates low utilization of the textile. Under these assumptions, it can be seen that the stresses differ for each beam due to the different geometric reinforcing ratios. The anticipated maximum textile stress at service occurs for the ACR beam (422 MPa), while the stress for EPX beam were slightly lower than 200 MPa (less than half of ACR). Regarding the concrete compressive stress, values ranging between 13.3 and 13.9 MPa were observed.

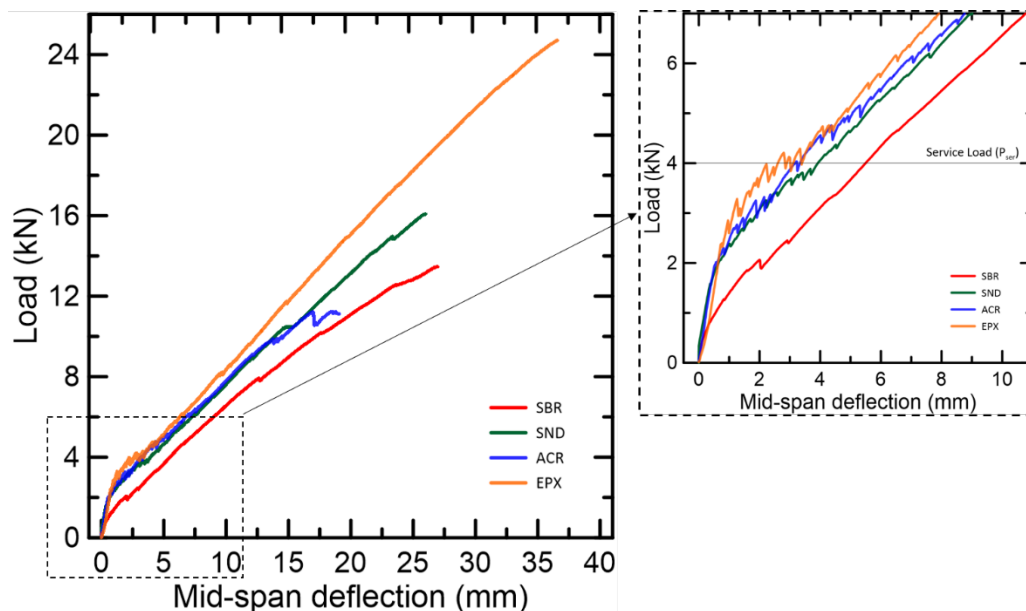


Figure 5.7– Load-deflection curves from monotonic test for beams with different textile reinforcements and reinforcing ratios.

Figure 5.8 shows the crack patterns at the constant moment region obtained with DIC technique for all beams at two different instants of time: at a service load P_s of 4 kN and immediately before failure (P_u). The number and width of the cracks, the distance between them and the crack associated with the corresponding analyzed loads were monitored using DIC. At first, it can be seen that the service load does not correspond to the end of the crack formation stage, particularly for SND, ACR and EPX beams, for which the number of cracks significantly increased with loading. This figure reveals an excellent bond performance for SND and EPX beams and a poor cracking behavior for SBR. ACR exhibited a lower number of cracks in comparison to SND and EPX, which can be partially associated to its lower reinforcing ratio.

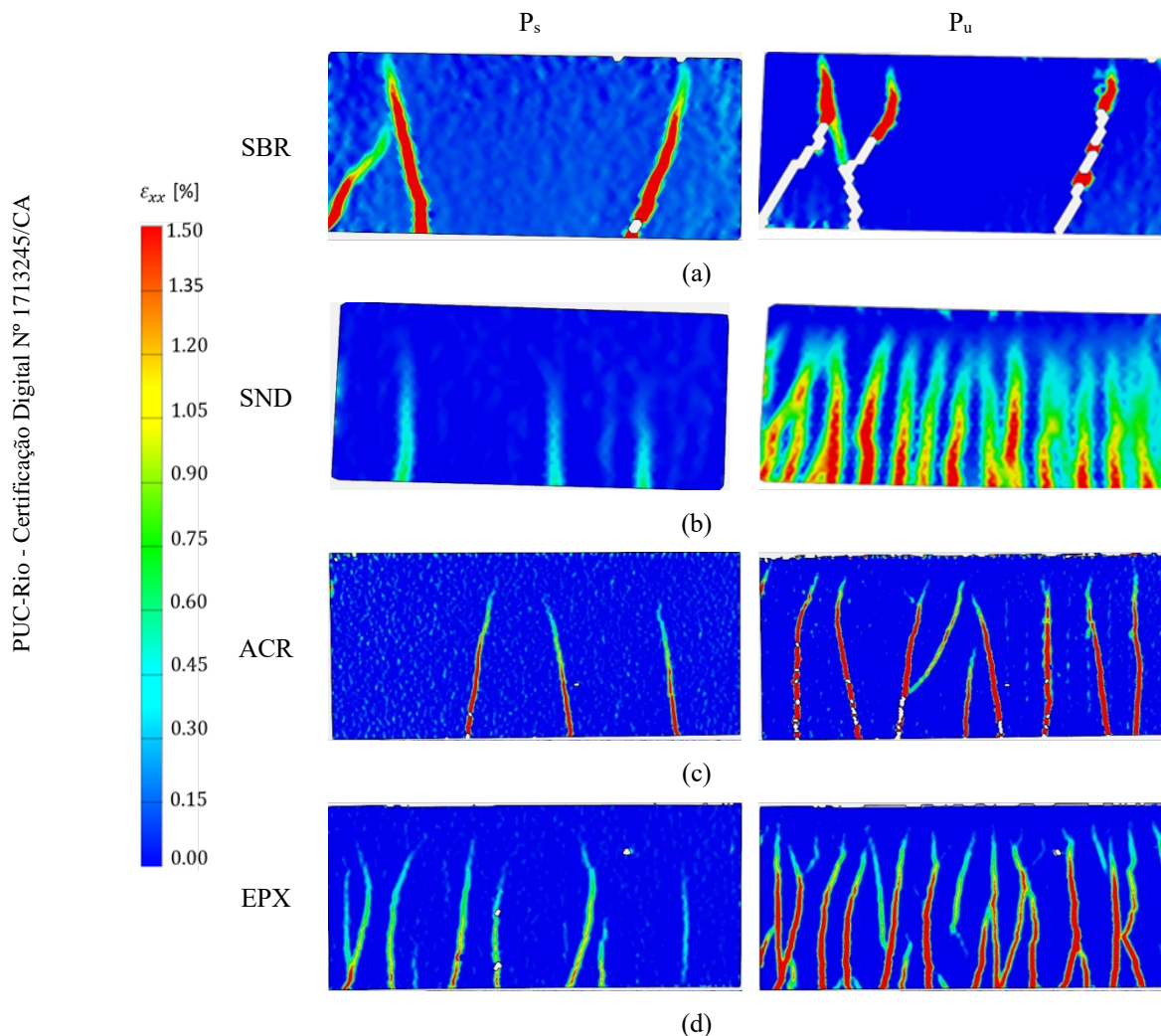


Figure 5.8– Cracking pattern of beams not in scale, only for crack pattern observation purposes): a) SBR; b) SND; c) ACR; d) EPX.

Crack growth was also analyzed through the moment *vs* crack opening relation ($M \times w$), as shown in Figure 5.9, where the average crack opening was estimated as the total elongation monitored at the bottom of the beam within the constant region divided by the final number of cracks formed at this region. This figure indicates an excellent bond performance for EPX beam, with very thin cracks formed. ACR also exhibited cracks, despite the lower ρ_f and larger stresses applied. Finally, it can be seen that the additional sand-coating strategy for SBR led to a significant improvement of cracking performance, as already observed in previous works [49, 66-70]. Values of crack opening and spacing load are also presented in Table 2 for reference. Since cracking openings are dependent on a number of parameters that are different for each beam such as the applied stress, modulus of elasticity, concrete tensile strength and reinforcing ratio, an attempt was made to compare the performances in terms of the nominal bond stress, τ_b . To do so, the model described in Appendix A was used and τ_b was determined indirectly through regression to minimize the error between the slopes of theoretical and experimental $M \times w$ curves at the stabilized cracking stage. Based on the values of τ_b reported in Table 2, it can be confirmed that EPX has the strongest bond strength (37.6 MPa), which is about 100 times that of SBR (0.36 MPa). On the other hand, values of τ_b for ACR and SND were near and respectively equal to 4.08 and 5.04 MPa.

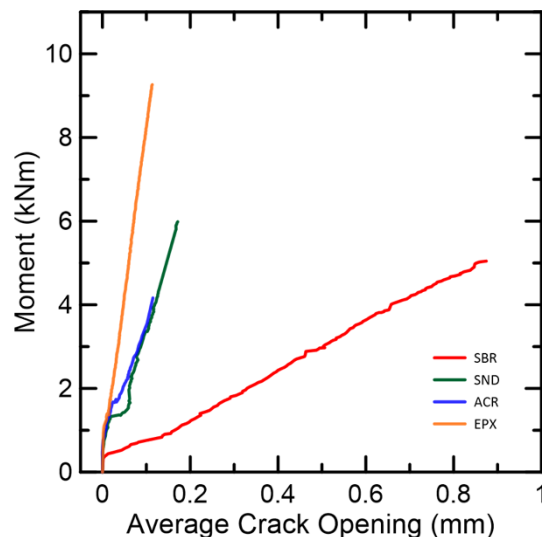


Figure 5.9– Moment vs average crack opening.

5.3.2. Long-term Tests

Table 5.3 summarizes the global results obtained during the long-term tests campaign, while typical load *vs* deflection and deflection *vs* time curves are

presented in Figures 5.10a and 5.10b, respectively. In Figure 10b, relevant creep parameters such as the immediate deflection (δ_0), the long-term deflection (δ_{90}) and deflection recovery (δ_r) are defined. In the discussions presented hereafter, these and other similar parameters related to crack opening (w_0 , w_{90} and w_r) and compressive strain (ε_0 , ε_{90} , ε_r) are adopted. Additionally, the numbers used in the subscript correspond to the age at which the parameter was evaluated, e.g. ε_{90} corresponds to the strain measured at 90 days.

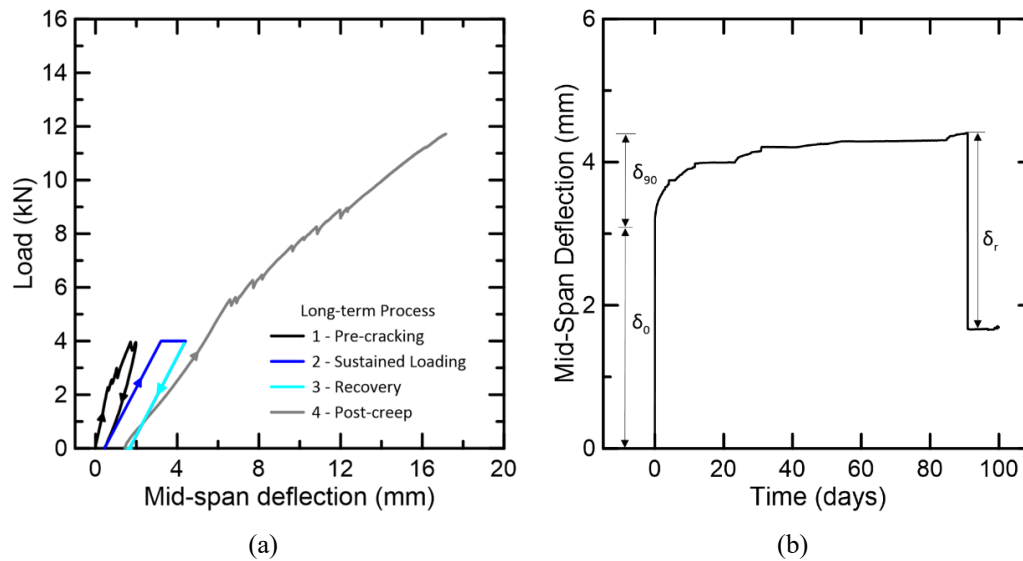


Figure 5.10– Flexural creep test graphical representation of the (a) process and (b) creep parameters over time.

Table 5.3– Summary of long-term tests results.

Specimen		SBR	SND	ACR	EPX
Pre-cracking	P_{cr} (kN)	2.22	3.66	2.27	2.13
	P_u (kN)	13.45	21.15	11.12	25.04
	δ_u (mm)	25.63	29.13	15.71	35.51
Post-creep tests	M_u (kN.m)	5.19	7.93	4.40	9.39
	$s_{m,u}$ (mm)	156.00	13.12	36.98	12.00
	Failure mode	Shear	Shear (Yarn rupture)	Shear	Shear (Yarn rupture)

P_{cr} – first crack load;

P_u – ultimate load;

δ_u – deflection at ultimate load;

M_u – ultimate moment;

$s_{m,u}$ – average spacing at ultimate load.

Figure 5.11 presents the load vs deflection curves for short and long-term tests, for each beam type. A good agreement between tests was achieved for the pre-cracking stage, with differences mainly associated to the inherent variability in concrete tensile. Higher cracking forces (P_{cr}) were particularly observed for SBR and SND beams, i.e. 74.8% and 108% with respect to the short-term tests. When unloaded and reloaded for the creep test, ACR and SND beams exhibited ‘jumps’ in the immediate deflection, with the formation of additional cracks that could not be captured in a controlled way. This may be attributed to the incremental manual force application procedure during the reloading of beams at the creep frames. Nonetheless, immediate deflections at the beginning of creep tests were similar to that observed at service load (4 kN) during short-term tests. Aspects of the behavior observed at the post-creep test will be discussed further.

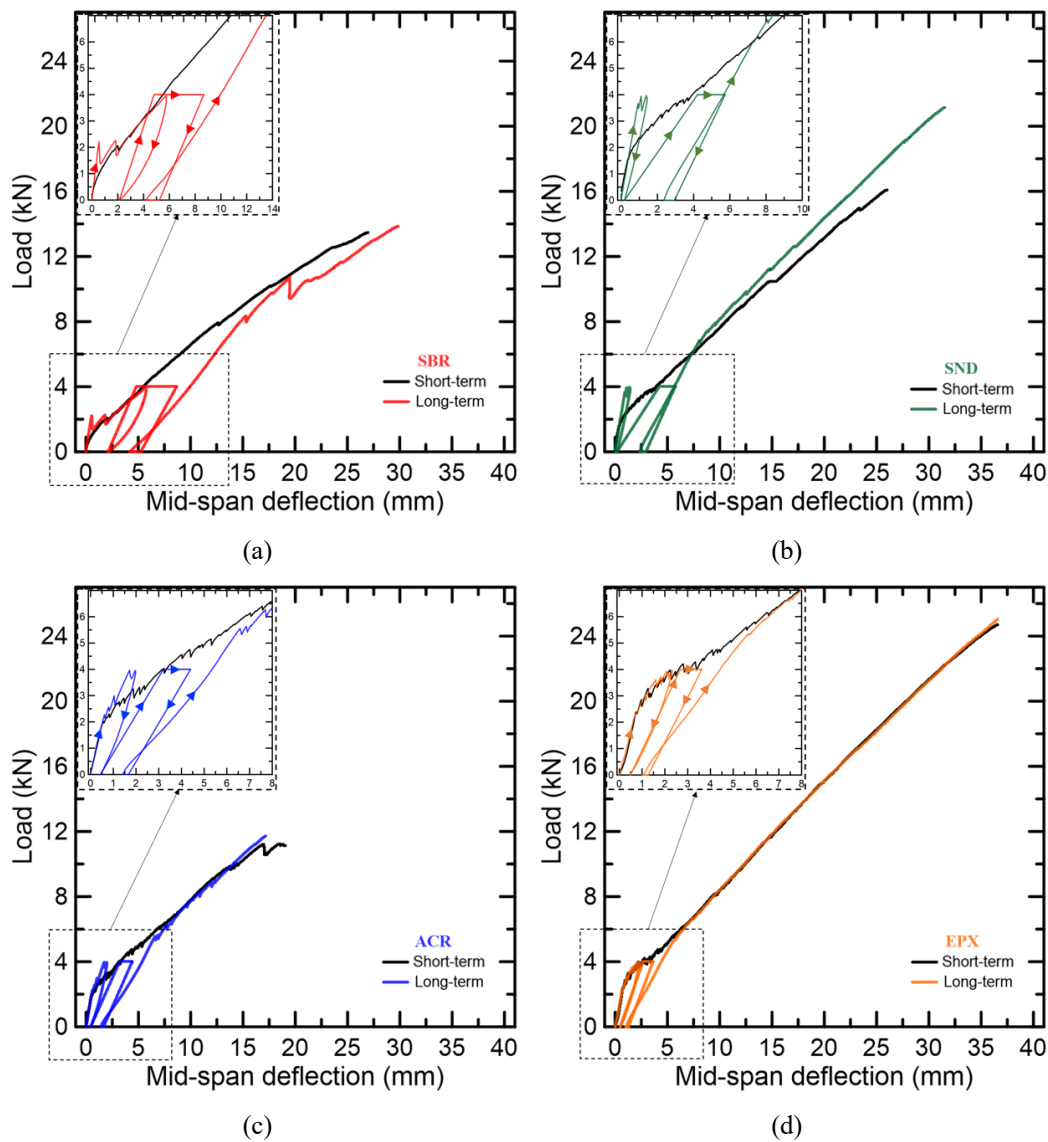


Figure 5.11– Load-deflection curves comparing the monotonic test with the creep process for a) SBR, b) SND, c) ACR and d) EPX.

The deflection response of the beams analyzed during the creep tests is presented in Figure 5.12a, whereas the evolution of creep deflection coefficient – $\varphi_{\delta,t} = \delta_t/\delta_0$ – is shown in Figure 5.12b, in which δ_0 and δ_t are deflections occurred at given times 0 and t, respectively, where 0 corresponds to the instant of time immediately after load application was completed. The behavior resembles a typical creep response, with well-marked primary and secondary creep stages – tertiary does not appear due to relatively short test duration. It can also be seen that deflections grow quickly immediately after loading for SBR specimen, which indicates a high creep rate at the primary creep stage. The deflections δ_0 and δ_{90} and some $\varphi_{\delta,t}$ values are presented in Table 5.4. As expected, SBR beam exhibited the greatest immediate deflection ($\delta_0 = 3.77$ mm) and EPX the lowest (2.49 mm). When analyzing the creep deflection coefficient, the SBR deflection after 90 days was 2.3 times the immediate value; in fact, a significant increase could already be seen after 10 days. Other beams also exhibited relevant creep coefficients, nearly 1.4-1.6 after 90 days, i.e. much lower than that SBR. In this context, it is interesting to compare the results for SBR and SND beams, which are reinforced with the same type of textile (but different coating conditions) and are subjected to similar tensile and compressive stresses (see Section 5.3.1), but have different $\varphi_{\delta,t}$ values. This difference indicates that the effective compliance of the reinforcement is dependent not only on the textile material properties, but also on its bond with the matrix. In the graphs, small discontinuities in the curves might be related to slight variations in temperature and humidity during the test.

Table 5.4– Long-term evolution of parameters related to overall beam performance.

Parameter	SBR	SND	ACR	EPX
δ_0 (mm)	3.77	3.55	2.97	2.49
δ_{90} (mm)	8.67	5.73	4.40	3.62
δ_r (mm)	3.43	2.80	2.74	2.35
$\varphi_{\delta,10}$	1.92	1.39	1.32	1.25
$\varphi_{\delta,30}$	2.07	1.48	1.40	1.34
$\varphi_{\delta,60}$	2.17	1.55	1.44	1.41
$\varphi_{\delta,90}$	2.30	1.61	1.48	1.45
ε_0 (mm)	-0.39	-0.30	-0.32	-0.30

ε_{90} (mm)	-0.69	-0.53	-0.66	-0.70
ε_r (mm)	*	-0.34	-0.37	-0.30
$\varphi_{\varepsilon,10}$	1.77	1.17	1.66	1.70
$\varphi_{\varepsilon,30}$	1.87	1.50	1.94	2.03
$\varphi_{\varepsilon,60}$	1.72	1.53	1.84	2.07
$\varphi_{\varepsilon,90}$	1.77	1.77	2.06	2.33
$E_{f,0}/E_{f,10}$	1.79	1.30	1.16	1.10
$E_{f,0}/E_{f,30}$	1.92	1.32	1.19	1.12
$E_{f,0}/E_{f,60}$	2.04	1.37	1.23	1.16
$E_{f,0}/E_{f,90}$	2.13	1.39	1.23	1.16

* After the unloading process, the compressive strain can not be measured for SBR specimen.

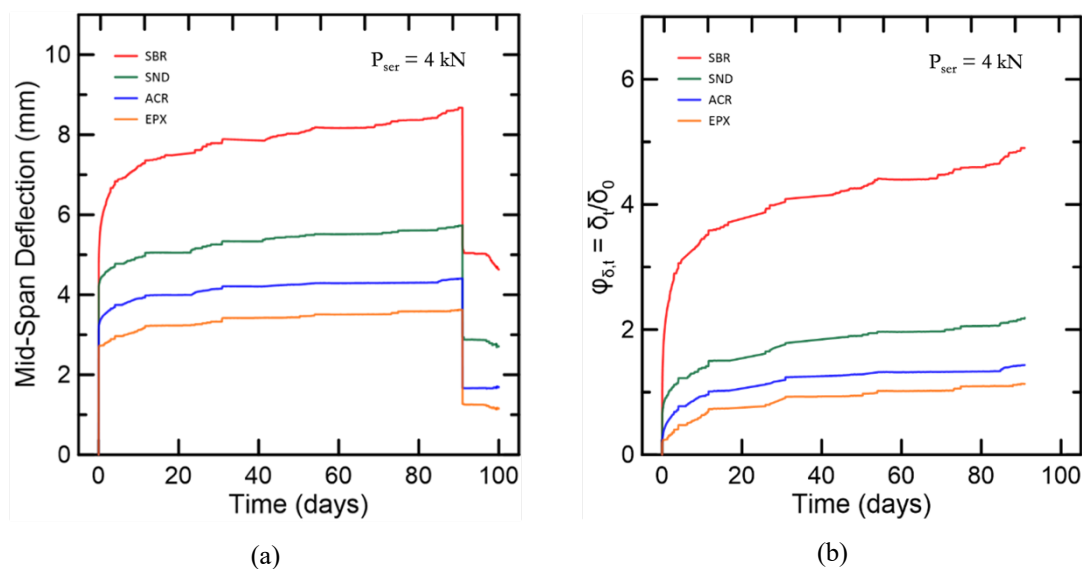


Figure 5.12– Long-term deflections: a) deflection-time curves and b) evolution of creep deflection coefficients.

The unloading process occurred after 90 days, and the deflection recovery (δ_r) was recorded (Figure 5.12a). Overall, the immediate elastic deflection recovery was slightly lower than the immediate deflection after loading. SND, ACR and EPX beam had a similar recovery of 2.80, 2.74 and 2.35 mm, respectively, while the SBR beam presented a recovery of 3.43 mm. Negligible long-term recovery was observed during the remaining 10 days for all beams.

In Table 5.4, the compressive strains measured at the beginning and by the end of the creep tests (ε_0 and ε_{90} , respectively) at the compression region of each beam are reported, as well as the creep strain coefficients at various t days of ages ($\varphi_{\varepsilon,t} = \varepsilon_t/\varepsilon_0$). It can be seen that, after 90 days, the strains roughly doubled. It is interesting

to point out that, although the compressive stresses at the SBR and SND beams are higher at the service load (Table 5.2), these beams exhibited lower creep coefficients than ACR and EPX beams. This may be associated to slight changes in the neutral axis depth during creep due to differential long-term deformations of concrete and textile reinforcement.

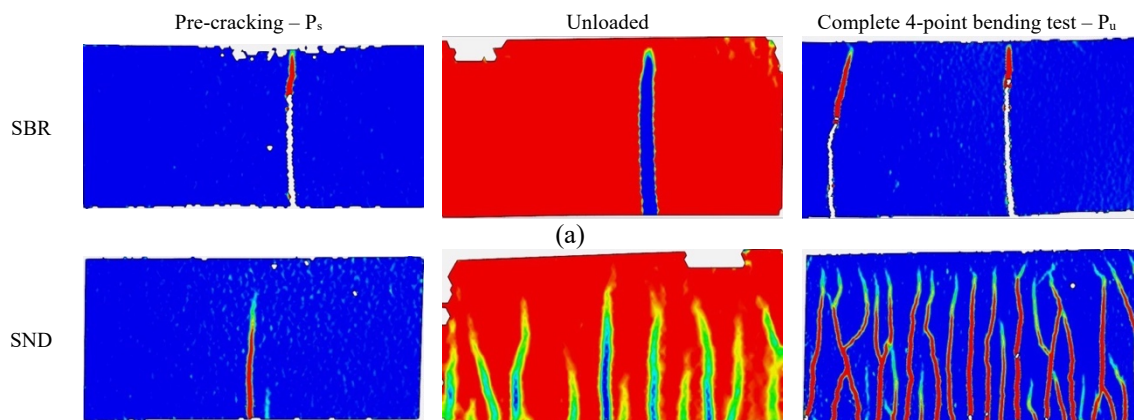
To estimate the textile compliance with time, two main hypotheses are assumed: i) the beam deflection at a given time t is obtained as the difference between the deflection calculated considering cracked stiffness (δ_{cr}) and the tension stiffness contribution (δ_c), following the model described in Appendix A; and ii) the variations in the concrete compressive strain with time described by parameter $\varphi_{e,t}$ can be interpreted as a reduction in the concrete modulus, i.e. $\varphi_{e,t} = E_{c,0}/E_{c,t}$, where $E_{c,0}$ and $E_{c,t}$ are the moduli at times 0 and t , respectively. As a consequence of these assumptions and considering negligible changes in the tension stiffening contribution with time, the time-dependent cracked stiffness $E_{c,t}I_{cr,t}$ can be correlated with the immediate cracked stiffness $E_{c,0}I_{cr,0}$ according to Eq. 5.1 – with δ_c/δ_0 estimated from short term tests for the service load. Then, having the concrete modulus and $E_{c,t}I_{cr,t}$ values for each instant of time t , the time-dependent textile effective modulus $E_{f,t}$ can be determined indirectly from the simple cross-sectional model (Appendix A). Values of $E_{f,0}/E_{f,t}$ – hereafter called normalized textile compliance – for different instants of time are reported in Table 5.4 and it can be seen that SBR-based textiles exhibit significant deformation under sustained load due to the viscoelastic nature of the coating. Comparing SND and SBR beams, it is clearly seen that the bond also plays an important role, avoiding slippage with time and keeping the effectivity of the reinforcement. In fact, the effective textile deformation after 90 days increased 113% and 39% for SBR and SND beams, respectively. On the other hand, epoxy- and acrylate-based textiles seem to be much less affected by sustained load – 16% of increase for EPX and 23% for ACR. Although simple, the strategy presented in this paragraph allows estimating the contribution of long-term textile performance to the creep behavior of the structural member.

$$E_{c,t}I_{cr,t} = E_{c,0}I_{cr,0} \frac{1 + \delta_c/\delta_0}{\varphi_{\delta,t} + \delta_c/\delta_0} \quad \text{Eq. 5.1}$$

Figure 5.13 shows the crack patterns for the constant moment region in three different stages: i) after the pre-loading stage at a 4 kN load (P_s); ii) after the creep

tests, with members unloaded; iii) immediately before failure, after post-creep test (P_u). It can be seen that additional cracks formed during the creep tests for SND, ACR and EPX beams. As mentioned previously, some cracks formed during the manual loading application, but a few formed also during the creep test, which may indicate a certain enhancement of nominal bond stresses. Additional cracks formed during the post-creep test. Graphs of moment vs crack opening for the widest crack of each beam are also presented in Figure 5.14, along with corresponding openings observed in the short-term tests. Creep crack coefficients – $\varphi_{\delta,t} = w_t/w_0$ – are summarized in Table 5.5, where w_0 and w_t are openings observed at 0 and t days, respectively. It can be seen that cracks for the SBR beam almost doubled after 90 days, while the ACR cracks showed increases as low as 6% in the same period. Cracks for EPX and SND beams increased by about 20%. It is important to note that precision and accuracy of crack opening measurements during creep tests were low and the coefficients presented in Table 5.5 correspond to rough approximations. Considering the simple crack model described in Appendix A, the long-term nominal bond stress $\tau_{b,t}$ at a time t can be related to its immediate value according to Eq. 5.2. The ratios between $\tau_{b,0}$ and $\tau_{b,t}$ for $t = 30, 60$ and 90 days are presented in Table 5.5. The results for all beams but EPX apparently reveal that two competing mechanisms developed with time: i) at early ages, nominal bond stress was enhanced due to late cement hydration and/or, in case of an ascending linear bond-slip law branch, due to small increments in textile slip; and ii) later, bond stress started decaying possibly due to long-term slippage at the matrix-textile interface. For the EPX beam, results are not conclusive.

$$\tau_{b,t} = \tau_{b,0} \frac{E_{f,0}/E_{f,t}}{\varphi_{w,t}} \quad \text{Eq. 5.2}$$



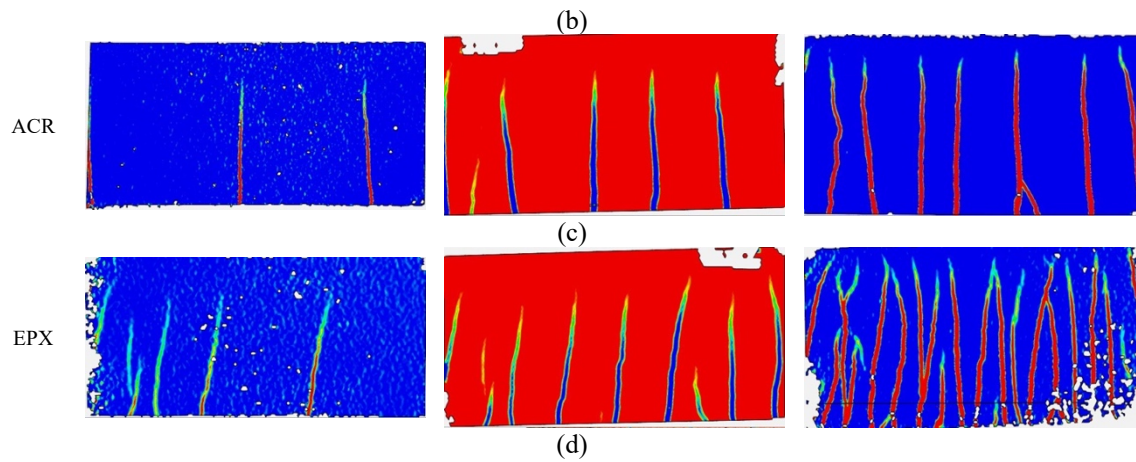
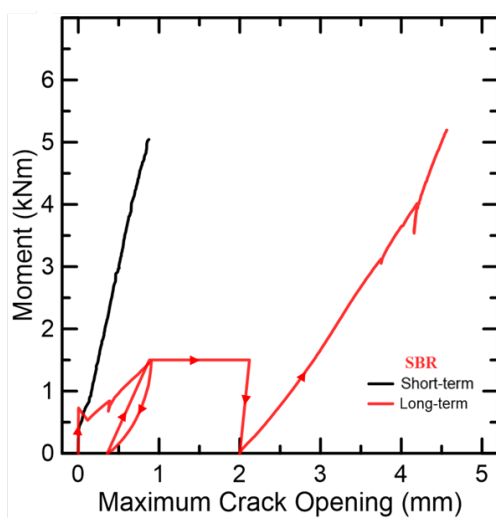


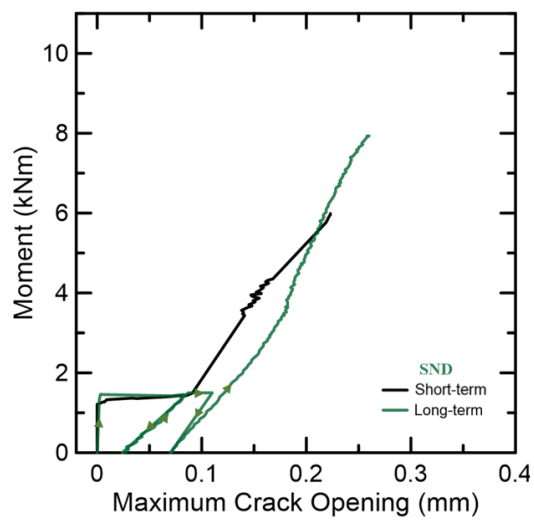
Figure 5.13– Cracking pattern of beams obtained using DIC: a) SBR; b) SND; c) ACR; d) EPX.

Table 5.5– Long-term evolution of parameters associated to cracking.

Parameter	SBR	SND	ACR	EPX
w_0 (mm)	1.07	0.10	0.12	0.09
w_{90} (mm)	2.21	0.12	0.13	0.11
$\phi_{w,30}$	1.35	1.10	1.00	1.11
$\phi_{w,60}$	1.68	1.10	1.00	1.22
$\phi_{w,90}$	1.98	1.20	1.08	1.22
$\tau_{b,0}/\tau_{b,30}$	0.70	0.83	0.84	0.99
$\tau_{b,0}/\tau_{b,60}$	0.83	0.80	0.81	1.05
$\tau_{b,0}/\tau_{b,90}$	0.92	0.86	0.88	1.05



(a)



(b)

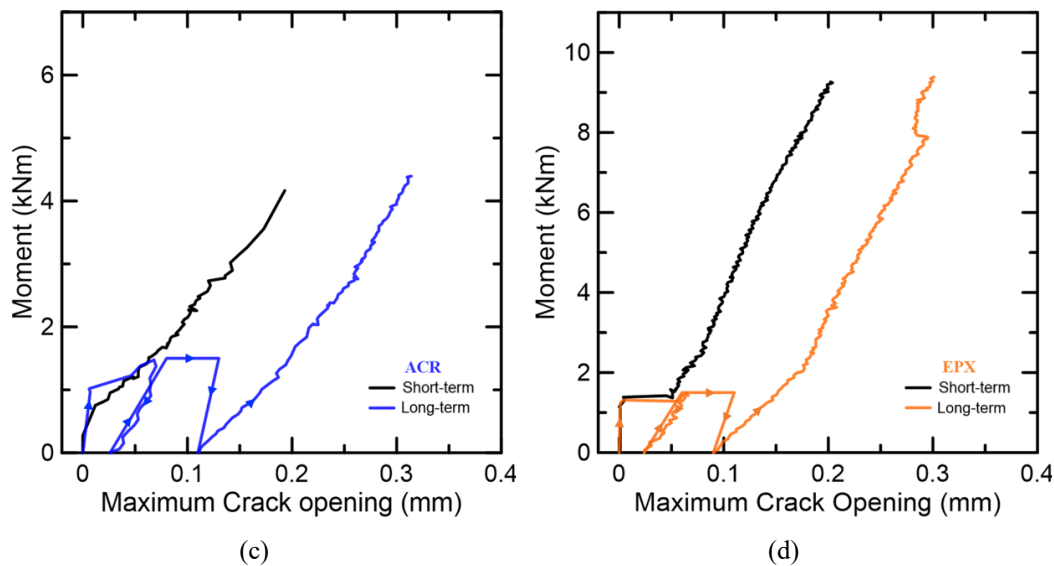


Figure 5.14– Moment vs maximum crack opening for: a) SBR; b) SND; c) ACR and d) EPX beams.

The failure modes for the beams after long-term testing are shown in Figure 5.15. All beams presented a similar abrupt and shear failure mode, with one critical diagonal crack between one of the supports and the nearest load application point. A similar failure was observed for SBR and ACR specimens for both short-term (Section 5.3.1) and post-creep tests, with slight changes in the crack shape and position. In the case of ACR, the diagonal crack failure region was larger and showed greater concrete spalling, whereas for the EPX beam no difference in the failure mode was found. Nevertheless, reinforcement failure was observed for the latter and beam was separated into two parts instantly once ultimate load was achieved. The SND beam presented the most significant difference rupture among tested beams; as shown in Figure 5.15b, rupture of web warp yarn occurred, followed by longitudinal tearing along web-to-flange junction across the entire length between the support and the load application point. This beam also showed an increase of about 32% in the load-carrying capacity when compared to its short-term counterpart, while the other had similar ultimate loads for both tests. This difference may be associated to inherent variabilities of material and fabrication procedure and more tests are necessary to confirm this trend. In general, no strength loss was observed for carbon-TRC beams after being subjected to a sustained load for 90 days, in agreement to the behavior observed by Spelter *et al.* [56] for carbon-TRC plates subject to tension. Finally, Figure 5.11 shows that all the specimens

tested followed load-displacement paths similar to that for short-term tests, indicating negligible loss of stiffness after the sustained loading period.

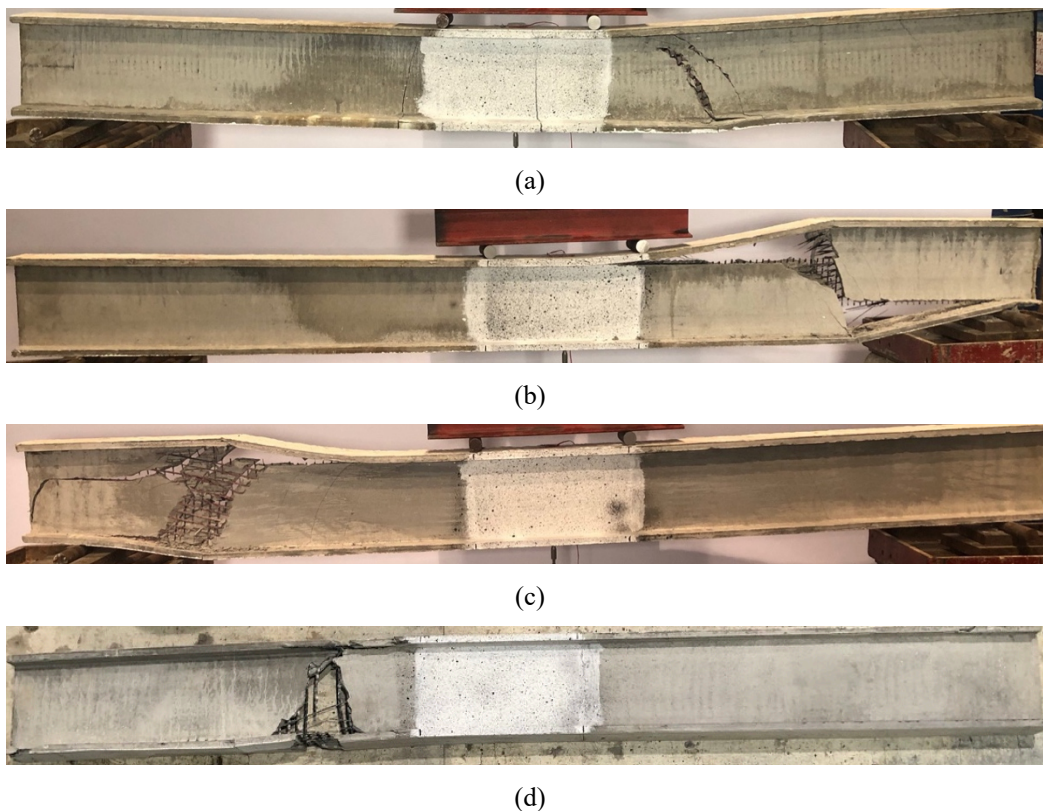


Figure 5.15– Failure mode of beams after residual bending tests: a) SBR; b) SND; ACR and EPX.

5.4. Conclusions

To investigate the long-term behavior of the carbon-TRC beams, short and long-term bending tests were performed for beams with different coating conditions (styrene-butadiene rubber - SBR, acrylate - ACR and epoxy - EPX, and SBR with an extra sand-coating - SND). It is important to highlight that although important conclusions were provided for the knowledge of the creep behavior of TRC beams, the number of samples was small, requiring further investigation. The main conclusions that can be drawn from this paper are:

- 1) All beams, in both tests, presented an abrupt failure at ultimate load, mainly governed by shear. Beams subjected to post-creep test did not show any sign of reduction in capacity; SND beam, in fact, showed a significant increase, but this trend needs to be confirmed with additional tests.
- 2) Since beams had different reinforcing ratios, an analytical linear model was successfully used to derive indirectly the effective textile moduli, concrete

tensile strength and the nominal bond stress, leading to results similar to those observed in literature.

- 3) The aforementioned model was later used to assess the evolution of long-term textile modulus and bond stress. The method indicates that SBR textiles are strongly affected by sustained load and have their effective deformation increased by 113% beams after 90 days, while increases of 39, 23 and 16% were seen for SND, ACR and EPX, respectively, under the same load. The differences between SND and SBR beams seem to indicate the bond also plays an important role, avoiding slippage with time and keeping the effectivity of the reinforcement.
- 4) With respect to cracking, SBR beam exhibited few wider cracks that grew significantly over time, while EPX had the closest and finest cracks among all beams. SND, ACR and EPX beams formed new cracks during the manual loading application procedure, as well as during the creep test. The reduction in effective modulus was not accompanied by the crack width. In fact, the results revealed an enhancement of bond stress at early ages, which may be partially attributed to late cement hydration. As time increased, the bond stress started decaying, possibly due to long-term slippage at the matrix-textile interface.
- 5) Results presented in the current work may raise interesting discussion about the different mechanisms affecting creep behavior and the parameters obtained may be useful for the development of a design strategy.

5.5. References

- [1] S. Rempel, C. Kulas, J. Hegger, Extremely light and slender precast pedestrian bridge made out of textile-reinforced concrete (TRC). High tech concrete: where technology and engineering meet. Switzerland (Cham): Springer Verlag, (2017) 2530–2537. https://doi.org/10.1007/978-3-319-59471-2_288.
- [2] A. Scholzen, R. Chudoba, J. Hegger, Thin-walled shell structures made of textile-reinforced concrete: Part I: Structural design and construction, Struct. Concr. 16, (2015) 106–114. <https://doi.org/10.1002/suco.201300071>.
- [3] E. Sharei, A. Scholzen, J. Hegger, R. Chudoba, Structural behavior of a

- lightweight, textile-reinforced concrete barrel vault shell, *Compos. Struct.* 171 (2017) 505-514. <http://dx.doi.org/10.1016/j.compstruct.2017.03.069>.
- [4] A. Schumann, H. Michler, F. Schladitz, M. Curbach, Parking slabs made of carbon reinforced concrete, *Struct. Conc.* 19 (2018) 647–655. <https://doi.org/10.1002/suco.201700147>.
- [5] Helbig, T., Unterer, K., Kulas, C., Rempel, S., & Hegger, J. (2016). Fuß-und Radwegbrücke aus Carbonbeton in Albstadt-Ebingen: Die weltweit erste ausschließlich carbonfaserbewehrte Betonbrücke. *Beton-und Stahlbetonbau*, 111(10), 676-685.
- [6] May, S., Steinbock, O., Michler, H., & Curbach, M. (2019, April). Precast slab structures made of carbon reinforced concrete. In *Structures* (Vol. 18, pp. 20-27). Elsevier. <https://doi.org/10.1016/j.istruc.2018.11.005>
- [7] Scholzen A, Chudoba R, Hegger J. Thin-walled shell structures made of textilereinforced concrete: Part I: Structural design and construction. *Struct Concr* 2015;16:106–14. <https://doi.org/10.1002/suco.201300071>.
- [8] Scholzen A, Chudoba R, Hegger J. Thin-walled shell structures made of textilereinforced concrete: part II: experimental characterization, ultimate limit state assessment and numerical simulation. *Struct Concr* 2015;16:106–14. <https://doi.org/10.1002/suco.201400046>.
- [9] Schumann A, Michler H, Schladitz F, Curbach M. Parking slabs made of carbon reinforced concrete. *Struct Concr* 2018;19:647–55. <https://doi.org/10.1002/suco.201700147>
- [10] Bruckner A, Ortlepp R, Curbach M (2006) Textile reinforced concrete for strengthening in bending and shear. *Mater Struct* 39:741–748. <https://doi.org/10.1617/s11527-005-9027-2>.
- [11] Ambrisi AD, Focacci F (2011) Flexural strengthening of RC beams with cement-based composites. *J Compos Constr* 15:707–720. [https://doi.org/10.1061/\(ASCE\)CC.1943-5614.0000218](https://doi.org/10.1061/(ASCE)CC.1943-5614.0000218).
- [12] Nahum, Lior, Alva Peled, and Erez Gal. The flexural performance of structural concrete beams reinforced with carbon textile fabrics. *Composite Structures* 239 (2020): 111917. <https://doi.org/10.1016/j.compstruct.2020.111917>.
- [13] Tetta, Zoi C., Lampros N. Koutas, and Dionysios A. Bournas. (2016) Shear strengthening of full-scale RC T-beams using textile-reinforced mortar

- and textile-based anchors." *Composites Part B: Engineering* 95: 225-239. <http://dx.doi.org/10.1016/j.compositesb.2016.03.076>.
- [14] Tetta ZC, Koutas LN, Bournas DA. (2015) Textile-reinforced mortar (TRM) versus fiber-reinforced polymers (FRP) in shear strengthening of concrete beams. *Compos Part B* 77: 338e48. <http://dx.doi.org/10.1016/j.compositesb.2015.03.055>.
- [15] Ortlepp, Regine, and Sebastian Ortlepp. Textile reinforced concrete for strengthening of RC columns: A contribution to resource conservation through the preservation of structures." *Construction and Building Materials* 132 (2017): 150-160. <http://dx.doi.org/10.1016/j.conbuildmat.2016.11.133>.
- [16] Kouris LAS, Triantafillou TC (2018) State-of-the-art on strengthening of masonry structures with textile reinforced mortar (TRM). *Constr Build Mater* 188:1221–1233. <https://doi.org/10.1016/j.conbuildmat.2018.08.039>.
- [17] Koutas LN, Tetta Z, Bournas DA, Triantafillou TC (2019) Strengthening of concrete structures with textile reinforced mortars: state-of-the-art review. *J Compos Constr.* [https://doi.org/10.1061/\(ASCE\)CC.1943-5614.0000882](https://doi.org/10.1061/(ASCE)CC.1943-5614.0000882).
- [18] Dvorkin D, Peled A (2016) Effect of reinforcement with carbon fabrics impregnated with nanoparticles on the tensile behavior of cement-based composites. *Cem Concr Res* 85:28–38. <https://doi.org/10.1016/j.cemconres.2016.03.008>
- [19] Dvorkin D, Poursaee A, Peled A, Weiss WJ (2013) Influence of bundle coating on the tensile behavior, bonding, cracking and fluid transport of fabric cement-based composites. *Cem Concr Compos* 42:9–19. <https://doi.org/10.1016/j.cemconcomp.2013.05.005>.
- [20] Halvaei M, Latifi M, Jamshidi M (2018) Study of the microstructure and flexural behavior of cementitious composites reinforced by surface modified carbon textiles. *Constr Build Mater* 158:243–256. <https://doi.org/10.1016/j.conbuildmat.2017.10.044>.
- [21] Zhu D, Gencoglu M, Mobasher B (2009) Low velocity flexural impact behavior of AR glass fabric reinforced cement composites. *Cem Concr Compos* 31:379–387. <https://doi.org/10.1016/j.cemconcomp.2009.04.011>
- [22] de Silva FA, Butler M, Mechtcherine V et al (2011) Strain rate effect on the tensile behaviour of textile-reinforced concrete under static and dynamic loading. *Mater Sci Eng A* 528:1727–1734.

- <https://doi.org/10.1016/j.msea.2010.11.014>.
- [23] Du Y, Zhang M, Zhou F, Zhu D (2017) Experimental study on basalt textile reinforced concrete under uniaxial tensile loading. *Constr Build Mater* 138:88–100. <https://doi.org/10.1016/j.conbuildmat.2017.01.083>
- [24] Du Y, Zhang X, Zhou F et al (2018) Flexural behavior of basalt textile-reinforced concrete. *Constr Build Mater* 183:7–21. <https://doi.org/10.1016/j.conbuildmat.2018.06.165>
- [25] Sneed LH, D'Antino T, Carloni C. Investigation of bond behavior of PBO fiberreinforced cementitious matrix composite-concrete interface. *ACI Mater J* 2014;111(5):569e80.
- [26] Caggegi C, Carozzi FG, De Santis S, Fabbrocino F, Focacci F, Hojdis L, et al. Experimental analysis on tensile and bond properties of PBO and Aramid fabric reinforced cementitious matrix for strengthening masonry structures. *Compos Part B Eng*, <http://dx.doi.org/10.1016/j.compositesb.2017.05.048>.
- [27] Silva F de A, Filho RDT, Filho JAM, Fairbairn EMR (2007) Effect of reinforcement ratio on the mechanical response of compression molded sisal fiber textile reinforced concrete. In: *High performance fiber reinforced cement composites (HPFRCC5)*, pp 175–182
- [28] de Silva FA, Mobasher B, Filho RDT (2009) Cracking mechanisms in durable sisal fiber reinforced cement composites. *Cem Concr Compos* 31:721–730. <https://doi.org/10.1016/j.cemconcomp.2009.07.004>
- [29] Teixeira, Felipe Pinheiro, and Flávio de Andrade Silva. "On the use of natural curaua reinforced cement based composites for structural applications." *Cement and Concrete Composites* 114 (2020): 103775. <https://doi.org/10.1016/j.cemconcomp.2020.103775>.
- [30] Fidelis MEA, de Andrade Silva F, Toledo Filho RD (2014) The influence of fiber treatment on the mechanical behavior of jute textile reinforced concrete. *Key Eng Mater* 600:469–474. <https://doi.org/10.4028/www.scientific.net/KEM.600.469>
- [31] Perry G, Dittel G, Gries T, Goldfeld Y. Mutual effect of textile binding and coating on the structural performance of TRC beams. *J Mater Civ Eng* 2020;32 (8):04020232. [https://doi.org/10.1061/\(ASCE\)MT.1943-5533.0003331](https://doi.org/10.1061/(ASCE)MT.1943-5533.0003331).

- [32] Bielak, J., Li, Y., Hegger, J., & Chudoba, R. (2018) Characterization procedure for bond, anchorage and strain-hardening behavior of textile-reinforced cementitious composites. Multidisciplinary Digital Publishing Institute Proceedings. Vol. 2, 395. <https://doi:10.3390/ICEM18-05224>.
- [33] Krüger, M., Reinhardt, H.W., Fichtlscherer, M. Bond behaviour of textile reinforcement in reinforced and prestressed concrete, *Otto-Graf-J.* 12 (2001) 33–50.
- [34] Yin, S. P., Xu, S. L., and Wang, F. (2015). Investigation on the flexural behavior of concrete members reinforced with epoxy resin-impregnated textiles. *Materials and Structures*, 48(1), 153-166. <https://doi.org/10.1617/s11527-013-0174-6>.
- [35] Raupach, M., Orlowsky, J., Büttner, T., Diltthey, U., Schleser, M., & Hegger, J. (2006, September). Epoxy-impregnated textiles in concrete-load bearing capacity and durability. In *Proceedings of the 1st International RILEM Conference* (pp. 77-88).
- [36] Wagner, J., & Curbach, M. Bond fatigue of TRC with epoxy impregnated carbon textiles. *Applied Sciences* (2019), 9(10), 1980. <https://doi.org/10.3390/app9101980>.
- [37] Hegger, J., Will, N., Bruckermann, O., & Voss, S. (2006). Load-bearing behaviour and simulation of textile reinforced concrete. *Materials and structures*, 39(8), 765-776. <https://doi.org/10.1617/s11527-005-9039-y>.
- [38] Schleser, M., Walk-Laufer, B., Raupach, M., & Diltthey, U. (2006). Application of polymers to textile-reinforced concrete. *Journal of materials in civil engineering*, 18(5), 670-676. [https://doi.org/10.1061/\(ASCE\)0899-1561\(2006\)18:5\(670\)](https://doi.org/10.1061/(ASCE)0899-1561(2006)18:5(670)).
- [39] Gong, T., Heravi, A., Alsous, G., Curosu, I., & Mechtcherine, V. (2019). The impact-tensile behavior of cementitious composites reinforced with carbon textile and short polymer fibers. *Applied Sciences*, 9(19), 4048. <https://doi.org/10.3390/app9194048>.
- [40] Donnini J, Corinaldesi V, Nanni A. Mechanical properties of frcm using carbon fabrics with different coating treatments. *Compos Part B Eng* 2016;88:220–8. <https://doi.org/10.1016/j.compositesb.2015.11.012>.
- [41] Diltthey U, Schleser M., Hegger J, Voss S, Load-bearing behaviour of polymer impregnated textiles in concrete. In *Proceedings of the fifth*

- international RILEM workshop (HPFRCC5 PRO53), RILEM Publications SARL, Mainz (2007) 183–192.
- [42] Zhu, D., Peled, A., & Mobasher, B. (2011). Dynamic tensile testing of fabric–cement composites. *Construction and Building Materials*, 25(1), 385–395. <https://doi.org/10.1016/j.conbuildmat.2010.06.014>.
- [43] Mechtcherine, V. (2012). Towards a durability framework for structural elements and structures made of or strengthened with high-performance fibre-reinforced composites. *Construction and Building Materials*, 31, 94–104. <https://doi.org/10.1016/j.conbuildmat.2011.12.072>.
- [44] M. Hinzen, W. Brameshuber, Improvement of Serviceability and Strength of Textile Reinforced Concrete by Using Short Fibres. In *Proceedings of the 4th Colloquium on Textile Reinforced Structures*, (2009) 261–272.
- [45] Schneider, K., Mechtcherine, V. Serviceability limit state design for carbon reinforced concrete structures. In *Proceedings of the 12th 13. Carbon and Textile Reinforced Concrete Days*, (2020) 42-47.
- [46] Donnini, J., Corinaldesi, V., & Nanni, A. (2016). Mechanical properties of FRCM using carbon fabrics with different coating treatments. *Composites Part B: Engineering*, 88, 220-228. <http://dx.doi.org/10.1016/j.compositesb.2015.11.012>.
- [47] D'Antino, T., & Papanicolaou, C. (2017). Mechanical characterization of textile reinforced inorganic-matrix composites. *Composites Part B: Engineering*, 127, 78-91. <http://dx.doi.org/10.1016/j.compositesb.2017.02.034>.
- [48] Schütze E, Curbach M. Experimental characterization of the bond behaviour of carbon reinforced concrete with concrete splitting as significant failure mode. *Bauingenieur* 2019;94:133–41. doi.org/10.37544/0005-6650-2019-04-61.
- [49] de Silva RMC, de Silva FA. Carbon textile reinforced concrete: materials and structural analysis. *Mater Struct* 2020;530:1–17. <https://doi.org/10.1617/s11527-020-1448-4>.
- [50] Goliath, K. B., Cardoso, D. C., & Silva, F. D. A. Bearing behavior of Carbon-Textile-Reinforced Concrete Beams. In *Proceedings of the 12th 13. Carbon and Textile Reinforced Concrete Days*, (2020) 54-59.
- [51] Gong, T., Ahmed, A. H., Curosu, I., & Mechtcherine, V. (2020). Tensile

- behavior of hybrid fiber reinforced composites made of strain-hardening cement-based composites (SHCC) and carbon textile. *Construction and Building Materials*, 262, 120913. <https://doi.org/10.1016/j.conbuildmat.2020.120913>.
- [52] Cardoso, Daniel Carlos Taissum, and Kent A. Harries. (2019) A viscoelastic model for time-dependent behavior of pultruded GFRP." *Construction and Building Materials* 208: 63-74. <https://doi.org/10.1016/j.conbuildmat.2019.02.155>
- [53] Ascione, Luigi, Valentino Paolo Berardi, and Anna D'Aponte. (2012) Creep phenomena in FRP materials. *Mechanics Research Communications* 43: 15-21. <https://doi.org/10.1016/j.mechrescom.2012.03.010>
- [54] Freitag, S., Beer, M., Jesse, F., & Weiland, S. Experimental investigation and prediction of long-term behavior of textile. In *ICTRC'2006-1st International RILEM Conference on Textile Reinforced Concrete*, pp. 121-130 (2006). RILEM Publications SARL.
- [55] Ali, A. H., Mohamed, H. M., Benmokrane, B., & ElSafty, A. (2019). Effect of applied sustained load and severe environments on durability performance of carbon-fiber composite cables. *Journal of Composite Materials*, 53(5), 677-692. <https://doi.org/10.1177/0021998318789742>
- [56] Spelter, A., Bergmann, S., Bielak, J., & Hegger, J. "Long-term durability of carbon reinforced concrete: An overview and experimental investigations", *Applied Sciences*, 9(8), 2019, 1651. <https://doi.org/10.3390/app9081651>.
- [57] Yin, S., Jing, L., Yin, M., & Wang, B. (2019). Mechanical properties of textile reinforced concrete under chloride wet-dry and freeze-thaw cycle environments. *Cement and Concrete Composites*, 96, 118-127. <https://doi.org/10.1016/j.cemconcomp.2018.11.020>.
- [58] Ortlepp, S., & Jesse, F. (2006). Experimental investigation of static fatigue strength of textile reinforced concrete. In *1st International RILEM Conference on Textile Reinforced Concrete (ICTRC)*: RILEM Publications SARL (pp. 131-40).
- [59] CNR-DT 215/2018 - Guide for the Design and Construction of Externally Bonded Fibre Reinforced Inorganic Matrix Systems for Strengthening Existing Structures

- [60] ACI 549.4R, Guide to design and construction of externally bonded fabric-reinforced cementitious matrix (FRCM) systems for repair and strengthening concrete and masonry structures. ACI 549 committee, 2013.
- [61] ACI (American Concrete Institute). Guide test methods for fiber-reinforced polymers (FRPs) for reinforcing or strengthening concrete structures. ACI 440.3R-04. Farmington Hills, MI: Author, 2004.
- [62] Goliath, K. B., Cardoso, D. C., & Silva, F. D. A. (2021). Flexural Behavior of Carbon Fiber Textile-Reinforced Concrete I-Section Beams. *Special Publication*, 345, 196-206.
- [63] ASTM C39/C39M-18, Standard Test Method for Compressive Strength of Cylindrical Concrete Specimens, ASTM International, West Conshohocken, PA, 2018, www.astm.org.
- [64] Goliath, K. B., Cardoso, D. C., & Silva, F. D. A. (2021). Flexural behavior of carbon-textile-reinforced concrete I-section beams. *Composite Structures*, 260, 113540. <https://doi.org/10.1016/j.compstruct.2021.113540>.
- [65] Image J/Fiji 1.46, Version, 2012. <https://imagej.nih.gov/ij/index.html>
- [66] Cruz CM, Raupach M. Influence of the surface modification by sanding of carbon textile reinforcements on the bond and load-bearing behavior of textile reinforced concrete. *MATEC Web Conf* 2019;289:04006. <https://doi.org/10.1051/mateconf/201928904006>.
- [67] Valeri, P., Ruiz, M. F., & Muttoni, A. (2020). Tensile response of textile reinforced concrete. *Construction and Building Materials*, 258, 119517. <https://doi.org/10.1016/j.conbuildmat.2020.119517>.
- [68] Portal NW, Perez IF, Thrane LN, Lundgren K. Pull-out of textile reinforcement in concrete. *Constr Build Mater* 2014;71:63–71. <https://doi.org/10.1016/j.conbuildmat.2014.08.014>.
- [69] Dalalbashia A, Ghiassib B, Oliveira DV, Freitas A. Effect of test setup on the fiberto-mortar pull-out response in TRM composites: Experimental and analytical modeling. *Compos B* 2018;143:250–68. <https://doi.org/10.1016/j.compositesb.2018.02.010>.
- [70] Xu SL, Krüger M, Reinhardt HW, Ožbolt J. Bond characteristics of carbon, alkali resistant glass, and aramid textiles in mortar. *J Mater Civ Eng* 2004;16(4):356–64. [https://doi.org/10.1061/\(ASCE\)0899-1561\(2004\)16:4\(356\)](https://doi.org/10.1061/(ASCE)0899-1561(2004)16:4(356)).

- [71] Valeri P, Ruiz MF, Muttoni A. Modelling of textile reinforced concrete in bending and shear with elastic- cracked stress fields. *Eng Struct* 2020;215:. <https://doi.org/10.1016/j.engstruct.2020.110664110664>.
- [72] Kulas C, Zum Tragverhalten getränkter textiler Bewehrungselemente für Betonbauteile. PhD Thesis, Aachen, RWTH Aachen, 2013.
- [73] Bertolesi E, Carozzi FG, Milani G, Poggi C. Numerical modeling of fabric reinforce cementitious matrix composites (frcm) in tension. *Constr Build Mater* 2014; 70: 531–48.
- [74] Larrinaga P, Chastre C, Biscaia HC, San-José JT. Experimental and numerical modeling of basalt textile reinforced mortar behavior under uniaxial tensile stress. *Mater Des* 2014; 55: 66–74.
- [75] Hegger J, Will N, Bruckermann O, Voss S. Load bearing behaviour and simulation of textile reinforced concrete. *Mater Struct* 2006; 39: 765–76.
- [76] Messori M, Nobili A, Signorini C, Sola A. Mechanical performance of epoxy coated ar-glass fabric textile reinforced mortar: influence of coating thickness and formulation. *Compos Part B: Eng* 2018; 149: 135–43.
- [77] Contamine R, Larbi AS, Hamelin P. Contribution to direct tensile testing of textile reinforced concrete (trc) composites. *Mater Sci Eng: A* 2011; 528: 8589–98.
- [78] Rampini MC, Zani G, Colombo M, di Prisco M. Mechanical Behaviour of TRC composites: experimental and analytical approaches. *Appl Sci* 2019; 9:1492. <https://doi.org/10.3390/app9071492>.
- [79] Kromoser B, Preinstorfer P, Kollegger J. Building lightweight structures with carbon-fiber-reinforced polymer-reinforced ultra-high-performance concrete: Research approach, construction materials, and conceptual design of three building components. *Struct Concr* 2019;20:730–44. <https://doi.org/10.1002/suco.201700225>.
- [80] Rempel S, Kulas C, Hegger J. Bearing Behavior of Impregnated Textile. FERRO-11 – 11th Int Symp Ferrocem 3rd ICTRC - Int Conf Text Reinf Concr 2015:71–8.

6 General Conclusions

This work presented the results of an investigation including the experimental characterization of carbon-TRC and the response of I-beams made with the material. For such, a literature review was exposed to demonstrate the TRC application and to evaluate the composite properties, as well as its response in short- and long-term test. Finally, the experimental mechanical characterization of these carbon-TRC composites was widely analyzed and then investigated their flexural response as a profiled beam.

The general conclusions are:

- cracking behavior was greatly improved with the use of SHCC matrix with respect to a plain matrix. The use of short fibers in combination with textile was not able to enhance the bond performance between carbon-textile and concrete and the load-bearing beam capacity. However, the SHCC matrix was able to improve the ductility and cracking load due to concrete softening mechanism and fiber bridging mechanism, respectively.
- the effectiveness of the sand surface treatment in SBR laminate fabric was confirmed by the stiffer and stronger interface compared to plain SBR fabric. Improvement in load-bearing capacity, the tension stiffening mechanism, the connection between warp and weft yarn, the crack pattern and bond performance were observed when sand-epoxy was used.
- a design model proposed to evaluate the bending performance of the TRC beams presented a good agreement for moment-curvature experimental and theoretical relations for beams. For the beam with SHCC, it is necessary to consider the premature softening mechanism through of a reduction factor. To measure crack opening in specimen with sand-impregnation, it is necessary to take into account the influence of the cross yarn.
- the characterization of the interface between matrix and yarn indirectly measured in tensile test was showed to be more effective in representing the bond performance between materials. In this way, it is possible to take into account the influence of connection between warp and weft yarn.

- despite the compressive strength of the matrix to decrease due to the incorporation of the textile, this reduction does not affect the flexural response of tension-governed carbon-TRC beams.
- the tensile tests revealed that there was a strong influence of dimensions and setup test on the TRC composite response, as well as the different coating of the fabrics. The major difference in test configuration was observed in terms of effective modulus of elasticity, when analyzed the use of this parameter in analytical model. The gauge length has more impact on crack pattern and tensile strength, but slight difference in terms of effective modulus of elasticity. Tensile tests for different carbon textiles showed the great influence of coating, mesh dimensions and stiffness of the fabric in tensile properties. Suitable values can be derived from the tensile parameters and to characterize the composite, making it possible to predict the bending response of carbon-TRC elements with a great agreement of experimental curves.
- carbon-TRC beams subjected to post-creep test did not show no loss in flexural capacity. All beams, in short and long-term tests, presented an abrupt failure at ultimate load, mainly governed by shear. An analytical linear model was successfully used to derive indirectly the effective textile moduli, concrete tensile strength and the nominal bond stress, leading to results similar to those observed in literature.
- the aforementioned model indicated that SBR beam is strongly affected by sustained load and it was observed a poorer creep behavior in terms of deflection and crack width for this beam. The use of sand-impregnation in SBR-laminate textile indicated the bond also plays an important role in sustained loading, avoiding slippage with time and keeping the effectivity of the reinforcement. SND, ACR and EPX beams formed new cracks during creep and the reduction in effective modulus observed was not accompanied by increase in crack width. This can be explained by an improvement in bond stress at early ages.

6.1. Suggestions for Future Works

This study has presented novel results to contribute to TRC knowledge regarding the material characterization and flexural creep behavior. However, it is evident that, in parallel, it demonstrates new demands for specific investigations that may be explored in future works, such as:

- Investigate the long-term behavior of TRC-beams with SHCC matrix;
- Production of beams with better flange-to-web connection (better “assemble cage reinforcement”) as well as increased reinforcement rate;
- Investigation of the parameters that influence the shear strength of carbon-TRC beams;
- Creep tests of the fabric and composite under tensile stresses as well as the fabric-matrix interface.

7 APPENDIX A

In this Section, the simplified model adopted throughout the present work to analyze the behavior of an I-section is presented. First of all, the moment \times average curvature ($M \times \Phi$) is assumed according to Figure 7.1a, where $M_{cr} = 2 I_g f_{ct} / h$ is the I-section moment at cracking (I_g is the moment of inertia of the gross section about major axis, f_{ct} is the effective concrete tensile strength and h is the beam depth), $E_c I_{cr}$ is the cracked flexural stiffness (E_c is the concrete modulus of elasticity and I_{cr} is the cracked moment of inertia) and $\Delta\Phi$ is the reduction in curvature due to tension stiffening effect. The slope of the curve before M_{cr} is reached is equal to $E_c I_g$. The value of I_g can be estimated assuming a plain concrete I-section, whereas the value of I_{cr} can be obtained from the transformed section method, considering usual beam theory hypotheses, linear elastic materials and neglecting influence of concrete in tension. Finally, $\Delta\Phi$ is defined as $\Delta\Phi = \Delta M / E_c I_{cr}$, in which ΔM is the additional moment produced by the average concrete tensile stresses acting at the tension portion – vary from 0 at the cracked section to approximately f_{ct} between cracks. For sake of simplicity, superposition of effects and plastic stress distribution are assumed and, therefore, $\Delta M = Z_{pl} (f_{ct}/2)$, where Z_{pl} is the cross-section plastic modulus.

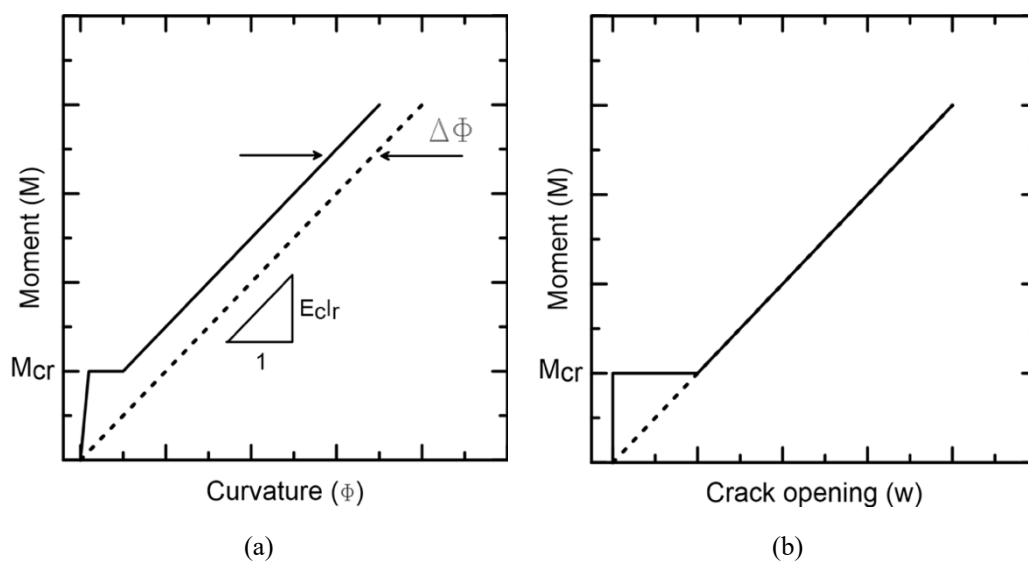


Figure 7.1– Models adopted for theoretical analysis: a) moment vs curvature; b) moment vs crack opening.

With the theoretical moment-curvature ($M-\Phi$) relation properly defined, its correlation with load-displacement ($P-\delta$) at mid-span can be estimated through the classic elastic line equation for a four-point bending configuration, as follows:

$$\Phi = \frac{24\delta}{3L^2 - 4a^2} \quad \text{Eq. 7.1}$$

in which L and a are the beam length and shear span, respectively. Moreover, correlation between the total load P and the bending moment M is simply given as $M = Pa/2$.

In Figure 16b, the simple moment x crack opening relation adopted in the work is presented, which is divided in two stages: i) sudden crack growth (plateau); and ii) linear crack growth (stabilized). As a first step, the average crack spacing, s_m , can be determined according to the model described by Goliath et al. [64], as follows:

$$s_m = 2 \frac{f_{ct}}{\tau_b (U_f/A_f) \rho_f} \quad \text{Eq. 7.2}$$

where τ_b is the nominal bond stress, ρ_f is the reinforcing ratio and U_f/A_f is ratio between reinforcement perimeter and cross-sectional area. Finally, assuming that the textile tensile stress remains approximately constant between cracks at the stabilized crack stage and considering negligible deformation of concrete, the crack opening in the linear range can be estimated according to Eq. 7.3. In this equation, E_f is the textile modulus of elasticity and the term in parenthesis represents the stress at the outermost yarn.

$$w = \frac{s_m}{E_f} \left(\frac{M}{I_{cr}} \frac{h}{2} \right) \quad \text{Eq. 7.3}$$